THE JOURNAL
OF
CHEMICAL PHYSICS

VOLUME 8 APRIL, 1940 NUMBER 4

A Vibrational Analysis of the Absorption Spectrum of Furan in the Schumann Region

LUCY W. PICKETT
Department of Chemistry, Mount Holyoke College, South Hadley, Massachusetts
(Received January 12, 1940)

The absorption spectrum of furan vapor between 2200 and 1550A shows three band systems which overlap slightly. The second of these with a 0−0 band at 52,230 cm^{-1} has sharp bands which could be analyzed to reveal three prominent totally symmetrical vibration frequencies of the excited molecule of 1395 cm^{-1}, 848 cm^{-1} and 1068 cm^{-1}. Other characteristic frequency differences in the more diffuse bands are noted. Since the furan was found to be comparatively stable to photochemical decomposition, measurements of the intensity of absorption were made.

THE ultraviolet absorption spectrum of furan at wave-lengths above 2100A has been studied by a number of investigators who have used both solution and the vapor phase.[1] Some of these have found evidences of narrow shallow bands while others have observed only a broad stepout with no evidence of structure. All agree, however, that the absorption in this longer wave-length region is of very low intensity and thus one may safely conclude that any electronic transition here is of the forbidden type. The measurements also show that the absorption is increasing rapidly to a band of high intensity beyond the short wave-length limit of observation and hence indicate that the lowest excited electronic states to which transitions are allowed are to be studied in the Schumann region.

The present paper describes an investigation of the absorption spectrum of furan vapor at wave-lengths 2200–1550A which shows three distinct band systems of high intensity, in one of which a vibrational analysis was possible. The results of this study are to be correlated with an analysis of the vibrational frequencies of the normal furan molecule from infra-red data which will soon be published.

EXPERIMENTAL

Preparation and purification of furan

Furan was prepared by heating the highest grade of furoic acid obtainable from Eastman Kodak Company and passing the vapor through a tower of sodium hydroxide pellets in an apparatus previously filled with nitrogen. A layer of glass wool placed over the furoic acid together with a careful regulation of the temperature prevented any appreciable quantity of the acid from subliming. The product was dried over lime and fractionally distilled in a one-meter Crismer column in a nitrogen atmosphere; the furan so obtained boiled at 31.3° at 760 mm and had a refractive index $n_D^{20°}=1.4214$. The measurements of absorption spectra were made immediately following distillation. The data were later duplicated with some furan kindly supplied by

[1] W. Hartley and J. Dobbie, J. Chem. Soc. **73**, 598 (1898); J. E. Purvis, J. Chem. Soc. **97**, 1648 (1910); S. Menczel, Zeits. f. physik. Chemie **125**, 161 (1927); I. Kaswagi, Bull. soc. chim. Japan **1**, 145 (1926); E. C. Hughes and J. R. Johnson, J. Am. Chem. Soc. **53**, 737 (1931); O. V. Fialkovskaya, Acta Physico-chimica (U.S.S.R.) **9**, 215 (1938); V. Henri and D. C. Foster (private communication).

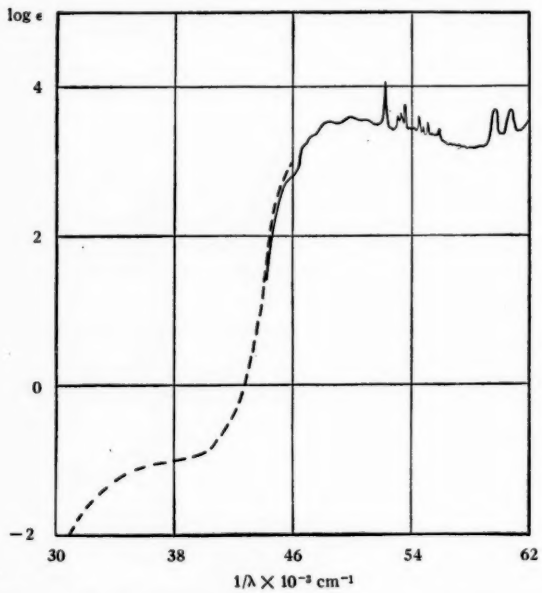

FIG. 1. Absorption spectrum of furan. —— vapor; ------ solution in hexane.

Professor G. B. Kistiakowsky which had been carefully purified for heats of hydrogenation measurements.[2]

Spectral measurements

The absorption spectrum below 2200A was measured with a Hilger fluorite prism vacuum spectrograph and a hydrogen discharge as light source. Photographs were first made of a continuously flowing stream of furan vapor at different pressures in a 60-cm absorption tube whose windows were protected by a layer of flowing nitrogen, using a technique which has been described.[3] Next, furan vapor was irradiated in the absorption tube for periods up to thirty minutes and the spectrum photographed at intervals of ten, twenty and thirty minutes in order to determine the extent of photochemical decomposition. Finally, since this substance was found to be quite stable to the action of the ultraviolet light, some measurements were made on the nonflowing vapor at different measured pressures.

The Ilford *Q* plates which were used were so satisfactory as to permit of densitometer records, the first of which were made on the Moll microphotometer at the Massachusetts Institute of Technology used through the courtesy of Professor G. R. Harrison. Those made from the photographs of the flowing vapor were used to determine the position and relative intensities of the bands. The results were checked by measurements of the positions of the sharp bands with a Hilger comparator. In order to get a measure of absolute intensities, exposures of furan at different pressures were compared photometrically with definitely timed exposures of the hydrogen lamp through the evacuated tube and extinction coefficients calculated for the wave-lengths where there was equal blackening of the two spectra.

[2] M. A. Dolliver, T. L. Gresham, G. B. Kistiakowsky, E. A. Smith and W. E. Vaughan, J. Am. Chem. Soc. **60**, 440 (1938).

[3] E. P. Carr and H. Stücklen, J. Chem. Phys. **4**, 760 (1936).

RESULTS

Since measurements of the furan vapor in the quartz region have been recently made and will be published by Henri and Foster[4] only preliminary experiments in this region were made. No evidence of narrow bands was obtained either in vapor or in hexane solution. A set of 15 narrow bands at wave-lengths 2500 to 2650A were found in the vapor by both Purvis and

TABLE I.

	Wave number in cm^{-1}	Intens.	$1/\lambda$	Calc., for assignment	Assignment
a'	48,890				
b'	50,105		1215		
c'	51,200		1095		
a	52,230	v.s.			0-0 band
b	52,685	w.	465		ν_4
c	53,078	m.s.	848		ν_2
d	53,298	m.s.	1068		ν_3
e	53,625	s.	1395		ν_1
f	53,930	v.w.	1700	1696	$2\nu_2$
g	54,136	w.	1906	1916	$\nu_2+\nu_3$
h	54,455	s.	2225	2243	$\nu_1+\nu_2$
i	54,690	m.	2460	2463	$\nu_1+\nu_3$
j	55,010	m.s.	2780	2790	$2\nu_1$
k	55,195	m.	2965		ν_5
l	55,317	w.	3087	3091	$\nu_1+2\nu_2$
m	55,435	w.	3205	3255	$2\nu_1+\nu_4$
n	55,540	w.	3310	3311	$\nu_1+\nu_2+\nu_3$
o	55,875	m.s.	3645	3638	$2\nu_1+\nu_2$
p	56,055	w.	3825	3858	$2\nu_1+\nu_3$
q	56,290	w.	4060	4103	$2\nu_1+\nu_4+\nu_2$
r	56,410	w.	4180	4185	$3\nu_1$
s	56,535	w.	4305	4360	$\nu_5+\nu_1$
t	56,660	w.	4430	4486	$2\nu_1+2\nu_2$
u	56,968	w.	4738	4739	$2\nu_1+\nu_2+\nu_3$
v	57,325	w.	5095	5033	$3\nu_1+\nu_2$

[4] Private communication, D. C. Foster.

Fialkovskaya[1] but the present measurements showed complete transmission up to 2300A at the highest vapor pressures measured[5] (400 mm in a 60-cm tube). The solution spectrum which shows a broad step-out from about 32,000 cm^{-1} to 42,000 cm^{-1} and a steep rise to a maxmium beyond 45,000 is reproduced in Fig. 1.

In the Schumann region, three distinct band systems were noted, the first two of which may be seen in Fig. 2 which is a microphotometer record of a photograph of the region from 48,000 to 59,000 cm^{-1}. The bands on this are lettered for identification, and in Table I are given the corresponding frequencies with an estimated possible error of ± 10 cm^{-1} which may be somewhat greater for the broader bands. The dispersion of the spectrograph is 200 cm^{-1} per mm at 56,000 cm^{-1}.

The first region of absorption consists of the three broad bands a', b' and c' with separations of 1215 cm^{-1} and 1095 cm^{-1}. These resemble in appearance the bands of cyclohexadiene, 1, 3[6] and cyclopentadiene[7] which are to be observed at much lower frequencies in the quartz ultraviolet. Similar broad diffuse bands at slightly lower frequencies than those of the furan are to be observed in the spectra of all of the aliphatic hydrocarbons with conjugated double bonds studied in this laboratory[7] and would seem to be characteristic of this grouping. There are also three step-outs or very shallow bands to be observed on the long wave-length side of these maxima which are not shown in the record. These step-outs were found at 45,960 cm^{-1}, 46,760 cm^{-1} and 47,480 cm^{-1} with separations of 800 cm^{-1} and 720 cm^{-1}, respectively.

The second band system comprising bands a to x is characterized by sharply defined maxima. The densitometer record gives a somewhat misleading picture of the relative intensity of a as compared with the other strong bands because there is total absorption, and records of photographs taken at lower pressures show that band a is much more intense than any of the other bands of this series. Thus it is assumed that a represents the vibrationless or 0−0 transition.

[5] Measurements of the vapor were made by Miss Elinor Sackter, Mount Holyoke College.
[6] V. Henri and L. Pickett, J. Chem. Phys. 7, 439 (1939).
[7] E. P. Carr and H. Stücklen, unpublished work.

The next strongest band is e with a wave number difference of 1395 cm^{-1} (ν_1) which is interpreted as the totally symmetrical ring vibration in the excited molecule corresponding to 1499 cm^{-1}, the wave number of the very intense band of furan vapor in the infra-red. Bands c and d are assigned as fundamentals of wave number 848 cm^{-1} (ν_2) and 1068 cm^{-1} (ν_3), respectively. The band labeled b is so weak as to be almost questionable but it is tentatively assigned as a fundamental

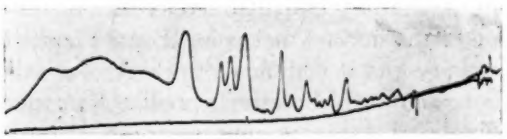

FIG. 2. Microphotometer tracing of furan spectrum from 48,000 to 59,000 cm^{-1} showing second band system and a part of the first and third, together with exposure of hydrogen lamp for comparison.

of 465 cm^{-1}. It is not impossible to interpret this either as a transition from a higher vibrational level of the normal molecule (i.e., $\nu_2''-\nu_1'$) or as a part of the first band system of broader bands which overlaps this one. Thirteen of the remaining seventeen bands seem to be transitions to combinations or overtones of these three vibrational states, ν_1, ν_2 and ν_3, from the lowest vibrational level of the ground state. The strongest of these, somewhat surprisingly, corresponds to the combination frequency, $\nu_1+\nu_2$, while that which has been identified as $2\nu_1+\nu_2$ is also abnormally strong. The overtones of all bands show a rapid and regular falling off of intensity so that no overtone higher than the third can be distinguished with certainty. Thus all of the prominent bands may be represented by the series $1/\lambda=52230+1395m+848n+1068p$ (where $m=0,1,2,3$, $n=0,1,2$, $p=0,1,2$). The assignment of the other bands, all of which are very weak, is less certain. Band k with a difference of 2965 cm^{-1} from a may measure a symmetrical C−H stretching frequency of the excited molecule (ν_5) and the other four bands be combination frequencies of ν_4 and ν_5. They may represent two quanta of vibrational energy of any of the other possible nontotally symmetrical furan vibrations alone or in combination with ν_1. Table I gives the assignment considered the most probable in each case with calculated

TABLE II.

PRESSURE	TIME	LOG ϵ	WAVE NUMBER OF LIGHT ABSORBED
2.2 mm	4 min.	2.76	Beyond 45,600 cm^{-1}
.60	4	3.33	46,250–55,550; beyond 59,120 peak at 55,875
.27	6	3.78	Peak at 52,230; beyond 62,700

frequencies without anharmonicity corrections for comparison with the observed values.

The best test of the probability of the assignment is in the comparison of vibrations with those of the normal molecule. If furan has a C_{2v} symmetry and it is difficult to think of it otherwise,[8] group theory methods predict[9] four totally symmetrical internal vibrations of the ring. Reitz[10] has tentatively selected these four frequencies from a study of depolarization factors of Raman lines of liquid furan as 1137 cm^{-1}, 986 cm^{-1}, 1483 cm^{-1} and 724 cm^{-1},[11] the last of which has however a depolarization factor of 0.63. Two totally symmetrical C−H stretching frequencies are to be expected of a furan molecule of C_{2v} symmetry; at least two frequencies have been reported between 3100–3200 cm^{-1}.

Since the moderately high intensity of the Schumann band system under consideration indicates that it represents an allowed transition, selection rules would permit totally symmetrical vibrational changes only and experience has shown that only the ring vibrations are likely to appear with any intensity. The finding of three prominent vibration frequencies in the excited molecule which correspond to three of the four totally symmetrical ring frequencies of the normal molecule with a decrease in each case of about 100 cm^{-1} seems strong confirmatory evidence for the present assignment. That the possible excited vibrational level of 465 cm^{-1} is the counterpart of the normal 724 cm^{-1} level is much more open to question not only because of the difference of these numbers but also because of the uncertainty that this is a real frequency of the excited molecule as previously discussed and because of the further question raised by the high depolarization factor of 0.63 as to the validity of the assignment in the normal molecule. It may be that a frequency so near in magnitude to one of the other three that it is not resolved, is the missing fourth totally symmetrical ring vibration.

All of the bands in this system have been considered to be transitions from the lowest vibrational level of the normal molecule. The reason for the absence of others is thought to be due to two factors. First, the energy of the totally symmetrical vibrational levels of the normal molecule is sufficiently high so that the number of molecules existing in them would be comparatively low at room temperatures. The Boltzmann factor for a 724 level is 0.031, for a 986 level is 0.009. Secondly, the overlapping band system on the long wave-length side which has been previously discussed would be likely to mask such weak bands.

The third band system begins at the point where the hydrogen spectrum is discontinuous and this makes the bands difficult of measurement so that only strong bands may be determined with certainty. There is a band of high intensity at 59,580 cm^{-1} and a second band of nearly equal intensity at 60,810 cm^{-1} followed by an absorption region which includes a maximum about 62,800 cm^{-1} and seems to have other less well defined peaks. There is also a shallow broad band at 58,765 cm^{-1} or 815 cm^{-1} to the long wave-length side of the first strong band. This may represent a transition from a higher vibrational state of the normal molecule although it does not correspond exactly to any of the vibrations which have been identified. The separation of the two strongest bands, 1230 cm^{-1}, seems to be the vibration frequency corresponding to the 1483 of the normal molecule and 1395 of the first excited state.

The results of the intensity studies are embodied in the curve in Fig. 1, while Table II gives the pressures, exposure times, log ϵ values and absorption limits of a series of measurements in an absorption cell of 8.5 cm length.

While these measurements are somewhat crude

[8] G. B. Bonino who has made careful studies of the Raman spectrum of furan has suggested that the molecule may exist in a dimeric form with C_{2h} symmetry to explain the anomalous Raman results. Atti x° Cong. Inter. Chim 2, 141 (1938).

[9] This number is found by applying the formula $n=1/N\Sigma_R \chi_R \chi_R'$, where N is the number of symmetry operations (4), χ_R is the character of each and χ_R' is the character as applied to each of the original coordinates of the 5 atoms of the ring.

[10] Reitz, Zeits. f. physik. Chemie **B38**, 381 (1938).

[11] Infra-red measurements of the vapor give corresponding frequencies which are slightly larger.

and do not take into consideration the photochemical decomposition during the exposure (which preliminary experiments indicated is small) or certain minor optical errors, they are presented here as giving a semi-quantitative measure of intensity in the Schumann region where almost no intensity data exists because of the difficulties of measurement. It is of interest to note that the solution curve is slightly higher than the vapor curve in the region of overlapping data.

Mulliken[12] has predicted that there should be an absorption maximum for furan in the neighborhood of 58,500 cm^{-1} corresponding to an $N \rightarrow V$, or rather four $N \rightarrow V$ transitions of very similar frequency, which would have a total f value of 0.3. It seems possible that the third band system may represent this transition, although the observed f value, uncertain because of lack of knowledge of the high frequency limit of the band, would seem to be below this predicted value.

The second band system has the characteristics attributed to Rydberg series bands in that the bands are sharp with an intense 0−0 band and short vibrational progressions starting from a ground vibrationless state. This may be a transition of the Rydberg type superimposed on the other band system. Studies of the unsaturated hydrocarbons[13] have shown that Rydberg series bands are to be expected in this part of the spectrum often superimposed on other bands.

Examination of the photographs of the furan which had been exposed to the short wavelength radiation for periods up to thirty minutes showed that the furan was not destroyed in this time. Unlike the unsaturated hydrocarbons studied in this laboratory no absorbing layer was formed on the windows of the absorption cell. However, there was evidence of the development of a substance with an absorption band from about 57,000 to 60,700 cm^{-1}, a doublet with the stronger peak at 55,860, and a peak at 55,500 during the exposure.

I wish to acknowledge with appreciation the grant of a fellowship from the Lalor Foundation during which these measurements were made, and to thank Doctors E. P. Carr and G. B. Kistiakowsky for helpful suggestions.

[12] R. Mulliken, J. Chem. Phys. **7**, 121 (1939).

[13] E. P. Carr and H. Stücklen, J. Chem. Phys. **7**, 631 (1939).

APRIL, 1940 JOURNAL OF CHEMICAL PHYSICS VOLUME 8

Bond Strength and Potential Energy Relationships in Acetylene

HYMAN HENKIN AND MILTON BURTON
Department of Chemistry, New York University, New York, New York

(Received January 15, 1940)

The spectroscopic value for the heat of formation of free CH and Herzberg's value for the heat of sublimation of graphite lead to a value of ∼137.9 kcal. for the C≡C bond strength in acetylene. This value is employed in a study of the potential energy levels of that compound and is shown to be the only one consistent with the most recent studies of its absorption spectrum. The fact that the known energy levels of free CH fit into the scheme is further evidence for the 125.1 kcal. value for the heat of sublimation of graphite.

FOUR widely divergent values for the C≡C bond strength appear in the literature.[1] The value of 220.5 kcal. given by Norrish[2] is based upon an older value for the heat of combustion of acetylene and the value of 150 kcal. for the heat of sublimation of carbon, taking into account the reorganization from tetravalent to divalent carbon as is probable in free CH. That of ∼200 kcal. given in an early work by Pauling[3]

[1] Cf. G. K. Rollefson and M. Burton, *Photochemistry and the Mechanism of Chemical Reactions* (Prentice-Hall, Inc., New York, 1939), pp. 349 and 422.

[2] R. G. W. Norrish, Trans. Faraday Soc. **30**, 103 (1934).

[3] L. Pauling, J. Am. Chem. Soc. **54**, 3570 (1932). Cf. L. Pauling and J. Sherman, J. Chem. Phys. **1**, 606 (1933),

derives from a similar calculation, but takes no account of this reorganization energy. A later calculation[3a] yielding a value of ~123 kcal. for the C≡C bond strength, while using the more recent considerations of Herzberg for the heat of sublimation of graphite still employs a value for the heat of formation of free CH derived from that of methane instead of from spectroscopic data.

On the other hand the value of ~187 kcal. given by Price is based simply on the observation of predissociation broadening in the ultraviolet absorption spectrum of acetylene.[4] The broadening places an upper limit on the strength of the bond concerned. The nature of the spectrum makes it improbable that a C−H bond is involved. Thus, the 187 kcal. value becomes an upper limit for the strength of the C≡C bond. On the assumption that the true value lies close to this maximum,[5] Price was able to suggest a consistent system of potential energy curves which seemed to fit the known data on acetylene.

We have re-examined the available data relating to the chemistry and spectroscopy of acetylene and have concluded that the C≡C bond strength is ~137.9 kcal. In this discussion we retain the definition of bond strength previously used:[6] the strength of a bond in a particular compound is the energy difference (per mole) between the lowest energy state of that compound and the summed lowest energy state of the products formed by rupture of that bond; thus, the calculation is relative to two CH radicals in the $^2\Pi$ state.[7] It should be emphasized that the extremely low value we have obtained derives essentially from the fact that we have accepted Herzberg's 125.1-kcal. value[8] for the heat of sublimation of graphite.[9]

In the estimation of the C≡C bond strength the reliability of the following data has been assumed.[10]

$$C_2H_2+(5/2)O_2\rightarrow 2CO_2+H_2O(1);\quad \Delta H=-311.1 \text{ kcal.} \qquad (1)^{11}$$

$$C(gr)+O_2=CO_2;\quad \Delta H=-94.030\pm 0.011 \text{ kcal.} \qquad (2)^{12}$$

$$H_2+\tfrac{1}{2}O_2=H_2O(1);\quad \Delta H=-68.37 \text{ kcal.} \qquad (3)^{11}$$

$$C(gr,0°K)=C(gr);\quad \Delta H=0.2 \text{ kcal.} \qquad (4)^{6}$$

$$H_2(g,0°K)=H_2;\quad \Delta H=1.9 \text{ kcal.} \qquad (5)^{6}$$

$$2H=(n)H_2(g,0°K);\quad \Delta H=-102.48\pm .02 \text{ kcal.} \qquad (6)^{13}$$

$$CH=C+H;\quad \Delta H=80.0 \text{ kcal.} \qquad (7)^{14}$$

$$C=C(gr,0°K);\quad \Delta H=-125.1 \text{ kcal.} \qquad (8)^{8}$$

In addition, we assume

$$C_2H_2=C_2H_2(g,0°K);\quad \Delta H=-2.2 \text{ kcal.} \qquad (9)^{15}$$

From these data the relationship

$$C_2H_2(g,0°K)=2CH:\quad \Delta H\backsimeq 137.9 \text{ kcal.} \qquad (10)$$

follows directly. This value may properly be compared with the C−C bond strength in ethane given variously as 72 kcal.[7] and 97.6

who give a value of 198.5 kcal. for all acetylenic hydrocarbons.

[3a] L. Pauling, *The Nature of the Chemical Bond* (Cornell University Press, Ithaca, New York, 1939), p. 122.

[4] W. C. Price, Phys. Rev. **47**, 444 (1935).

[5] In general such correspondence is not to be expected. Cf. M. Burton, J. Chem. Phys. **7**, 1072 (1939).

[6] M. Burton, J. Chem. Phys. **6**, 817 (1938).

[7] R. S. Mulliken, Rev. Mod. Phys. **4**, 1 (1932).

[8] G. Herzberg, Chem. Rev. **20**, 145 (1937). Herzberg actually gives 124.1 kcal. See, however, reference 6.

[9] Recent further investigations by Professor H. L. Johnston on the sublimation of graphite, as well as other considerations, lead him to the conclusion that the 125.1-kcal. value is correct. This work will be the subject of a shortly forthcoming paper. The authors wish to thank him for the opportunity to quote this result prior to publication.

[10] Unless otherwise indicated all chemically stable compounds are referred to their standard states. C(gr) represents graphite at 18°. Radicals and atoms are taken in the states corresponding to 0°K.

[11] F. R. Bichowsky and F. D. Rossini, *The Thermochemistry of the Chemical Substances* (Reinhold Publishing Corp., New York, 1936).

[12] F. D. Rossini, J. Chem. Phys. **6**, 569 (1938); F. D. Rossini and R. S. Jessup, Nat. Bur. Stand. J. Research **21**, 491 (1938).

[13] H. Beutler, Zeits. f. physik. Chemie **B29**, 315 (1935).

[14] G. Herzberg, *Molecular Spectra and Molecular Structure. I. Diatomic Molecules* (Prentice-Hall, Inc., New York, 1939), p. 485. G. W. King, J. Chem. Phys. **6**, 378 (1938), uses the value 78.9 kcal. Here ΔH is from spectroscopic data for D_0.

[15] This is an approximation obtained by comparison with the cases of CH_4 and C_2H_6 (see reference 6). The error probably does not exceed ±0.2 kcal. The same result is obtained by approximation from available thermal data. (Int. Crit. Tab.)

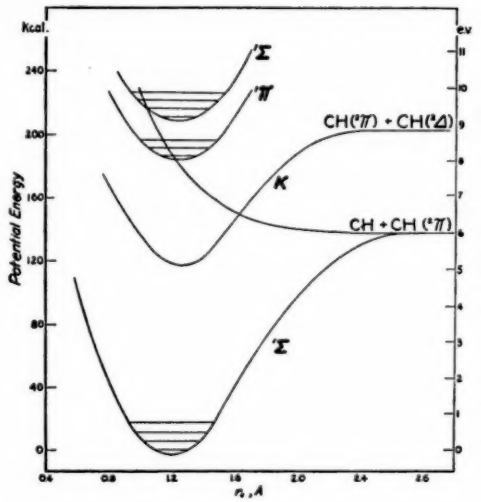

FIG. 1. Potential energy relationships in acetylene. The upper curves are from the data of Price (ref. 4). The lower part of the normal curve is obtained from data on the fundamental frequency and the moment of inertia. For the K curve, r_e is given by Kistiakowsky (reference 17).

kcal.[16] The striking fact is that, if we accept the 125.1-kcal. value for the heat of sublimation of graphite, we must conclude that the strength of the C≡C bond is less than two times the strength of the normal C−C bond.

SPECTRAL DATA AND POTENTIAL CURVES

It will now be shown that the value of 137.9 kcal. accords with data derived from a study of absorption bands in the near ultraviolet (at 2400–1900A), first described by Kistiakowsky.[17] These bands have been further investigated by Jonesco[18] who was able to represent the band heads by the formula[19]

$$\nu = \nu_0 + 1034.6v' - 9.6v'^2, \qquad 1$$

where $v = 0, 1, 2, 3\cdots$. From this equation he derived a value of ∼204 kcal. as the convergence limit for the band heads.

If this convergence limit is taken as the beginning of the region where the split into one normal ($^2\Pi$) and one excited ($^2\Delta$)CH radical occurs, then it may very simply be correlated to the C≡C bond strength of normal acetylene. Mulliken[7] has given 2.85 ev (65.5 kcal.) as the energy difference $^2\Delta - {}^2\Pi$ for the CH radical. If we use the 137.9 kcal. value for the C≡C bond strength, it follows that the dissociation in the first excited state should require 203.4 kcal., in very good agreement with Jonesco's value of ∼204 kcal.

The acetylene spectrum has been more thoroughly investigated in the same region by Woo and his co-workers.[20] They found that their data for what they designated as C bands could be represented by the relationship

$$\nu = 42{,}227.51 + 529.56v_5' - 2.450v_5'^2, \qquad 2$$

where $v_5' = 0, 2, 4\cdots$. The convergence limit derived from this equation is 201.6 kcal. Since v_5 represents transverse vibration of the C≡C bond

$$\nu_5: \quad \underset{\downarrow}{\mathrm{H}}-\overset{\uparrow}{\underset{\downarrow}{\mathrm{C}}}\equiv\overset{\uparrow}{\underset{\downarrow}{\mathrm{C}}}-\underset{\uparrow}{\mathrm{H}}.$$

and the C bands in Woo's classification are those with $v_4' = 2$,

$$\nu_4: \quad \underset{\downarrow}{\mathrm{H}}-\overset{\uparrow}{\underset{\downarrow}{\mathrm{C}}}\equiv\overset{\uparrow}{\underset{\downarrow}{\mathrm{C}}}-\underset{\uparrow}{\mathrm{H}},$$

the convergence limit corresponds to somewhat distended radicals with vibration frequencies slightly higher than in the normal state. This additional energy amounts to ∼3 kcal. Thus using the data of Woo and his co-workers we find that the energy required to dissociate C_2H_2 into CH($^2\Pi$) and CH($^2\Delta$) in their lowest states is ∼199 kcal. Considering the extrapolations involved and the assumptions made, the agreement with our ∼203 kcal. is good.

From the above data we may draw a more nearly correct picture of the C≡C positions of the acetylene potential energy hypersurfaces. The assumption made by Price that the beginning of the predissociation in the spectrum corresponds to the bond strength has recently been shown[5] to be invalid in several cases where it might have been expected to hold; this assumption is at best an approximation, not holding well in a relatively large number of cases. However, Price's value does fix an upper limit for the bond strength.

[16] Trenner, Morikawa and Taylor, J. Chem. Phys. **5**, 203 (1937).
[17] G. B. Kistiakowsky, Phys. Rev. **37**, 276 (1931).
[18] M. A. Jonesco, Comptes rendus **199**, 710 (1934).
[19] In Jonesco's article, the coefficient, 9.6, was omitted, perhaps because of a typographical error. We have determined it directly from his data.
[20] Woo, Lui, Chu and Chih, J. Chem. Phys. **6**, 240 (1938).

The potential energy curves which we have drawn for the various states of acetylene are shown in Fig. 1.[21] The normal curve flattens out at ~137.9 kcal., not at 187 kcal. as previously suggested by Price.[4] He postulated that the K curve also approached 187 kcal. asymptotically and that the interaction of that curve with the upper excited states produces predissociation, observed both at 1520A and 1350A. He thought it likely that this curve might represent the upper state of the Kistiakowsky bands which are found in the near ultraviolet. From the work of Jonesco and of Woo and his co-workers, it now appears, however, that this level dissociates, not at 187 kcal., but at ~203 kcal., so that we cannot explain the observed predissociations as due to interactions of this state with the higher electronic levels. The Kistiakowsky bands require a minimum in the K curve at slightly less than 120 kcal., as shown on the diagram; this value is fixed by the work of Jonesco and of Woo for the 0−0 transition from this state to the ground state.

To explain the predissociations at 1520A and 1350A, we postulate a repulsive curve as shown on the graph, coming down to the asymptotic value for the ground state. The interaction of this curve with the $n=3$ levels of Price's Class I and II bands would account for the predissociation at 1350A and 1520A, respectively. There has been some question as to whether another predissociation region occurs at ~1900A. Herzberg[22] has observed a continuum in this region at higher pressures. It may be that this is an example of an induced predissociation, which might be expected under such conditions. On the basis of these potential energy curves it would be explained as an interaction of the K curve with the repulsive curve. This predissociation is possible, but not required, according to our diagram; that it has not been observed by all workers may be due to different pressures used by various investigators or perhaps even to the occasional presence of paramagnetic impurities, e.g., oxygen.

Price has shown that the K state would fit into the Rydberg series for his Class I system of electronic bands, those involving a $^1\Sigma \rightarrow {}^1\Sigma$ transition. He doubts that this is anything more than a coincidence, inasmuch as the intensity of the bands he observed is at least 100,000 times as great as that of the Kistiakowsky bands, and the latter contain P, Q, and R branches whereas Price's are double-branched.

It is immaterial for the purpose of our discussion just what the quantum designation of the K level is. The excellent work by Woo and his collaborators is unfortunately incomplete; it is thus impossible to check Jonesco's $^1\Sigma$ designation[23] which, in view of the work of Woo, of Göpfert,[24] and of Kistiakowsky,[17] seems improbable. However, it is clear from the weakness of the Kistiakowsky bands that the transition $^1\Sigma + h\nu \rightarrow K$ seems to be forbidden by some selection rule for it is unlikely that application of the Franck-Condon principle could by itself account for such an effect.

In conclusion, we may emphasize that the choice of Herzberg's 125.1-kcal. value for the heat of sublimation of graphite has led to the 137.9-kcal. value for the C≡C bond strength. This is the only value so far suggested for that bond strength which is consistent with the known energy levels of free CH. Thus the system of potential energy relationships here demonstrated lends further support to the 125.1-kcal. value for the heat of sublimation of graphite.

[21] Cf. G. B. B. M. Sutherland, Phys. Rev. **43**, 883 (1933); Herzberg, Patat and Spinks, Zeits. f. Physik **92**, 87 (1934).
[22] G. Herzberg, Trans. Faraday Soc. **27**, 378 (1931). According to Price (reference 4), Dieke was unable to detect predissociation at 1900A.
[23] M. A. Jonesco, Comptes rendus **200**, 817 (1935).
[24] H. Göpfert, Zeits. f. wiss. Phot. **34**, 156 (1935).

The Exchange of Oxygen Between NO and NO_2*

EDGAR LEIFER†
Department of Chemistry, Columbia University, New York, New York

(Received February 19, 1940)

The reaction $N^{14}O+N^{15}O_2=N^{15}O+N^{14}O_2$ has been studied in the gas phase at $-35°C$ and at a total pressure of 2.5 cm of Hg. Although the reaction rate constant could not be determined due to the speed of reaction a lower limit for its value is 10^6 cc moles^{-1} second^{-1}. The equilibrium constant for the exchange at 298.1°K calculated from spectroscopic data is 0.967 as compared with 0.96 ±0.02 which was observed. By combining the data obtained in this investigation with the equilibrium data for N_2O_3 which is assumed to be the intermediate in the exchange reaction an approximate value for the energy of activation for the formation of N_2O_3 is determined.

THE existence of N_2O_3 as a stable compound in the gas phase has been shown by measurements of the equilibrium constant for the reaction

$$NO+NO_2=N_2O_3 \qquad (1)$$

by Verhoek and Daniels[1] and by a study of the absorption spectra of mixtures of NO and NO_2 by Melvin and Wulf.[2] Although its structure has never been determined, a study of the electronic states for NO and for NO_2 molecules makes it seem highly reasonable that the bond which is formed in their association is between oxygen of NO_2 and nitrogen of NO. This is most probable since the main resonating structure of NO is the one having an odd electron on the nitrogen atom, and that for NO_2 having an odd electron on either of the two oxygens. Proof for this structure can be obtained from a study of the oxygen exchange reaction between NO and NO_2 as traced by isotopic nitrogen.

In this research an attempt was made to study the kinetics of the exchange of nitrogen between NO and NO_2 in the gas phase. Owing to the speed of this reaction, only a lower limit for the rate constant could be established. However, the exchange itself established some interesting points about N_2O_3, which will be reported here. The reaction studied was

$$N^{14}O+N^{15}O_2=N^{15}O+N^{14}O_2. \qquad (2)$$

The equilibrium constant for this reaction has been calculated from spectroscopic data for the ordinary compounds by the method of Urey and Greiff.[3] The molecular constants used in the calculation are given in Table I. The molecular constants for the rarer isotopic molecules have been calculated from the spectral data of the more abundant molecules. The equilibrium constant for reaction (2) is given by

$$K=f_{(N^{15}O)}f_{(N^{14}O_2)}/f_{(N^{15}O_2)}f_{(N^{14}O)}.$$

The ratio of the partition functions is given by the following formulae:*

$$f_{(N^{14}O)}/f_{(N^{15}O)}=\left(\frac{M_1}{M_2}\right)^{\frac{3}{2}}\left(\frac{I_1}{I_2}\right)\times\exp\left[-\frac{hc}{2kT}(\omega_1-\omega_2)\right]\left(\frac{1-e^{-hc\omega_2/kT}}{1-e^{-hc\omega_1/kT}}\right),$$

$$f_{(N^{14}O_2)}/f_{(N^{15}O_2)}=\left(\frac{M_1}{M_2}\right)^{\frac{3}{2}}\left(\frac{A_1B_1C_1}{A_2B_2C_2}\right)^{\frac{1}{2}}\times\exp\left[-\frac{hc}{2kT}\left(\sum_i\omega_{1i}-\sum_i\omega_{2i}\right)\right]\prod_i\frac{1-e^{-hc\omega_{2i}/kT}}{1-e^{-hc\omega_{1i}/kT}}.$$

At 298.1°K $K_{calc}=0.967$.

TABLE I.

	ω_0(CM^{-1})	I_2/I_1*
$N^{14}O$[4]	1891.3	1.0369
$N^{15}O$	1857.4	

	ω_1	ω_2	ω_3	α(half-angle)	A_2/A_1	B_2/B_1	C_2/C_1
$N^{14}O_2$[5]	1373	641	1615	60°	1.0044	1.0486	1.0000
$N^{15}O_2$	1356	634	1581	60°			

* Publication assisted by the Ernest Kempton Adams Fund for Physical Research of Columbia University.

† Fellow of the Charles A. Coffin Foundation, 1939–1940.

[1] Verhoek and Daniels, J. Am. Chem. Soc. **53**, 1250 (1931).

[2] E. H. Melvin and O. R. Wulf, J. Chem. Phys. **3**, 755 (1935).

[3] H. C. Urey and L. G. Greiff, J. Am. Chem. Soc. **57**, 321 (1935).

* Subscript 1 refers to ordinary molecule and 2 to rarer isotopic molecule.

[4] Nielsen and Gordy, Phys. Rev. **56**, 781 (1939).

[5] Sutherland and Penney, Nature **136**, 146 (1935).

Experimental

NO was prepared by the method of Johnston and Giauque.[6] $N^{15}O_2$ was prepared by the catalytic oxidation of ammonia (2.4 percent N^{15}), prepared by Thode and Urey,[7] over a single layer of 80-mesh platinum gauze. The products of oxidation were caught in a trap surrounded by a Dewar flask containing liquid nitrogen. They were then distilled through one meter of a P_2O_5 drying tube, oxidized with excess oxygen and then frozen to dry ice temperature. The excess of oxygen was then pumped off with a mercury diffusion pump. The NO_2 was kept at temperature of dry ice at all times to prevent its attacking the "Apiezon" stopcock grease which is attacked if allowed to remain in contact with NO_2 for any period of time. Since the reaction discussed is so very rapid, the "Apiezon" grease used to lubricate the stopcocks of the reaction vessel and filling chamber was not attacked even after many runs.

In the attempted kinetic runs measured amounts of NO were admitted from a filling chamber into a reaction vessel which already contained a known amount of NO_2 (heavy in N^{15}). The reaction vessel was immersed in a Dewar flask containing bath of chloroform at $-35°C$. The total pressure in the reaction vessel was 2.5 cm. More than half of the pressure was always due to NO. After about 15 seconds the reaction vessel was opened to an evacuated system which contained a trap and sample tube in series. The trap, which was kept at $-118°C$ with solid-liquid ethyl bromide, separated quantitatively all N_2O_3 and the excess NO was frozen into the sample tube which was immersed in a Dewar flask containing liquid nitrogen. The NO was then analyzed for its isotopic ratio with a mass spectrometer of the Bleakney[8] type. Since the reaction was found to be very rapid, it was necessary to design the reaction vessel so as to eliminate the error which might arise due to the rate of diffusion of gases. The rate of diffusion of gases in an ordinary bulb proved to be slower than the rate of reaction even at the low pressures in the experiments. The reaction vessel was a 125-ml bulb; through a ring seal in it a one-millimeter capillary tube extended about two-thirds of the way into the bulb. Attached to this tube was a three-way stopcock, one opening of which was to the bulb, another to the filling system, and the third to the analysis system. The jet effect produced by allowing NO from a higher pressure in the filling system into the reaction vessel, and the fact that NO is lighter than NO_2 already in the bulb caused the gases to mix rapidly so that diffusion was completed within 15 seconds.

The equilibrium constant for the reaction was determined by mixing larger amounts of NO and $N^{15}O_2$. Since the original isotopic ratios were known for both NO and NO_2, a mass spectrometer analysis for the isotopic ratio of NO at equilibrium would give us the equilibrium constant.

Experiments were also performed on solid N_2O_3. Solid N_2O_3 containing a high isotopic content of nitrogen was mixed with NO at $-118°C$ using a solid-liquid ethyl bromide mixture as the cooling bath. The excess of NO was analyzed for its isotopic ratio after remaining in contact with N_2O_3 for several minutes.

Results and Discussion

The mere fact that we have obtained exchange proves that in its structure N_2O_3 has an oxygen bridge between both nitrogens. This follows immediately from the assumption that the exchange which was observed occurs through the formation of N_2O_3. Although the kinetics for this reaction could not be measured by the method used since all samples were at equilibrium within 15 seconds, a lower limit for the rate constant "k" defined by

$$d(N^{15}O)/dt = K_p k(N^{14}O)(N^{15}O_2) - k(N^{15}O)(N^{14}O_2),$$

where K_p is the equilibrium constant for reaction (2), is approximately 10^6 cc moles^{-1} second^{-1} at $-35°C$ and at a total pressure of 2.5 cm of Hg. Since the rate constant for this reaction is so high even at so low a temperature, it must mean that the energy of activation for the formation of N_2O_3 is very small and is most probably less than one kilocalorie. Since ΔH for reaction (1) is 10,300 calories,[1] the energy of activation for the

[6] Johnston and Giauque, J. Am. Chem. Soc. **51**, 3194 (1929).
[7] Thode and Urey, J. Chem. Phys. **7**, 34 (1939).
[8] Bleakney, Phys. Rev. **40**, 496 (1932).

dissociation of N_2O_3 into NO and NO_2 is approximately 10.5 kilocalories. These results compare favorably with those for the association of NO_2 to form N_2O_4[9] where a similar situation exists. We should normally expect these results since it is probable that very little energy of activation is required to form a bond between two molecules, both of which have odd electrons.

The equilibrium constant determined experimentally is 0.96 ± 0.02 as compared with the value 0.967 at 25°C calculated from spectroscopic data. This reaction might, therefore, also be used for concentrating isotopic nitrogen, although it seems less feasible from an experimental point of view than the method used by Thode and Urey.[7]

From the exchange which was found between NO and solid N_2O_3 at −118°C, it appears that solid N_2O_3 is unstable and can exist only in equilibrium with its components.

The author wishes to express his appreciation to Professor Harold C. Urey for his helpful advice throughout the course of this investigation.

[9] Richards and Reid, J. Chem. Phys. **1**, 114 (1933).

APRIL, 1940 JOURNAL OF CHEMICAL PHYSICS VOLUME 8

The Molecular Structure of Isobutane

J. Y. Beach and John Walter
Frick Chemical Laboratory, Princeton, New Jersey

(Received January 15, 1940)

The two published electron diffraction investigations of isobutane led to slightly conflicting results. We have repeated the calculation of the theoretical scattering curves using $Z-F$ instead of Z for the atom form factor and including the temperature factor. The final results are: C−C distance, 1.54 ± 0.02A; C−C−C angle 111° 30′±2°.

TWO electron diffraction investigations of isobutane have been published. Both led to a C−C bond distance of 1.54 ± 0.02A. There was a slight disagreement, however, on the value of the C−C−C angle. Beach and Stevenson[1] reported 113° 30′±2°. Pauling and Brockway[2] reported 111° 30′±2°. In this paper we shall attempt to resolve this discrepancy. The positons and intensities of the electron diffraction maxima and minima obtained in the two investigations do not differ significantly. In this re-examination of the problem we shall use the average of the two sets of data. The averages of the observed values of s ($s_{obs}=(4\pi \sin \theta/2)/\lambda$) and I (visually estimated intensities) are given in Table I.

In both investigations the usual visual method[3] was used to interpret the photographs. In this procedure the visual estimates of the positions and intensities of the maxima and minima are compared with the positions of the maxima and minima on the simplified theoretical curve, $I=C\sum_i\sum_j Z_iZ_j \sin sr_{ij}/sr_{ij}$. In this expression the atom form factors $(Z_i-F_i)/s^2$ have been replaced by Z_i. This involves two simplifications. First, the neglect of $1/s^2$ changes the curve from

TABLE I.*

MAX.	MIN.	I	C_k	s_{OBS}	s_{CALC}[a]	s_{CALC}/s_{OBS}
1		10	16	3.00	2.77	(0.923)
	2			4.36	4.10	(0.940)
2		28	80	5.48	5.75	1.049
	3			6.99	6.94	0.993
3		11	42	7.88	8.04	1.020
	4			8.63	9.11	(1.056)
4 (shelf)		8	33	9.31	9.60	1.031
	5			11.38	11.13	0.978
5		19	85	12.88	12.94	1.005
6		12	44	17.69	17.79	1.006
7		6	17	21.12	20.83	0.986
					Average	1.009
					C−C	1.55

* Values in parentheses not included in the average.
[a] Curve *D*, Fig. 1.

[1] J. Y. Beach and D. P. Stevenson, J. Am. Chem. Soc. **60**, 475 (1938).
[2] L. Pauling and L. O. Brockway, J. Am. Chem. Soc. **59**, 1223 (1937).
[3] L. Pauling and L. O. Brockway, J. Chem. Phys. **2**, 867 (1934).

a rapidly falling one to an approximately horizontal one possessing a series of maxima and minima. This curve represents the visual appearance of the photographs much more closely than the complete curve. Second, it is assumed that $Z-F$ is proportional to Z for different atoms, with the same proportionality factor, at a given angle. It is easy to check the accuracy of the first simplification. We can be sure that $Z-F$ is proportional to Z by considering a molecule in which all the atoms are of the same kind. This is true of the halogen molecules. These molecules have been treated by the visual method[3] and interatomic distances are obtained which agree with the spectroscopic values. This is good proof that the first simplification introduces no serious error. The second simplification is not completely justified,[4] although it introduces only a slight error for atoms in the same row in the periodic system. In order to eliminate a possible source of error in isobutane we have used $Z-F$ in the scattering function. The Pauling and Sherman[5] F values were used in the calculations.

In both of the investigations of isobutane the effect of the thermal motion of the molecule on the scattering curve was not considered. We have now included the temperature factor in the calculations. To include the temperature factor it is necessary to know the mean of the square of the deviation of each interatomic distance in the molecule from the equilibrium value. To know this accurately requires a complete normal coordinate treatment of the molecule. The mean square displacement of each interatomic distance can then be calculated for each normal vibration. The total mean square displacement for an interatomic distance is the sum of the mean square displacements for all the normal vibrations.[6] Expressions have not been obtained for all the normal vibrations of isobutane. We have split the problem into two parts. We consider first the vibrations of a pyramidal XY_3 molecule. As normal coordinates we have used the symmetry coordinates of Howard and Wilson.[7] Their symmetry coordinates correspond quite closely to either stretching vibrations or bending vibrations. This is a fairly good approximation. We use this treatment to obtain the two C−C mean square displacements. The two shortest C−H and the shortest H−H mean square displacements we obtain from a similar treatment of the XYZ_3 molecule.

This accounts for all the terms in the scattering formula that do not change with the orientation of the methyl groups. The scattering formula including $Z-F$ and temperature factor but not including rotation terms, in the case of a tetrahedral C−C−C angle, is:

$$I=3(Z_C-F_C)^2(\sin 1.54s/1.54s)\exp(-0.0014s^2)+3(Z_C-F_C)^2(\sin 2.52s/2.52s)\exp(-0.0020s^2)$$
$$+10(Z_C-F_C)(Z_H-F_H)(\sin 1.09s/1.09s)\exp(-0.0028s^2)+12(Z_C-F_C)(Z_H-F_H)$$
$$\times(\sin 2.16s/2.16s)\exp(-0.0034s^2)+9(Z_H-F_H)^2(\sin 1.78s/1.78s)\exp(-0.0074s^2).$$

This curve is shown in Fig. 1, curve B. It is only slightly different from the curve calculated without $Z-F$ and temperature factor, curve A. The introduction of $Z-F$ and temperature factor does not have an important effect on the C−C−C angle. As before[1] we find that the assumed orientation of the methyl groups has a considerable effect on this angle. Previously[1] the methyl groups were supposed to be stationary in an orientation which allowed the H−H distances to be as large as possible. Pauling and Brockway omitted the rotation terms. To determine the most reasonable orientation of the methyl groups we have constructed a model of isobutane from a set of atom models.[8] From an examination of the H−H distances we found that the most stable orientation giving the molecule the symmetry C_3 (not C_{3v}) is the one used before.[1] However, it is evident that the methyl groups can rotate to all positions more or less as cog wheels without having the H−H

[4] M. H. Pirenne, J. Chem. Phys. **7**, 144 (1939).
[5] L. Pauling and J. Sherman, Zeits. f. Krist. **A81**, 1 (1932).
[6] R. W. James, Physik Zeits. **33**, 737 (1932).
[7] J. B. Howard and E. B. Wilson, J. Chem. Phys. **2**, 630 (1934).
[8] Fischer-Hirschfelder models, obtained from the Fischer Scientific Company. The radii in bond directions are obtained from observed interatomic distances. The radii in other directions are kinetic theory radii.

distances become seriously smaller. For any orientation of a given methyl group the other two can be oriented in such a way that the H−H distances remain reasonably large. We have therefore assumed, in calculating the long C−H terms, that the methyl groups rotate freely. Each methyl group was assumed to have an equal chance of occupying one of the twelve orientations differing by 30° (or n 30°). The long C−H terms might have been accounted for by considering stationary methyl groups and using a large ($\langle \delta l_{ij}^2 \rangle_{Av}$ large) temperature factor. Free rotation is probably a much better representation of the motion of the molecule. Only the long H−H terms were not included in the calculation. The short H−H terms were included.

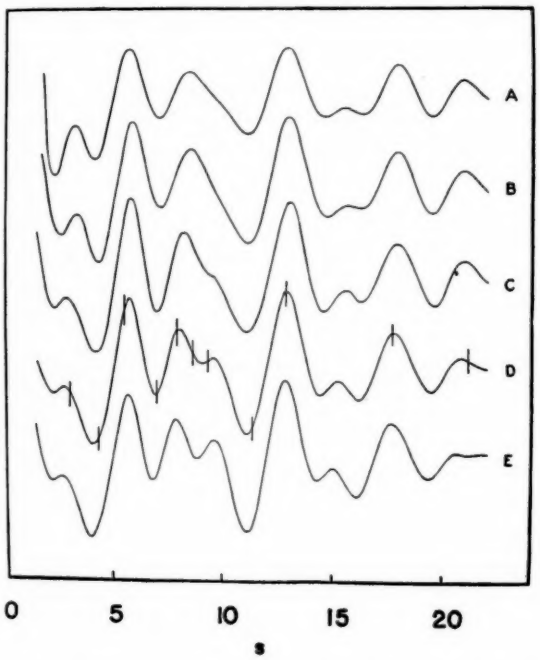

FIG. 1. Theoretical intensity curves for isobutane. Curve A: C−C−C angle, 109° 28′; Z-F, temperature factor and long C−H terms not included. Curve B: C−C−C angle, 109° 28′; Z-F and temperature factor included. Curve C: C−C−C angle, 109° 28′; Z-F, temperature factor and long C−H terms included. Curve D: C−C−C angle, 111° 30′; Z-F, temperature factor and long C−H terms included. Curve E: C−C−C angle, 113° 30′; Z-F, temperature factor and long C−H terms included. The vertical lines indicate the observed positions of the maxima and minima.

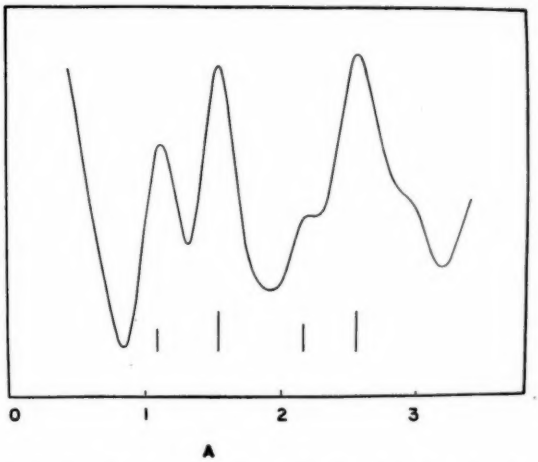

FIG. 2. Modified radial distribution function for isobutane. Vertical lines indicate the final values for the interatomic distances and their importance in the scattering function.

Curves C, D and E were calculated using $Z-F$, temperature factor and long C−H terms. The C−C−C angles are 109° 28′, 111° 30′ and 113° 20′, respectively. The fourth maximum on the photographs is reproduced most closely in the 111° 30′ curve. In curve C it is too low and in curve E it is too high. Quantitative comparison of curve D and the photographs is made in Table I. The radial distribution function calculated by the method of Schomaker[9] is shown in Fig. 2. The C−C bond distance is 1.55A in Table I and 1.54A in Fig. 2. The long C−C distance is 2.56A in Fig. 2 giving an angle of 112°.

The final results are: C−C distance, 1.54 ±0.02A; C−C−C angle 111° 30′±2°.

[9] V. F. Schomaker, Baltimore meeting of the American Chemical Society, April, 1939.

Errors in the Determination of the Dissociation Constant of a Weak Acid by the Extrapolation Method

MARY L. KILPATRICK
Department of Chemistry and Chemical Engineering, University of Pennsylvania, Philadelphia, Pennsylvania
(Received February 12, 1940)

In the extrapolation method for determining the dissociation constant of a weak acid the value of the limiting equivalent conductance is not known from independent measurements, and both the limiting equivalent conductance Λ_0 and the dissociation constant K are obtained from conductimetric measurements on solutions of the acid. While clearly convenient, the reliability of the method has been questioned. In the present paper equations are derived which express the effect on K and on Λ_0 of errors in the experimental quantities. For water as solvent, tables are given showing the numerical values of the errors. The possibility of detecting constant errors is discussed.

WITH the realization that the relationship between the structure of an acid and its dissociation constant requires a knowledge of the thermodynamic quantities, free energy, heat content, and entropy, the importance of the accurate determination of dissociation constants over a range of temperature becomes evident. The conductimetric determination of the thermodynamic dissociation constant of a weak acid HX commonly requires a knowledge of the equivalent conductance of the acid at infinite dilution, obtained by measurement of the conductances of the salts MX and MY and that of the strong acid HY. It has been proposed by Ives,[1] Fuoss and Kraus,[2] Fuoss,[3] and Shedlovsky,[4] that the dissociation constant may be evaluated from measurements on the weak acid alone. This procedure, known as the extrapolation method, has however been criticized by Shedlovsky and by Belcher.[5] After comparing the values of the dissociation constant computed by the extrapolation method for a number of weak acids in water with the values obtained in the customary manner using the conductance of the alkali salt, Belcher concluded that the extrapolation method is reliable if the electrolyte is not too weak ($K \geqq 10^{-3}$), but that if the electrolyte is much weaker ($K \leqq 10^{-5}$) the method may give Λ_0 and K values that are seriously in error.

In solvents in which all electrolytes are weak the experimental determination of Λ_0 is not possible, and the extrapolation method is perforce applied. Although Λ_0 is experimentally determinable in water, the experimental determination presents a laborious task if the conductances of HY and MY are not already available. It therefore appears worth while to examine the problem of the accuracy with which the conductance of the weak acid HX must be measured in order that the extrapolation method may yield a reliable value of the dissociation constant.

The extrapolation method is based upon the assumption of obedience to the equation of Onsager for the equivalent conductance of a completely dissociated solute,* and to the equation of Debye and Hückel for the activity coefficient of an ion. Let Λ be the equivalent conductance of the weak acid HX present at total concentration C. The sum of the ion conductances at this acid concentration, Λ_e, is given by the equation

$$\Lambda_e = \Lambda_0 - (L\Lambda_0 + M)(C\Lambda/\Lambda_e)^{\frac{1}{2}} = \Lambda_0 - (L\Lambda_0 + M)C_i^{\frac{1}{2}}, \quad (1)$$

where L and M are constants for a given solvent and temperature, and $C_i = C\Lambda/\Lambda_e$ represents the concentration of each ionic species. The dissociation constant K is given by the equation

$$K = \frac{C_i^2 f^2}{C - C_i} = \frac{\Lambda^2 C f^2}{\Lambda_e(\Lambda_e - \Lambda)},$$

[1] D. J. G. Ives, J. Chem. Soc. 731 (1933).
[2] R. M. Fuoss and C. A. Kraus, J. Am. Chem. Soc. **55**, 476 (1933).
[3] R. M. Fuoss, J. Am. Chem. Soc. **57**, 488 (1935).
[4] T. Shedlovsky, J. Frank. Inst. **225**, 739 (1938).
[5] D. Belcher, J. Am. Chem. Soc. **60**, 2744 (1938).

* In the development given by Shedlovsky, reference 4, an extended form of the Onsager equation is employed.

where f is the mean ionic activity coefficient, that of the undissociated molecules being taken as unity. Upon setting

$$\log_{10} f = -AC_i^{\frac{1}{2}} = -A(C\Lambda/\Lambda_e)^{\frac{1}{2}},$$

A being a constant for a given solvent and temperature, we have

$$K = \frac{\Lambda^2 C \cdot 10^{-2AC_i^{\frac{1}{2}}}}{\Lambda_e(\Lambda_0 - (L\Lambda_0 + M)C_i^{\frac{1}{2}} - \Lambda)}$$

or

$$\Lambda + (L\Lambda_0 + M)(C\Lambda/\Lambda_e)^{\frac{1}{2}} = \Lambda_0 - \frac{1}{K}\left[\frac{\Lambda^2 C \cdot 10^{-2A(C\Lambda/\Lambda_e)^{\frac{1}{2}}}}{\Lambda_e}\right]. \quad (2)$$

$$[\Lambda + (L\Lambda_0 + M)(C\Lambda/\Lambda_e)^{\frac{1}{2}}] = y$$

is a linear function of

$$[\Lambda^2 C \cdot 10^{-2A(C\Lambda/\Lambda_e)^{\frac{1}{2}}}/\Lambda_e] = x,$$

the slope of the line being $-1/K$ and the intercept Λ_0. The solution of (1) and (2) for Λ_0 and K is effected by a series of approximations from an initial approximate value of Λ_0.[6] The reader is referred to the papers cited for details of solution.

Two points (Λ_1, C_1 and Λ_2, C_2) furnish two equations of the form of (1) and two of the form of (2); from these values of the four unknowns Λ_{e1}, Λ_{e2}, Λ_0, K may be obtained. For n experimental points there are $n+2$ unknowns, $\Lambda_{e1}, \cdots \Lambda_{en}$, Λ_0, K and $2n$ equations, n of the form of (1), n of the form of (2). The n equations of the form of (2) may be written briefly as

$$y_1 = \Lambda_0 - \frac{1}{K}x_1,$$
$$\cdots\cdots$$
$$y_n = \Lambda_0 - \frac{1}{K}x_n.$$

For n points of equal weight the theory of least squares gives as the best value of K and of Λ_0

$$K = \frac{n\Sigma x^2 - (\Sigma x)^2}{\Sigma x \Sigma y - n\Sigma xy}, \quad (3)$$

$$\Lambda_0 = \frac{\Sigma x \Sigma xy - \Sigma x^2 \Sigma y}{(\Sigma x)^2 - n\Sigma x^2}. \quad (4)$$

Eqs. (3) and (4), together with the n equations of the form of (1), furnish $n+2$ equations. From these one may compute the effect upon K and Λ_0 of error in the experimental quantities, concentration and specific conductance.

The Partial Derivatives

Upon differentiating (1), there results for the kth point

$$d\Lambda_{ek} = 2\Lambda_{ek}\left[\frac{1 - L(C_k\Lambda_k/\Lambda_{ek})^{\frac{1}{2}}}{3\Lambda_{ek} - \Lambda_0}\right]d\Lambda_0 - \frac{\Lambda_{ek}(\Lambda_0 - \Lambda_{ek})}{3\Lambda_{ek} - \Lambda_0}\left[\frac{d\Lambda_k}{\Lambda_k} + \frac{dC_k}{C_k}\right]. \quad (5)$$

Upon differentiating

$$x_k = \frac{\Lambda_k^2 C_k \cdot 10^{-2A(C_k\Lambda_k/\Lambda_{ek})^{\frac{1}{2}}}}{\Lambda_{ek}} = \frac{\Lambda_k^2 C_k}{10^{2A((\Lambda_0 - \Lambda_{ek})/(L\Lambda_0 + M))}\Lambda_{ek}}$$

and introducing the expression above for $d\Lambda_{ek}$, there results

$$dx_k = u_k d\Lambda_k + v_k dC_k + w_k d\Lambda_0, \quad (6)$$

[6] It may be asked what is the effect upon the linearity of (2) when x and y are computed from an incorrect value of Λ_0. The effect is small, as the following figures show. Brockman and Kilpatrick (J. Am. Chem. Soc. **56**, 1483 (1934)), found Λ_0 for benzoic acid in water at 25° to be 382.10; the values of ordinate and abscissa in (2) computed therefrom are designated as y_0 and x_0, respectively. Letting the values computed from $\Lambda_0 = 1000$ be y' and x', it is found that the maximum deviation of $y' - 0.4$ from y_0, and of $2.563x' - 0.00019$ from x_0, is less than 0.2 percent. Since x' and y' are obtainable (within the accuracy stated) by linear transformation of x_0 and y_0, respectively, y' is an approximately linear function of x'.

where, letting

$$j=\frac{2.303(2A)}{L\Lambda_0+M},$$

$$u_k=\frac{x_k}{\Lambda_k}\left[2+\frac{\Lambda_0-\Lambda_{ek}}{3\Lambda_{ek}-\Lambda_0}(1-j\Lambda_{ek})\right]$$

$$v_k=\frac{x_k}{C_k}\left[1+\frac{\Lambda_0-\Lambda_{ek}}{3\Lambda_{ek}-\Lambda_0}(1-j\Lambda_{ek})\right]$$

$$w_k=x_k\left\{\frac{1}{3\Lambda_{ek}-\Lambda_0}\left(\frac{L\Lambda_{ek}+M}{L\Lambda_0+M}\right)[j(\Lambda_0-\Lambda_{ek})-2]\right\}$$

and similarly from

$$y_k=\Lambda_k+(L\Lambda_0+M)(C_k\Lambda_k/\Lambda_{ek})^{\frac{1}{3}}=\Lambda_k+\Lambda_0-\Lambda_{ek}$$

there results

$$dy_k=r_k d\Lambda_k+s_k dC_k+t_k d\Lambda_0, \tag{7}$$

where

$$r_k=1+\frac{1}{\Lambda_k}\left\{\Lambda_{ek}\left(\frac{\Lambda_0-\Lambda_{ek}}{3\Lambda_{ek}-\Lambda_0}\right)\right\}$$

$$s_k=\frac{1}{C_k}\left\{\Lambda_{ek}\left(\frac{\Lambda_0-\Lambda_{ek}}{3\Lambda_{ek}-\Lambda_0}\right)\right\}$$

$$t_k=1-\frac{2\Lambda_{ek}(L\Lambda_{ek}+M)}{(3\Lambda_{ek}-\Lambda_0)(L\Lambda_0+M)}.$$

From Eq. (3) it follows that

$$dK=\sum_{k=1}^{n}\left\{\frac{\partial K}{\partial x_k}dx_k+\frac{\partial K}{\partial y_k}dy_k\right\}, \tag{8}$$

where

$$\frac{\partial K}{\partial x_k}=\frac{1}{\Sigma x\Sigma y-n\Sigma xy}\{2[nx_k-\Sigma x]+K[ny_k-\Sigma y]\}$$

$$\frac{\partial K}{\partial y_k}=\frac{K[nx_k-\Sigma x]}{\Sigma x\Sigma y-n\Sigma xy}$$

and from (4) it follows that

$$d\Lambda_0=\sum_{k=1}^{n}\frac{\partial\Lambda_0}{\partial x_k}dx_k+\frac{\partial\Lambda_0}{\partial y_k}dy_k, \tag{9}$$

where

$$\frac{\partial\Lambda_0}{\partial x_k}=\frac{1}{(\Sigma x)^2-n\Sigma x^2}\{[\Sigma xy+y_k\Sigma x-2x_k\Sigma y]+2\Lambda_0[nx_k-\Sigma x]\}$$

$$\frac{\partial\Lambda_0}{\partial y_k}=\frac{x_k\Sigma x-\Sigma x^2}{(\Sigma x)^2-n\Sigma x^2}.$$

When the expressions for dx_k and dy_k from (6) and (7) are introduced into (9), there results

$$d\Lambda_0=\frac{1}{l}\left\{\sum_{k=1}^{n}m_k d\Lambda_k+n_k dC_k\right\}, \tag{10}$$

where

$$l=1-\left\{\sum_{k=1}^{n} w_k\frac{\partial\Lambda_0}{\partial x_k}+t_k\frac{\partial\Lambda_0}{\partial y_k}\right\};\quad m_k=\frac{\partial\Lambda_0}{\partial x_k}u_k+\frac{\partial\Lambda_0}{\partial y_k}r_k;\quad n_k=\frac{\partial\Lambda_0}{\partial x_k}v_k+\frac{\partial\Lambda_0}{\partial y_k}s_k.$$

We are now in a position to express dK in terms of the dC_k's, $d\Lambda_k$'s. Upon introducing into (8) the expressions for dx_k and dy_k given in (6) and (7), with $d\Lambda_0$ replaced by its value from (10), there results

$$dK=\sum_{k=1}^{n}\frac{\partial K}{\partial x_k}\left[u_k d\Lambda_k+v_k dC_k+\frac{w_k}{l}\left\{\sum_{j=1}^{n} m_j d\Lambda_j+n_j dC_j\right\}\right]$$

$$+\sum_{k=1}^{n}\frac{\partial K}{\partial y_k}\left[r_k d\Lambda_k+s_k dC_k+\frac{t_k}{l}\left\{\sum_{j=1}^{n} m_j d\Lambda_j+n_j dC_j\right\}\right]. \quad (11a)$$

Since the specific conductance $\tilde{\kappa}_k$ is the directly measured quantity, rather than the equivalent conductance Λ_k, $d\Lambda_k$ will be replaced by its value in terms of $d\tilde{\kappa}_k$ and dC_k.

(7)
$$\Lambda_k=\frac{1000\tilde{\kappa}_k}{C_k},\quad d\Lambda_k=\Lambda_k\left[\frac{d\tilde{\kappa}_k}{\tilde{\kappa}_k}-\frac{dC_k}{C_k}\right].$$

Eq. (11a) then becomes

$$dK=\sum_{k=1}^{n}\frac{\partial K}{\partial x_k}\left[u_k\Lambda_k\left(\frac{d\tilde{\kappa}_k}{\tilde{\kappa}_k}-\frac{dC_k}{C_k}\right)+v_k dC_k+\frac{w_k}{l}\left\{\sum_{j=1}^{n} m_j\Lambda_j\left(\frac{d\tilde{\kappa}_j}{\tilde{\kappa}_j}-\frac{dC_j}{C_j}\right)+n_j dC_j\right\}\right]$$

$$+\sum_{k=1}^{n}\frac{\partial K}{\partial y_k}\left[r_k\Lambda_k\left(\frac{d\tilde{\kappa}_k}{\tilde{\kappa}_k}-\frac{dC_k}{C_k}\right)+s_k dC_k+\frac{t_k}{l}\left\{\sum_{j=1}^{n}\cdots\right\}\right], \quad (11b)$$

from which it follows that

(8)
$$\frac{\partial K}{\partial\tilde{\kappa}_k}=\frac{1}{\tilde{\kappa}_k}\left[\Lambda_k\left\{u_k\frac{\partial K}{\partial x_k}+r_k\frac{\partial K}{\partial y_k}+\frac{m_k}{l}\sum_{j=1}^{n} w_j\frac{\partial K}{\partial x_j}+t_j\frac{\partial K}{\partial y_j}\right\}\right]=\frac{Q_k}{\tilde{\kappa}_k},$$

$$\frac{\partial K}{\partial C_k}=\frac{1}{C_k}\left[C_k\left\{v_k\frac{\partial K}{\partial x_k}+s_k\frac{\partial K}{\partial y_k}+\frac{n_k}{l}\sum_{j=1}^{n} w_j\frac{\partial K}{\partial x_j}+t_j\frac{\partial K}{\partial y_j}\right\}-Q_k\right]=\frac{1}{C_k}[P_k-Q_k]. \quad (12)$$

Upon introducing into (10) $d\Lambda_k$'s value in terms of $d\tilde{\kappa}_k$ and dC_k, there results

$$d\Lambda_0=\frac{1}{l}\left[\sum_{k=1}^{n} m_k\Lambda_k\frac{d\tilde{\kappa}_k}{\tilde{\kappa}_k}+\{n_k C_k-m_k\Lambda_k\}\frac{dC_k}{C_k}\right], \quad (13)$$

from which it follows that

(9)
$$\frac{\partial\Lambda_0}{\partial\tilde{\kappa}_k}=\frac{m_k\Lambda_k}{l}\frac{1}{\tilde{\kappa}_k},\quad \frac{\partial\Lambda_0}{\partial C_k}=\left[\frac{n_k C_k}{l}-\frac{m_k\Lambda_k}{l}\right]\frac{1}{C_k}. \quad (14)$$

Evaluation of Errors for a Weak Acid in Water

Before proceeding further it is necessary to discuss the range of applicability of the equations derived. It is known that when for a weak acid of the type of HX

(10)
$$\log\frac{\Lambda^2 C}{\Lambda_e(\Lambda_e-\Lambda)}=\log K_c$$

is plotted against $C_i^{\frac{1}{2}}=(C\Lambda/\Lambda_e)^{\frac{1}{2}}$, a linear relationship obtains up to a certain concentration, after which $\log K_c$ drops off. Thus for benzoic acid in water at 25°

$$\log_{10} K_c=\log_{10} K+1.011 C_i^{\frac{1}{2}}$$

for solutions of ion concentration less than $2.9\times10^{-4}N$.[6] Since the slope 1.011 is close to the theoretical value of $2A$ for this solvent and

temperature, the conclusion is drawn that in the case of benzoic acid in water, Eq. (2) is valid for solutions sufficiently dilute so that C_i does not exceed $2.9\times10^{-4}N$. When the data for the acids listed by Belcher[7] in Table IV of his paper are similarly examined, it is seen that for carbonic ($K=4.31\times10^{-7}$) the limiting ion concentration is not reached experimentally, i.e., $(C_i)_l>1.2\times10^{-4}$; for propionic ($K=1.343\times10^{-5}$), $(C_i)_l=3.7\times10^{-4}$; for *n*-butyric ($K=1.508\times10^{-5}$), 2.5×10^{-4}; for acetic ($K=1.753\times10^{-5}$), 2.0×10^{-4}; for benzoic ($K=6.312\times10^{-5}$), 2.9×10^{-4}; for *o*-chlorobenzoic ($K=1.197\times10^{-3}$), 1.5×10^{-3}; and for monochloroacetic ($K=1.396\times10^{-3}$), 2.7×10^{-3}. For weak acids in water the range $C_i=4\times10^{-5}$ to $C_i=2\times10^{-4}$ is selected for examination, that is to say, the assumption is made that over this range Eqs. (1) and (2) and the partial derivatives derived therefrom are valid. At these low concentrations of univalent ions it does not appear necessary to use Shedlovsky's extended equation for Λ_e in place of Eq. (1); according to Shedlovsky,[4] Onsager's equation is valid up to a concentration of 0.001 or $0.002N$ for uni-univalent electrolytes in water.

In Table I are given values of the partial derivatives for an acid for which in water at 25°C, $K=1\times10^{-4}$ and $\Lambda_0=400$. The constants L, M, and A have been taken as 0.2274, 59.79, and 0.5065, respectively. The concentrations have been chosen so as to give equal increments of x on the graph of Eq. (2), and the range of ion concentration is from 4×10^{-5} to $2\times10^{-4}N$. In all instances concentration is expressed in molarity, specific conductance in ohm^{-1} cm^{-1}. The partial derivatives listed are computed from formulas (12) and (14). Since the points lie on the line of Eq. (2),

$$\frac{\partial K}{\partial x_k}=\frac{1}{K}\frac{\partial K}{\partial y_k} \quad \text{and} \quad \frac{\partial \Lambda_0}{\partial x_k}=\frac{1}{K}\frac{\partial \Lambda_0}{\partial y_k}.$$

The probable error in K resulting from random errors in the experimental quantities is

$$\Delta K=\left(\sum_{k=1}^{11}\left(\frac{\partial K}{\partial \bar{\kappa}_k}\Delta\bar{\kappa}_k\right)^2+\left(\frac{\partial K}{\partial C_k}\Delta C_k\right)^2\right)^{\frac{1}{2}}.$$

If the relative errors in the $\bar{\kappa}$'s and C's are less than ϵ,

$$\frac{\Delta K}{K}<\frac{\epsilon}{K}\left(\sum_{k=1}^{11}\left(\bar{\kappa}_k\frac{\partial K}{\partial \bar{\kappa}_k}\right)^2+\left(C_k\frac{\partial K}{\partial C_k}\right)^2\right)^{\frac{1}{2}}<6.6\epsilon,$$

and similarly

$$\frac{\Delta\Lambda_0}{\Lambda_0}<2.1\epsilon.$$

Turning to the consideration of constant errors, we have for the case of a constant relative error in specific conductance

$$[\Delta K]_{\bar{\kappa}}=\sum_{k=1}^{11}\frac{\partial K}{\partial \bar{\kappa}_k}\Delta\bar{\kappa}_k=\frac{\Delta\bar{\kappa}}{\bar{\kappa}}\sum\bar{\kappa}_k\frac{\partial K}{\partial\bar{\kappa}_k}=-7\times10^{-7}\frac{\Delta\bar{\kappa}}{\bar{\kappa}},$$

$$\frac{[\Delta K]_{\bar{\kappa}}}{K}=-7\times10^{-3}\frac{\Delta\bar{\kappa}}{\bar{\kappa}},$$

i.e., an error of 1 percent in all specific conductances causes an error of -0.007 percent in K. Error in the cell constant is therefore of little consequence in the determination of K by the extrapolation method. This point has been stressed by Ives.[1] For the case of a constant relative error in concentration

$$[\Delta K]_C=\sum\frac{\partial K}{\partial C_k}\Delta C_k=\frac{\Delta C}{C}\sum C_k\frac{\partial K}{\partial C_k}=+0.990\times10^{-4}\frac{\Delta C}{C},$$

$$\frac{[\Delta K]_C}{K}=+0.99\frac{\Delta C}{C},$$

i.e., an error of 1 percent in all concentrations causes an error of practically 1 percent in K.

TABLE I. *Values of the partial derivatives. $K=1\times10^{-4}$; $\Lambda_0=400$; $n=11$; $C_i=4\times10^{-5}$ to 2×10^{-4}.*

$Ci\times10^4$	$C\times10^4$	$\bar{\kappa}\times10^3$	$\bar{\kappa}\frac{\partial K}{\partial\bar{\kappa}}\times10^4$	$C\frac{\partial K}{\partial C}\times10^4$	$\bar{\kappa}\frac{\partial\Lambda_0}{\partial\bar{\kappa}}\times10^{-2}$	$C\frac{\partial\Lambda_0}{\partial C}\times10^{-2}$
0.4000	0.5577	1.596	−2.423	+1.890	+3.426	−2.672
0.4860	0.7184	1.939	−1.985	+1.501	+2.874	−2.173
0.5720	0.8935	2.282	−1.568	+1.154	+2.348	−1.728
0.6720	1.115	2.680	−1.112	+0.797	+1.772	−1.270
0.7860	1.391	3.133	−0.628	+0.438	+1.160	−0.809
0.9130	1.728	3.639	−0.131	+0.092	+0.531	−0.372
1.064	2.169	4.240	+0.406	−0.269	−0.149	+0.099
1.239	2.735	4.935	+0.964	−0.625	−0.855	+0.554
1.442	3.464	5.742	+1.536	−0.973	−1.580	+1.001
1.693	4.474	6.739	+2.149	−1.330	−2.358	+1.459
2.000	5.870	7.957	+2.785	−1.685	−3.165	+1.915

[7] D. Belcher, reference 5. References to the original papers are given by Belcher.

TABLE II. *Relative errors in K, from measurements at two concentrations.*

K	$C_1\times10^4$	$C_2\times10^3$	$\frac{1}{K}\left[\bar{\kappa}_1\frac{\partial K}{\partial\bar{\kappa}_1}\right]$	$\frac{1}{K}\left[\bar{\kappa}_2\frac{\partial K}{\partial\bar{\kappa}_2}\right]$	$\frac{1}{K}\left[C_1\frac{\partial K}{\partial C_1}\right]$	$\frac{1}{K}\left[C_2\frac{\partial K}{\partial C_2}\right]$
$Ci_1=4\times10^{-5}$, $\bar{\kappa}_1=1.596\times10^{-5}$; $Ci_2=2\times10^{-4}$, $\bar{\kappa}_2=7.957\times10^{-5}$.						
1×10^{-3}	0.4158	0.2387	−9.729	+9.717	+9.365	−8.358
1×10^{-4}	0.5577	0.5870	−5.622	+5.615	+4.385	−3.397
5×10^{-5}	0.7153	0.9740	−7.245	+7.236	+5.034	−4.051
1×10^{-5}	1.977	4.070	−22.32	+22.30	+12.44	−11.49
1×10^{-6}	16.17	38.90	−168.5	+168.3	+85.48	−84.82
1×10^{-7}	158.1	387.2	−692.4	+691.6	+347.6	−347.8
$Ci_1=2\times10^{-4}$, $\bar{\kappa}_1=7.957\times10^{-5}$; $Ci_2=1\times10^{-3}$, $\bar{\kappa}_2=3.952\times10^{-4}$.						
1×10^{-2}	2.039	1.093	−16.86	+16.82	+16.51	−15.45
5×10^{-3}	2.077	1.186	−10.09	+10.06	+9.707	−8.691
1×10^{-3}	2.387	1.929	−5.357	+5.343	+4.608	−3.628

TABLE III. *Relative errors in Λ_0, from measurements at two concentrations.*

K	$C_1\times10^4$	$C_2\times10^3$	$\frac{1}{\Lambda_0}\left[\bar{\kappa}_1\frac{\partial\Lambda_0}{\partial\bar{\kappa}_1}\right]$	$\frac{1}{\Lambda_0}\left[\bar{\kappa}_2\frac{\partial\Lambda_0}{\partial\bar{\kappa}_2}\right]$	$\frac{1}{\Lambda_0}\left[C_1\frac{\partial\Lambda_0}{\partial C_1}\right]$	$\frac{1}{\Lambda_0}\left[C_2\frac{\partial\Lambda_0}{\partial C_2}\right]$
$Ci_1=4\times10^{-5}$, $\bar{\kappa}_1=1.596\times10^{-5}$; $Ci_2=2\times10^{-4}$, $\bar{\kappa}_2=7.957\times10^{-5}$.						
1×10^{-3}	0.4158	0.2387	+1.354	−0.354	−1.303	+0.305
1×10^{-4}	0.5577	0.5870	+2.238	−1.237	−1.745	+0.748
5×10^{-5}	0.7153	0.9740	+3.216	−2.214	−2.235	+1.239
1×10^{-5}	1.977	4.070	+10.92	−9.90	−6.085	+5.104
1×10^{-6}	16.17	38.90	+84.30	−83.20	−42.78	+41.94
1×10^{-7}	158.1	387.2	+347.3	−345.9	−174.3	+174.0
$Ci_1=2\times10^{-4}$, $\bar{\kappa}_1=7.957\times10^{-5}$; $Ci_2=1\times10^{-3}$, $\bar{\kappa}_2=3.952\times10^{-4}$.						
1×10^{-2}	2.039	1.093	+1.311	−0.312	−1.283	+0.287
5×10^{-3}	2.077	1.186	+1.359	−0.360	−1.307	+0.311
1×10^{-3}	2.387	1.929	+1.743	−0.744	−1.500	+0.505

Similarly,

$$[\Delta\Lambda_0]_{\bar{\kappa}}=+4.004\times10^2\frac{\Delta\bar{\kappa}}{\bar{\kappa}},$$

and

$$\frac{[\Delta\Lambda_0]_{\bar{\kappa}}}{\Lambda_0}=+1.00\frac{\Delta\bar{\kappa}}{\bar{\kappa}};$$

$$[\Delta\Lambda_0]_C=-3.996\times10^2\frac{\Delta C}{C},$$

and

$$\frac{[\Delta\Lambda_0]_C}{\Delta_0}=-1.00\frac{\Delta C}{C};$$

i.e., 1 percent errors in all $\bar{\kappa}$'s and in all C's cause errors of +1 percent and −1 percent, respectively, in Λ_0. For the case of a constant absolute error in specific conductance, such as would be caused by the presence of a small amount of neutral salt,

$$[\Delta K]_{\bar{\kappa}\text{ abs}}=\Delta\bar{\kappa}\sum\frac{\partial K}{\partial\bar{\kappa}_k}=-26.53\Delta\bar{\kappa},$$

$$\frac{[\Delta K]_{\bar{\kappa}\text{ abs}}}{K}=-2.65\times10^5\,\Delta\bar{\kappa};$$

for $\Delta\bar{\kappa}=4\times10^{-8}$ ohm^{-1} cm^{-1}, the error in K is −1.1 percent. The corresponding error in Λ_0 is

$$[\Delta\Lambda_0]_{\bar{\kappa}\text{ abs}}=\Delta\bar{\kappa}\sum\frac{\partial\Lambda_0}{\partial\bar{\kappa}_k}=+4.604\times10^7\,\Delta\bar{\kappa},$$

$$\frac{[\Delta\Lambda_0]_{\bar{\kappa}\text{ abs}}}{\Lambda_0}=+1.15\times10^5\,\Delta\bar{\kappa};$$

for $\Delta\bar{\kappa}=4\times10^{-8}$ ohm^{-1} cm^{-1}, the error in Λ_0 is +0.5 percent.

In contrast to neutral salt, a small amount of basic impurity causes a diminution in specific conductance and an increase in the calculated value of the dissociation constant. For example, if it is assumed that the water used as solvent contains $NaHCO_3$ and H_2CO_3, and has a specific conductance of 2×10^{-7} ohm^{-1} cm^{-1} and a hydrogen-ion concentration of $4\times10^{-7}N$, the $\Delta\bar{\kappa}$'s for the solutions listed in Table I range from -5.5×10^{-8} for the most dilute to -3.9×10^{-8} ohm^{-1} cm^{-1} for the most concentrated solution of acid. The resultant errors in K and Λ_0 are

$$\frac{\Delta K}{K}=\frac{1}{K}\sum\frac{\partial K}{\partial\bar{\kappa}_k}\Delta\bar{\kappa}_k=+1.55\text{ percent},$$

$$\frac{\Delta\Lambda_0}{\Lambda_0}=\frac{1}{\Lambda_0}\sum\frac{\partial\Lambda_0}{\partial\bar{\kappa}_k}\Delta\bar{\kappa}_k=-0.64\text{ percent}.$$

COMPARISON OF ERRORS FOR ACIDS OF DIFFERENT STRENGTHS

It can be shown that small constant errors in the experimental quantities have little effect upon the linearity of (2). That being the case, it appears justifiable to approximate the errors in K and Λ_0 by regarding K and Λ_0 as determined by two points, which correspond to the extremes of the range of ion concentration. For $n=2$ the computation is considerably shorter than in the previous instance where n was taken as 11. The values of the partial derivatives obtained from (12) and (14) for $n=2$ are listed in Tables II and III. The solvent is water, the temperature 25°, and Λ_0 is 400.

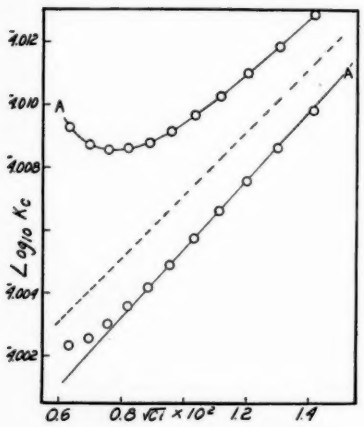

FIG. 1. Curve A, down 0.00200. Curve - - -, down 0.00300.

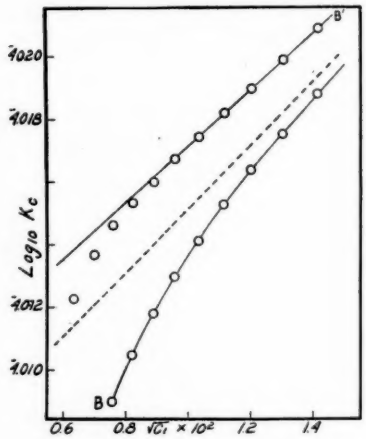

FIG. 2. Curve B, up 0.00500. Curve - - -, up 0.00500.

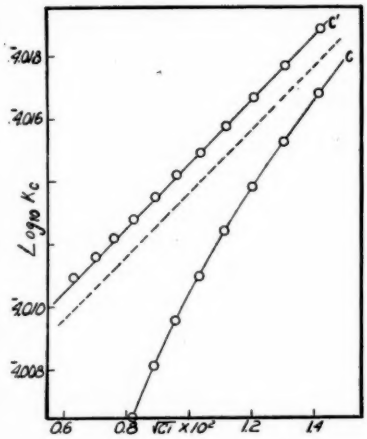

FIG. 3. Curve C, up 0.00900. Curve - - -, up 0.00350.

For $n=2$ the errors in K and Λ_0 due to a constant absolute error in specific conductance are, for an acid of dissociation constant 1×10^{-4},

$$\frac{[\Delta K]_{\bar{\kappa}\text{ abs}}}{K}=-2.82\times10^{5}\,\Delta\bar{\kappa},$$

and

$$\frac{[\Delta\Lambda_0]_{\bar{\kappa}\text{ abs}}}{\Lambda_0}=+1.26\times10^{5}\,\Delta\bar{\kappa},$$

as compared with $-2.65\times10^{5}\Delta\bar{\kappa}$ and $+1.15\times10^{5}\Delta\bar{\kappa}$, respectively, for $n=11$. The errors resulting from a constant relative error in specific conductance or in concentration are the same for $n=2$ as for $n=11$. The effects of constant errors in the experimental quantities are in general so little different for $n=2$ and $n=11$ that the approximation appears warranted.

It has already been mentioned that for *o*-chlorobenzoic and monochloroacetic acids, which in water have dissociation constants of the order of 1×10^{-3}, $\log K_c$ is a linear function of $C_i^{\frac{1}{2}}$ up to ion concentrations somewhat above $1\times10^{-3}N$. The lowest ion concentrations studied in these investigations were $5\times10^{-4}N$ for *o*-chlorobenzoic[8] and $1\times10^{-4}N$ for monochloroacetic acid.[9] It seemed worth while, therefore, to include in Tables II and III errors computed by use of the ion concentrations 2×10^{-4} and $1\times10^{-3}N$ in the case of the stronger acids.

[8] B. Saxton and H. F. Meier, J. Am. Chem. Soc. **56**, 1918 (1934).
[9] T. Shedlovsky, A. S. Brown, and D. A. MacInnes, Trans. Electrochem. Soc. **66**, 165 (1934).

The effect upon K of a constant relative error in specific conductance is seen to be minor. For acids of dissociation constant between 1×10^{-3} and 1×10^{-5} a 1 percent error in $\bar{\kappa}$ causes in K an error not exceeding 0.02 percent, and for the weakest acid listed ($K=1\times10^{-7}$) a 1 percent error in $\bar{\kappa}$ causes in K an error of 0.8 percent. The error in K caused by a constant error of 1 percent in concentration drops from 1 percent for the strongest to -0.2 percent for the weakest acid. The effect upon K of a constant absolute error in specific conductance increases markedly with diminution in K for acids weaker than 5×10^{-5}. As regards Λ_0, constant relative errors of 1 percent in $\bar{\kappa}$ and C cause errors of approximately 1 percent in Λ_0, except in the case of the weakest acid ($K=1\times10^{-7}$) where the effects are 1.4 percent and 0.3 percent, respectively. The error caused in Λ_0 by a constant absolute error in specific conductance increases with decrease in K.

The most striking conc usion to be drawn from Table II concerns the random errors. For acids of dissociation constant between 2 or 3×10^{-3} and 5×10^{-5}, the individual errors in K are of approximately the same magnitude for a given percentage error in $\bar{\kappa}$ or C. For acids in this range, therefore, the extrapolation method should yield about equally reliable values of the dissociation constant provided the experimental accuracy remains the same. The high values of the individual errors given in Table II for acids of dissociation constant 1×10^{-6} and 1×10^{-7} show that the determination of K by the extrapolation

method is not practicable in the case of acids which in water are very weak.

Detection of Constant Errors

As already mentioned, small constant errors in the experimental quantities have little effect upon the linearity of (2). They have a greater effect upon the linearity of the relationship between $\log K_e$ and $C_i^{\frac{1}{2}}$. In the accompanying figures $\log K_e$ is plotted against $C_i^{\frac{1}{2}}$ for an acid of dissociation constant 1×10^{-4}, for the cases where (Fig. 1, curves A and A') there is neutral salt present in the water, where (Fig. 2, curves B and B') the water contains basic impurity, and where (Fig. 3, curves C and C') the concentrations employed in the computation are 1 percent too high.

Data for the figures are taken from Table I; in A and A', 4.0×10^{-8} ohm^{-1} cm^{-1} is added to each specific conductance; in B and B', from each specific conductance is subtracted an amount varying from 5.5×10^{-8} ohm^{-1} cm^{-1} for the most dilute solution to 3.9×10^{-8} for the most concentrated, the impurity in the water used as solvent being regarded as $NaHCO_3$ and H_2CO_3 of such concentration as to give the water a specific conductance of 2×10^{-7} ohm^{-1} cm^{-1} and a hydrogen-ion concentration of $4\times10^{-7}N$; in C and C' the recorded concentrations are increased by 1 percent. The curves designated by the unprimed letters are constructed by use of $\Lambda_0=400$ and $\Lambda_e=400-(400L+M)(1000\bar{\kappa}/\Lambda_e)^{\frac{1}{2}}=400.00-150.75C_i^{\frac{1}{2}}$. Those designated by the primed letters are constructed by use of Λ_0 obtained by the extrapolation method, i.e., from the partial derivatives of Table I we have

for A', $\Delta\Lambda_0=+1.84$, $\Lambda_0=401.84$,
$\Lambda_e=401.84-151.17(1000\bar{\kappa}/\Lambda_e)^{\frac{1}{2}}$;
for B', $\Delta\Lambda_0=-2.56$, $\Lambda_0=397.44$,
$\Lambda_e=397.44-150.17(1000\bar{\kappa}/\Lambda_e)^{\frac{1}{2}}$;
for C', $\Delta\Lambda_0=-4.00$, $\Lambda_0=396.00$,
$\Lambda_e=396.00-149.84(1000\bar{\kappa}/\Lambda_e)^{\frac{1}{2}}$.

These cases are selected because they cause in K as given by the extrapolation method errors of approximately the same magnitude; from the partial derivatives of Table I we have

for A', $\Delta K=-1.06\times10^{-6}$;
for B', $\Delta K=+1.55\times10^{-6}$;
for C', $\Delta K=+0.99\times10^{-6}$.

The broken lines in the figures are drawn with intercept $\bar{4}.0000$ and slope 1.013, i.e., they represent the case of no errors. Continuous curves have not been drawn through the points of A', B', C' since they would obscure the lines drawn to show departure from linearity. It was not considered worth while to include a figure for the case of a constant relative error in specific conductance, since an error of 1 percent in all $\bar{\kappa}$'s causes in K as given by the extrapolation method an error of less than 0.01 percent for an acid of this strength.

The curves A, B, C show large deviation from linearity, and if lines are drawn through the points of higher ion concentration, their slopes differ from the theoretical. Deviation from linearity is less pronounced for the curves designated by the primed letters. A' and B' nevertheless show definite departure from linearity, A' being concave upward toward lower ion concentrations and concave downward toward higher, and B' being concave downward. The curve C' shows only slight departure from linearity; it is slightly concave upward. The slope of the line drawn through the points of higher ion concentration is greater than the theoretical for the curve A', and less than the theoretical for the curve B'. From curves A' and B' it appears that, if consistent data for the acid are at hand, it should be possible to detect the presence of neutral salt or basic impurity in the water, even though the plot of Eq. (2) exhibits a linear relationship. The detection of a constant relative error in concentration appears more difficult; the detection of a constant relative error in specific conductance is comparatively unimportant when the extrapolation method is employed to determine the dissociation constant of a weak acid in water.

Acknowledgment

The writer would like to express her appreciation of stimulating discussions with Professor J. A. Shohat and with Mr. E. A. Fackenthal.

A Note on the Efficiency of the Thermal Diffusion Process for Separating Isotopes

J. W. WESTHAVER* AND A. KEITH BREWER
Bureau of Agricultural Chemistry and Engineering, U. S. Department of Agriculture, Washington, D. C.
(Received February 1, 1940)

The mechanism proposed by Gillespie for the thermal separation of gases is correlated with the attendant conduction of heat; this is done by describing gaseous heat conduction as a heat exchange between two oppositely bombarding Maxwellian groups which differ in temperature at each isothermal surface by a finite ΔT. The resulting formulas enable a computation of ΔT the bombardment "equipartition distance" and the transport yield. An ideal system of cells each having temperature limits of 300°K and 500°K is found to require a minimum of 880 kw hours of conducted heat per gram $C^{13}H_4$ extracted to a concentration of 20 percent.

THE transport of the components of a gaseous mixture by action of a temperature gradient is receiving special attention as a method for segregating isotopes. Until the recent paper by Gillespie[1] no adequate attempt had been made to explain this action on the basis of elementary considerations.[2] The success of Gillespie's theory, particularly its agreement with observed equilibria separations, appears sufficient to warrant an application of its underlying mechanism to a study of other factors of the transport process.

The mechanism assumes that the difference dT in the average temperatures of contiguous thin gas layers normal to the temperature gradient can be regarded as the difference in the effective temperatures of the molecules which bombard the opposite sides of the plane separating the two layers. If these layers are of finite thickness the bombardment on the two sides of the plane results in a net flow of molecules in the direction of increasing temperature. To preserve the condition of uniform pressure this net flow of molecules must be exactly compensated in number by an opposite superimposed mass return flow. This action occurs in any stagnant gas when subjected to a temperature gradient. In the case of homogeneous mixtures of gases of unequal molecular weight, the numbers of molecules of a particular component flowing in the two directions are not equal; for this reason a transport occurs.

The following discussion relates particularly to the case of a vertical temperature gradient through a cell of gas in which the top wall is heated and the bottom wall is cooled; the confined gas is necessarily stagnant. The molecules in each element of volume can be classified into two groups one having components of velocity toward and the other away from the heated wall. In virtue of the fact that heat is conducted across the plane there must exist a finite difference in the heat energies carried by the two groups. Assuming that each group is composed of the same kind of molecules it follows that the groups differ in temperature at the plane by a finite amount, designated as ΔT.

It can be shown that the heat transport due to the net bombardment and corresponding mass return as above defined is proportional to the square of ΔT and hence can be neglected. In consequence, ΔT is found by dividing the rate of heat conduction $k dT/dx$ across the plane by $\Sigma c_i p_i (M_i/2\pi RT)^{\frac{1}{2}}$ where c_i is the specific heat at constant pressure and $p_i(M_i/2\pi RT)^{\frac{1}{2}}$ is Langmuir's[3] formula for molecular bombardment of a surface, expressed in g cm^{-2} sec.$^{-1}$ when p_i is the partial pressure in dynes cm^{-2}, M_i the molecular weight when $O=16$, and $R=8.315\times10^7$ ergs per mole$-$°K. The summation is over-all components of the mixture. As an example of its magnitude, ΔT is found to have the value 7.1×10^{-3} °K in methane at 40 cm Hg where $T=400$°K, $c=0.60$ cal. g^{-1} deg.$^{-1}$, $k=1.0\times10^{-4}$ cal. cm^{-1} sec.$^{-1}$ deg.$^{-1}$ and $dT/dx=200$°K cm^{-1}.

If dx is the finite thickness of the thin layers defined above, then dT is related to ΔT by

$$\Delta T=\frac{k dT/dx}{\Sigma c_i p_i (M_i/2\pi RT)^{\frac{1}{2}}}. \qquad (1)$$

* Now at the U. S. Patent Office.
[1] Gillespie, J. Chem. Phys. **7**, 530 (1939).
[2] Furry, Jones and Onsager, Phys. Rev. **55**, 1083 (1939).
[3] Langmuir, Phys. Rev. **2**, 329 (1914).

Also if dx is the mean distance along the gradient over which the two bombarding groups can move before they partition their energy, the medial planes of the contiguous layers may be regarded as the emission sources for the groups, and, since these sources have the average temperature of their respective layers, ΔT becomes identical with dT. The equipartition distance dx is then given by the expression

$$dx=\frac{k}{\Sigma c_i p_i (M_i/2\pi RT)^{\frac{1}{2}}}. \qquad (2)$$

When the same constants are used as in the previous example, dx has the value 3.6×10^{-5} cm. This is about $\frac{3}{2}$ the mean free path for collision in methane under the conditions stated; dx and dT are therefore finite quantities of reasonable value.

After an expression for ΔT has been obtained, Langmuir's formula can be used to find the net bombardment for any component q whose respective group temperatures at the plane are $T+\Delta T/2$ and $T-\Delta T/2$. By subtracting from the mole net bombardment of q the mole mass return of q the initial rate of transport of component q across the plane of temperature T is found. This computation gives for the initial transport of light component 1 toward the hot wall in g cm^{-2} sec.$^{-1}$

$$R_0=\frac{dQ}{dt}\frac{p_1}{2T\Sigma c_i p_i M_i^{\frac{1}{2}}}\left\{M_1^{\frac{1}{2}}-\frac{M_1\Sigma p^i/M_i^{\frac{1}{2}}}{\Sigma p_i}\right\}, \qquad (3)$$

where $dQ/dt=kdT/dx$ is the heat passing between the boundaries in cal. cm^{-2} sec.$^{-1}$ as conventionally computed. For a two-component system

$$R_0=\frac{dQ}{dt}\frac{p_1p_2M_1^{\frac{1}{2}}(M_2^{\frac{1}{2}}-M_1^{\frac{1}{2}})}{2T(p_1+p_2)M_2^{\frac{1}{2}}(c_1p_1M_1^{\frac{1}{2}}+c_2p_2M_2^{\frac{1}{2}})}, \qquad (4)$$

which is dependent on relative but not total pressures. When the molecular weights and specific heats are nearly the same, R_0 becomes a maximum when $p_1\doteq p_2$.

Since the rate of transport across the midsection decreases with time in the manner $R_t=R_0e^{-at}$, the corresponding change in partial pressure across the cell for either component is $\Delta p=\Delta p_e(1-e^{-at})$ where Δp_e is the equilibrium change. Maximum rate of separation occurs when $R_t\Delta p$ is maximum. This is at the time when $e^{-at}=\frac{1}{2}$; the maximum yield is therefore $R_0/2dQ/dt^{-1}$ and the small change in partial pressure is $\Delta p_e/2$.

The separation factor is conveniently defined as the ratio of the ratios of partial pressures at the hot and cold walls; for maximum rate of separation it may be written

$$S_{\frac{1}{2}}=1+\frac{\Delta p_e(p_1+p_2)}{2p_1p_2}, \qquad (5)$$

where Δp_e can be computed from Eq. (7) given by Gillespie. Since Δp_e is small, his equation can be rewritten

$$\Delta p_e=\frac{p_1p_2(M_2^{\frac{1}{2}}-M_1^{\frac{1}{2}})}{2(p_1M_1^{\frac{1}{2}}+p_2M_2^{\frac{1}{2}})}\ln T_2/T_1. \qquad (6)$$

For such isotopes as heavy carbon and nitrogen, p_2 will be small and M_1 nearly equal to M_2, so that the denominator of (6) is nearly $2(p_1+p_2)M_1^{\frac{1}{2}}$ and (5) becomes

$$S_{\frac{1}{2}}=1+\frac{M_2^{\frac{1}{2}}-M_1^{\frac{1}{2}}}{4M_1^{\frac{1}{2}}}\ln T_2/T_1. \qquad (7)$$

By assuming a mixture $0.01C^{13}H_4+0.99C^{12}H_4$ at 400°K average temperature, where $c_1=c_2=0.60$, the maximum yield $\frac{1}{2}R_0(dQ/dt)^{-1}$ is found from Eq. (4) to be 3.1×10^{-7} gram $C^{12}H_4$ toward the hot wall or 3.3×10^{-7} gram $C^{13}H_4$ toward the cold wall per calorie conducted heat. The corresponding energy requirement is 3.5 kw hours per gram $C^{13}H_4$ transported across the cell. For wall temperatures of 300°K and 500°K the cell separation factor $S_{\frac{1}{2}}$ from Eq. (7) is 1.0040. This half-equilibrium condition is reached in a time which varies as the square of the wall separation. In the present case $t_{\frac{1}{2}}$ is about 0.15 second at 40 cm Hg and wall spacing of 1.0 cm.

As an example of accumulative yield, assume that N cells of equal height, heated at the top and cooled at the bottom to the same temperatures, are connected in series so that the hot gas layer of one cell and the cold gas layer of the following cell undergo a continuous interchange of gas and thereby acquire the same composition. If the hot gas layer of the first cell mixes with a constant source of $0.01C^{13}H_4+0.99C^{12}H_4$, a

heavy mixture may be continuously bled from the cold layer of the final cell. Since Eq. (4) shows that the rate of transport for unit of transverse area varies as p_1p_2, the transverse area of the rth cell must be a fraction $p_1p_2/(p_1p_2)_r$ of the first cell area; this is necessary to insure a total rate which does not vary along the series of cells. If 20 percent $C^{13}H_4$ is desired an over-all separation factor of 25 is required. For this case $(1.0040)^N=25$ and 810 cells are required.

The total heat conducted across the gas is $\int_0^N p_1p_2(p_1p_2)_r^{-1}dr$ times that of the first cell. The integration is made by noting that

$$p_1p_2(p_1p_2)_r^{-1}=(p_2+p_1S_1^{-r})(p_1+p_2S_1^{r})$$

where $(p_1+p_2)_r=1$, the cell separation factor S_1 being the same for all cells. The result is $[2rp_1p_2-(p_1^2S_1^{-r}-p_2^2S_1^{r})(\ln S_1)^{-1}]_0^N$ which equals 250 for the present example. The maximum yield of the system is therefore 1/250 of the first cell, namely $3.3\times10^{-7}/250=1.3\times10^{-9}$ gram $C^{13}H_4$ per calorie for 20 percent concentration. The corresponding energy requirement is 880 kw hr. per gram $C^{13}H_4$. This neglects all heat transfer other than by conduction through the gas.

These calculations have been carried through primarily to show the applicability of the mechanism suggested by Gillespie for the thermal separation of gases. However, the theoretical yield obtained suggests the feasibility of a system in which the operating principle is that of a series of cells.

The writers wish to thank Dr. Arthur Bramley for his interest and constructive criticisms.

APRIL, 1940 JOURNAL OF CHEMICAL PHYSICS VOLUME 8

The Specific Heat of Tantalum at Low Temperatures and the Effect of Small Amounts of Dissolved Hydrogen*

K. K. KELLEY†
Metallurgical Fundamentals Section, Metallurgical Division, Bureau of Mines, United States Department of the Interior, Berkeley, California

(Received January 8, 1940)

Specific heat determinations of pure tantalum were made in the temperature range 53° to 298°K and the entropy was found to be $S_{298.1}=9.9\pm0.1$. Tantalum containing hydrogen in amounts ranging from Ta+0.0284 H to Ta+0.0958 H was shown to behave anomalously, the specific heat having a high maximum in the region 220° to 265°K depending on the composition. The height of the maximum and the difference in measureable heat content between hydrogenated and normal tantalum were shown to be approximately proportional to the amount of dissolved hydrogen. The temperature of the maximum increases as the hydrogen is increased. After dehydrogenation, the same specific heat was obtained as for the original unhydrogenated material. The density of the dehydrogenated product also was normal, whereas the hydrogenated materials had lower densities. It is postulated that differences in entropy between hydrogenated and pure tantalum may be attributed to differences in the number of possible ways of arranging the hydrogen particles among the positions in the tantalum lattice available at the higher and lower temperatures.

IN pursuance of one of the programs of study of the Pacific Experiment Station of the United States Bureau of Mines, low-temperature specific-heat measurements of a sample of electrolytic tantalum were made. This material, labeled "sample F" below, was found to have an unexpected, marked "hump" in its specific-heat curve centered near 275°K. The sample was known to contain about 6.4 atomic percent of hydrogen, and moreover it is probable that it did not consist of a single crystalline species. The desirability of obtaining a more adequate entropy figure for tantalum and the interest attached to the "hump" itself were the incentives for studying the effects of relatively small amounts of hydrogen on the low-temperature specific heats

* Published by permission of the Director, Bureau of Mines, U. S. Department of the Interior. (Not subject to copyright.)

† Chemist, Metallurgical Division, Bureau of Mines, U. S. Department of the Interior.

of tantalum with which this paper is concerned. Six samples were investigated, the electrolytic material already mentioned, three containing different amounts of hydrogen, one of wrought tantalum wire containing virtually no hydrogen, and one made by pumping the hydrogen from material previously hydrogenated to 8.74 atomic percent.

The scope of this investigation has been restricted intentionally to the range 0 to 12 atomic percent hydrogen, as Hagg[1] has shown by x-ray studies that it is near the latter composition that the structure begins to change from a body-centered cubic lattice to hexagonal close packing, the change being complete near 33 atomic percent. Hagg has stated that in the range below 12 atomic percent hydrogen the introduction of hydrogen merely causes an increase in the lattice parameter without change of structure. This swelling also has been noted by Pietsch and Lehl[2] and Chaudron, Portevin, and Moreau.[3]

Materials

The tantalum was loaned for this work by the Fansteel Metallurgical Corporation through the courtesy of Mr. J. H. Harper and Mr. F. L. Hunter.

Sample *A* consisted of pure wrought tantalum in the form of 0.006″ diameter wire. The wire was sheared into lengths averaging about 0.5 cm, washed consecutively with HCl solution, NaOH solution, distilled water, and alcohol, and then dried near 100°C.

Sample *B* was made from sample *A* by heating to 710°C in vacuum (10^{-5} mm Hg at room temperature to 2×10^{-4} mm Hg at 710°C) and then admitting hydrogen to give the atomic ratio 0.0676 : 1. The hydrogen was purified by passing through activated charcoal immersed in liquid nitrogen and was measured by filling a calibrated flask sealed to the system through a stopcock. About half the hydrogen was absorbed in a few seconds at 710°, and the remainder was taken up as the tantalum was cooled slowly to 300°.

Table I. *Density measurements.*

Sample	Density ($d_4^{25°}$)
A, no H	16.557
E, 0.0284 H	16.552
B, 0.0676 H	16.436
C, 0.0958 H	16.330
D, H pumped off *C*	16.614

[1] Hagg, Zeits. f. physik. Chemie **B11**, 433 (1931).
[2] Pietsch and Lehl, Kolloid Zeits. **68**, 226 (1934).
[3] Chaudron, Portevin, and Moreau, Comptes rendus **207**, 235 (1938).

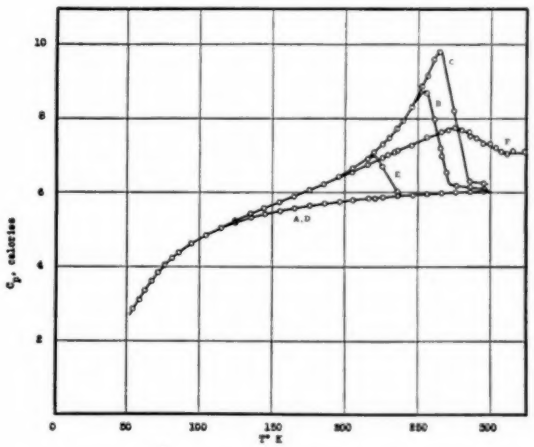

Fig. 1. Specific heats: *A*, *D*—pure Ta; *E*—Ta+0.0284 H; *B*—Ta+0.0676 H; *C*—Ta+0.0958 H.

Sample *C* was made from sample *B* by evacuating to 10^{-5} mm Hg at room temperature, heating to 700°C, and admitting additional hydrogen to raise the atomic ratio to 0.0958 : 1.

Sample *D* was prepared by pumping the hydrogen from sample *C* at 720°C. The pumping was continued until the pressure had fallen to and remained static at 2×10^{-4} mm Hg at 720° and, of course, during the cooling to room temperature.

Sample *E* was made by rehydrogenating sample *D* at 700°C to the atomic ratio 0.0284 : 1.

Sample *F* was the electrolytic powder mentioned in the introduction. According to the makers, this material contained 99.85 percent Ta, 0.11 percent C, 0.005 percent Fe, 0.02 percent residual impurities including oxide, and about 75 cc hydrogen, measured at atmospheric pressure and room temperature, per cc of metal. The last figure corresponds to 0.037 weight percent or 6.4 atomic percent hydrogen.

Density Measurements

The densities of all samples except the electrolytic powder were determined with a pyc-

TABLE II. *Specific heats.*

SAMPLE T °K	A C_p	D C_p	E C_p	B C_p	C C_p	F C_p
53	2.81					2.71
55	2.95					2.84
60	3.26					3.14
65	3.54					3.44
70	3.80					3.72
75	4.03					3.96
80	4.22	4.21	4.19	4.16	4.13	4.16
85	4.40	4.38	4.37	4.34	4.32	4.33
90	4.55	4.53	4.53	4.49	4.48	4.48
95	4.68	4.66	4.66	4.63	4.62	4.62
100	4.78	4.77	4.77	4.76	4.74	4.75
105	4.87	4.86	4.88	4.88	4.86	4.87
110	4.97	4.96	4.98	4.98	4.97	4.98
115	5.06	5.05	5.08	5.08	5.07	5.08
120	5.14	5.13	5.17	5.17	5.17	5.18
125	5.21	5.20	5.27	5.26	5.26	5.27
130	5.27	5.27	5.36	5.35	5.36	5.36
135	5.33	5.33	5.44	5.44	5.44	5.44
140	5.39	5.38	5.53	5.52	5.52	5.52
145	5.44	5.42	5.61	5.59	5.60	5.59
150	5.48	5.46	5.69	5.66	5.68	5.66
155	5.52	5.50	5.76	5.74	5.76	5.74
160	5.55	5.53	5.84	5.81	5.84	5.82
165	5.58	5.57	5.91	5.89	5.92	5.90
170	5.62	5.61	5.99	5.97	6.00	5.98
175	5.65	5.65	6.07	6.05	6.08	6.06
180	5.68	5.67	6.15	6.14	6.16	6.13
185	5.70	5.70	6.24	6.23	6.25	6.21
190	5.73	5.72	6.33	6.32	6.35	6.30
195	5.76	5.74	6.43	6.42	6.46	6.39
200	5.78	5.76	6.54	6.52	6.57	6.48
205	5.80	5.78	6.65	6.64	6.70	6.57
210	5.82	5.80	6.78	6.76	6.84	6.67
215	5.84	5.82	6.91	6.91	6.99	6.76
220	5.86	5.84	7.04	7.08	7.16	6.86
225	5.88	5.86	6.74	7.27	7.36	6.96
230	5.89	5.88	6.35	7.48	7.58	7.04
235	5.91	5.90	6.03	7.73	7.81	7.13
240	5.92	5.91	5.97	8.00	8.08	7.22
245	5.94	5.92	5.98	8.29	8.38	7.30
250	5.95	5.94	5.98	8.58	8.72	7.39
255	5.96	5.95	5.99	8.76	9.10	7.48
260	5.98	5.96	5.99	8.01	9.53	7.56
265	5.99	5.97	6.00	7.23	9.80	7.64
270	6.01	5.98	6.00	6.48	8.98	7.72
275	6.02	6.00	6.01	6.21	8.07	7.78
280	6.03	6.02	6.02	6.17	7.16	7.70
285	6.03	6.03	6.02	6.14	6.33	7.59
290	6.04	6.04	6.04	6.12	6.28	7.48
295	6.04	6.05	6.06	6.10	6.25	7.37
300						7.26
310						7.12
320						7.10

nometer, using distilled water as the fluid. Corrections were made for buoyancy and the temperature coefficient of the volume of the pycnometer flask. The measurements were made at 25±1°C. The results are contained in Table I.

These measurements show that as hydrogen is introduced in these rather low concentrations the tantalum swells, the rate of swelling increasing with the hydrogen content. If Hagg's[1] lattice parameter for tantalum containing 12 atomic percent hydrogen (hydrogen-tantalum ratio, 0.136 : 1), the composition at which the structure begins to change, is correct, then the density of such material is 15.82 and the swelling must become much more pronounced as this composition is approached.

Sample *D*, which was made by pumping the hydrogen from sample *C*, has about the density given by the best direct measurements in the literature[4] (ranging from 16.55 to 16.64) and by Hagg's[1] lattice parameter, 16.64. Sample *A*, which also contains virtually no hydrogen, has a lower density which may be attributed to the effects of cold working.[5] These effects apparently are entirely removed by hydrogenation followed by dehydrogenation at 700°C. Consequently, the density of sample *D* is more significant than that of sample *A* for comparison with the other results in Table I.

SPECIFIC-HEAT MEASUREMENTS

The apparatus and methods are very similar to those described in such detail elsewhere[6] that repetition is unnecessary here. The temperature scale employed is that of the laboratory of Professor Giauque.[7] The over-all error in the measurements is considered to be 0.5 percent or less.

The results, expressed in defined calories (1 calorie = 4.1833 int. joules) are given in Table II and shown graphically in Fig. 1. The figures in Table II were read from smooth curves while the plotted values are actual measured results. This procedure was followed to save space. All results are for 180.88 grams of tantalum plus contained hydrogen when present.

A number of items of interest are immediately evident on examination of Fig. 1. First, sample *A*, which is the original unhydrogenated material,

[4] Landolt-Börnstein, *Physikalisch-chemische Tabellen* (Julius Springer, Berlin, 1923), Vol. 1, p. 290; *ibid.* second suppl. (1931), Vol. 1, p. 212; *ibid.* third suppl. (1935), Vol. 1, p. 285.

[5] For example, see Maier, Trans. Am. Inst. Min. Met. Eng., Inst. of Metals Div. **122**, 121 (1936).

[6] a. Gibson and Giauque, J. Am. Chem. Soc. **45**, 93 (1923); b. Giauque and Wiebe, *ibid.* **50**, 101 (1928); c. Millar, *ibid.* **50**, 1875 (1928); d. Anderson, *ibid.* **52**, 2296 (1930).

[7] a. Giauque, Buffington, and Schulze, J. Am. Chem. Soc. **49**, 2343 (1927); b. Giauque, Johnston, and Kelley, *ibid.* **49**, 2367 (1927).

and sample *D*, which was prepared by pumping the hydrogen from sample *C* at 720°C, show the same specific heat within limits too small to be evident in Fig. 1 (average deviation observed <0.3 percent). From curves *B*, *C*, and *E* it is seen that the specific-heat maxima are of a higher order of magnitude than the quantity of hydrogen present. The ratio of the height of the maximum above the normal curve to the gram atoms of hydrogen present ranges from 39.7 to 41.3 and averages 40.7 for the three cases. Consequently, the virtual coincidence of the specific heats of *A* and *D* may be taken as evidence that the hydrogen was nearly completely removed in preparing sample *D*, as something of the order of 10^{-3} gram-atom of hydrogen per gram-atom of Ta should have resulted in a detectable effect. This removal of hydrogen is also indicated by the density measurements; and, in addition, it may be stated that rough pressure observations made with both increasing and decreasing temperatures in the range 400° to 700°C on samples *B* and *C* indicate that the hydrogenation process is approximately reversible.

Curves *B*, *C*, and *E* also show that both the temperature and the height of the maximum are increased by increasing the hydrogen content. Moreover, except for second-order differences, too small to be shown in Fig. 1, these three curves coincide below the maximum in *E*, and *B* and *C* coincide below the maximum in *B*. This indicates that the same quantity of change, whatever it may be, has taken place when a given temperature is reached independently of the amount of hydrogen present provided the temperature is below that of the lowest specific heat maximum. If the effect produced is attributed solely to the hydrogen, then the quantity changed from the low temperature to the high-temperature condition is independent of the total amount present, or of the amount unchanged, until the maximum in the specific-heat curve is reached.

At the lowest temperatures studied all the samples are shown in Fig. 1 to have the same specific heat. Actually this is not the case and small, but regular differences are evident on examination of Table II, showing that increasing hydrogen content is accompanied by slightly decreasing specific heats at temperatures below 100°K.

Curve *F*, for the electrolytic powder, cannot be considered a member of this group, although it very nearly coincides with the others at intermediate temperatures. It is believed that this sample did not consist of a single crystalline species, which is not at all unusual for electrolytic deposits of metals, and that there is present the resultant of the effects of hydrogen on the two (or more) crystalline species, which broadens the maximum and lowers its height. It was not considered advisable to attempt to stabilize this sample or to remove the hydrogen therefrom, as it was a special material of considerable value and its owners stated that removal of hydrogen would result in a material very active toward oxidation by air or moisture.

It was found possible to supercool the hydrogenated samples in the regions of the maxima. On rapidly cooling sample *B* from room temperature to 230°K the following results were obtained: 6.42 at 231.5°, 6.70 at 236.5°, and 7.01 at 241.3°. Similar results were obtained with sample *F*; namely, 6.34 at 222.7°, 6.78 at 232.3°, 7.17 at 242.3°, 7.39 at 252.5°, 7.60 at 262.6°, 7.70 at 270.5°, 7.75 at 274.6°, 7.67 at 282.0°, and 7.48 at 289.6°. Also the value 6.86 at 298.3° was obtained with sample *F* after rapidly cooling from 320°K to room temperature. However, the temperature extent of supercooling was limited, and it was found that quite reproducible results always were obtained after cooling to liquid nitrogen temperatures. In the case of sample *B*, two sets of determinations that agreed within 0.1 percent were made in the range 80°–90°K after cooling to 78° under virtually identical conditions. For this same sample duplicate determinations also were obtained in the range 215 to 273° after warming from 85°K to 215°K at rates differing by at least a factor of 3. These agreed within 0.3 percent. For sample *F*, duplicate determinations were made throughout the range 78° to 290°K after cooling from room temperature to 78°K under very different conditions. The first cooling was made in 2.5 hours, using helium for conduction, while the second was made in vacuum (*ca.* $10^{-3}-10^{-2}$ mm Hg), the process taking 50 hours. Agreement within 0.2 percent was obtained

except near the maximum, 265° to 275°K, where the greatest deviation was 0.7 percent.

The time required to reach equilibrium after energy input in the calorimeter for samples *B*, *C*, and *E* was 6 min. at the lower temperatures but increased to 15 min. at the temperatures of the maxima. Just above the temperature of the maximum this time interval decreased rapidly in each instance, returning to 6 min. In the case of sample *F*, the sluggishness of energy distribution was more marked in the neighborhood of the maximum and did not decrease above this region. In fact, for sample *F*, the uncertainty in obtaining equilibrium above 280°K was so great that the inaccuracies in the specific-heat measurements were several times as large as those normally present, as is apparent on examination of Fig. 1. It is to be emphasized, however, that this last remark does not apply to any of the other samples.

There is but little earlier work with which to compare the present measurements on pure tantalum. Good agreement is obtained with the value 6.024 calories per degree at 0°C that Jaeger and Veenstra[8] have reported as the extrapolation of their measurements in the range 300 to 1600°C. Simon and Ruhemann[9] have made six determinations in the range 71° to 79°K, employing a special apparatus that involved dropping samples from temperatures obtained with boiling oxygen and nitrogen to those obtained by boiling these liquids under reduced pressures. Their results are nearly 8 percent lower than those reported here. The reason for this difference is not apparent, as measurements made in this laboratory on chromium agree with the work of these investigators while measurements on antimony differ, as in the present instance.

TABLE III. *Entropy of pure* Ta.

$S_{53.1}$ (extrapolation)	$=1.40$
$S_{298.1}-S_{53.1}$ (graphical)	$=8.54$
$S_{298.1}$	$=9.9\pm0.1$

[8] Jaeger and Veenstra, Proc. Acad. Sci. Amsterdam **37**, 61 (1934).

[9] Simon and Ruhemann, Zeits. f. physik. Chemie **129**, 334 (1927).

TABLE IV. *Entropy calculations for hydrogenated* Ta.

MATERIAL	$S_{298.1}-S_0$ (DEBYE)	$S_{298.1}-S_0$	$\delta S_{298.1}$	CASE 1	CASE 2
Ta+0.0284 H	10.17	10.18	0.24	0.26	0.27
Ta+0.0676 H	10.43	10.45	0.50	0.49	0.52
Ta+0.0958 H	10.62	10.65	0.69	0.63	0.67

ENTROPY CALCULATIONS

The entropy of tantalum was calculated from the results for samples *A* and *D* in the usual manner. Extrapolation below 53°K was made by means of the Debye function with $\theta=224$, which adequately represents the measurements in the lower temperature range. The results are shown in Table III. The error has been taken as ±0.1 to allow safely for a possibly large error in the extrapolated portion. The value of $S_{298.1}$ is 0.5 unit higher than that previously in use.[10]

It cannot be stated that the entropies of the hydrogenated materials are zero at 0°K. However, calculations of $S_{298.1}-S_0$ may be made in the same manner, account being taken, of course, of the small decrease in specific heat at the lower temperatures accompanying hydrogenation. In Table IV, values are given in columns 2 and 3 based on two methods of extrapolation, the first involving Debye functions and the second the procedure of Kelley, Parks, and Huffman.[11] The two methods yield substantially the same results, and those of the first method are adopted. The differences between $S_{298.1}-S_0$ for the hydrogenated samples and $S_{298.1}$ for the pure metal are given in column 4 and designated $\delta S_{298.1}$.

DIFFERENCES IN MEASURED HEAT CONTENTS

Again using Debye extrapolations, the heat involved in raising the temperature of these substances from 0° to 298.1°K, $\int_0^T C_p dT$, may be computed. The results are given in column 2 of Table V. Differences between the values for the hydrogenated samples and pure tantalum, designated $\delta H_{298.1}$, are given in column 3, but it is not meant to imply that these substances have the same heat content at 0°K. Values in the last column give 1890, 2010, and 2000 calories,

[10] K. K. Kelley, Bureau of Mines Bull. **394**, 1936, p. 43.

[11] Kelley, Parks, and Huffman, J. Phys. Chem. **33**, 1802 (1929).

respectively, when computed to the bases of 1 gram-atom of hydrogen, the mean being 1970.

Discussion

It has been accepted practice for some time to consider hydrogen dissolved in metals as dissociated, because in many instances it has been found that the amount dissolved is proportional to the square root of the pressure, at least over certain temperature and pressure ranges. From the recent statistical mechanical treatments of the solution process by Fowler and Smithells[12] and Lacher,[13] it appears very highly probable that the dissolved hydrogen is largely dissociated into protons and electrons, the latter adding to the metal electrons already present. Consequently, in considering the change in any property, after hydrogen of the amounts under consideration is absorbed by tantalum, three factors are involved—the presence of protons, the increased number of metal electrons, and the swelling of the lattice without crystal structure change. When, as in the present instance, only some of the resultant effects are known, it may seem absurd to attempt to reach any definite conclusions concerning the relative importance of these three factors. However, the contribution to the specific heat made by electrons is ordinarily taken to be very small in the temperature range under consideration. Also, in spite of differences (although not uniform) known to occur in lattice parameters, Eucken and Werth,[14] for copper and nickel, and Maier and Anderson,[15] for copper and aluminum, have found no difference in specific heats between cold-worked and annealed metal in this temperature range. Consequently, it appears probable that the anomalous behavior observed here may be attributed primarily to the presence of protons.

If it is assumed that at temperatures far below the maximum in the specific-heat curve a single fixed stable position or set of fixed stable positions is available to each proton while at temperatures above the maximum a greater number of positions is available, then the entropy difference involved should be calculable from the number of possible ways of arranging the protons among the available positions in the two states. The expression for this entropy difference, derivable from probability considerations or by analogy with the ordinary entropy of mixing expression for gases or ideal solutions, is

$$\delta S = -nR\left[\ln\left(\frac{1}{p}\right)\left(\frac{p-1}{p}\right)^{p-1} - \ln\left(\frac{1}{q}\right)\left(\frac{q-1}{q}\right)^{q-1}\right]$$

in which n is the number of gram-atoms of hydrogen, R is the gas constant, p is the number of positions available to each proton at the higher temperatures, and q is the number of positions available to each proton at the lower temperatures. The number of positions available for either state is, of course, not determined by the data presented here. Two somewhat extreme cases will be considered, and the calculation will be restricted to whole numbers for p and q. Thus, if there is one position per tantalum atom available at the higher temperatures and if it is assumed that at the lower temperatures the protons arrange themselves in some stable fashion that limits each proton to a single fixed position, the calculations, given as case 1 in Table IV, are in agreement with the measured results. In case 2, 8 spaces per tantalum atom are considered available at the higher temperatures; but it must then be assumed, to obtain agreement, that as the lower temperatures each proton has a choice of 3 positions. The agreement obtained cannot be considered as proof of this point of view, but it may be noteworthy that the trend in the measured values with increasing hydrogen content as well as their magnitudes have been represented.

For any two compositions considered, as mentioned earlier, the extent of the transition reac-

Table V. *Calculation of* $\int_0^T C_p dT$.

Material	$\int_0^T C_p dT$	$\delta H_{298.1}$
Ta	1362.7	
Ta+0.0284 H	1416.4	53.7
Ta+0.0676 H	1498.9	136.2
Ta+0.0958 H	1553.9	192.2

[12] Fowler and Smithells, Proc. Roy. Soc. (London) **A160**, 37 (1937).
[13] Lacher, Proc. Roy. Soc. (London) **A161**, 525 (1937).
[14] Eucken and Werth, Zeits. f. anorg. allgem. Chemie **188**, 152 (1930).
[15] Maier and Anderson, J. Chem. Phys. **2**, 513 (1934).

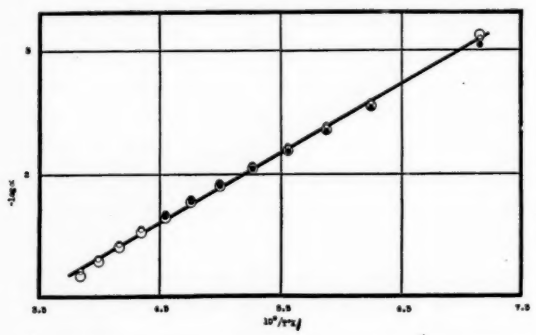

FIG. 2. Plot of $-\log \alpha$ against $1/T$: closed circle—Ta +0.0284 H; small open circle—Ta+0.0676 H; large open circle—Ta+0.0958 H.

tion at a given temperature is the same regardless of the concentration of hydrogen, for all temperatures below that of the lower specific-heat maxima. This phenomenon may be considered somewhat analogous to heating different small amounts of pure liquid in a closed tube of such size that the liquid volume is always negligible. At a given temperature for all cases the vapor pressure would be constant as long as any appreciable amount of liquid were present, and the amount vaporized would be virtually constant. Such an analogy, however, does not portray the slowness with which the specific heats drop with the temperature above the maxima. The observation under consideration makes it reasonable to expect, however, that all data for temperatures below those of the maxima may be represented by a straight line in a $\log \alpha$ *vs.* $1/T$ plot, where α is the quantity of protons changed to the higher temperature condition.

At any temperature, α may be computed approximately as the ratio of the observed $\int_0^T \Delta C_p dT$ for a given sample to the average $\int_0^{298.1} \Delta C_p dT = 1970$ calories computed for 1 gram atom of hydrogen present, the integrals being the areas between the hydrogenated specific heat curve and that of pure tantalum. The result is shown in Fig. 2. The slope of the line as drawn is too great compared with the 1970 calories average excess heat-content change previously mentioned, but not unreasonably so considering the possible errors in the α's, especially at the lower temperatures where ΔC_p is a small fraction of the measured specific heats.

SUMMARY

Specific-heat measurements of pure tantalum have been made in the range 52° to 298.1°K, and the entropy of tantalum has been computed as $S_{298.1} = 9.9 \pm 0.1$.

Specific-heat measurements of tantalum containing, respectively, 0.0284, 0.0676, and 0.0958 gram-atom of hydrogen have been made in the range 78° to 298°K. These substances have marked maxima in their specific-heat curves, the average excess specific heat at the maxima being 40.7 calories per degree per gram-atom of dissolved hydrogen. The excess specific heats at temperatures below all maxima concerned were shown to be independent of the amounts of hydrogen present, but both the temperatures and heights of the maxima are increased as the quantity of dissolved hydrogen is increased.

On dehydrogenation the same specific heat was obtained as for unhydrogenated tantalum, and the density of the dehydrogenated product was normal.

The entropy differences between the hydrogenated materials and pure tantalum perhaps may be attributed to differences in the number of positions in the tantalum lattice available to the hydrogen at the lower and higher temperatures.

Physics of Stressed Solids

ROY W. GORANSON
Geophysical Laboratory, Carnegie Institution of Washington, Washington, D. C.
(Received December 1, 1939)

The internal energy of a system is subdivided into a work or potential function and a thermal or kinetic function, the former expressed in terms of the current electrostatic theory of intercrystalline bonding, and these functions then examined for variations of temperature, hydrostatic pressure, unidirectional stress and combined hydrostatic and unidirectional pressure. From these considerations a theory is evolved which not only seems satisfactorily to explain and correlate phenomena of deformation, creep or plastic flow, cold working, elastic afterworking, rupture, shear and certain other phenomena hitherto described as "anomalous" effects but has been corroborated experimentally in some of its predictions, in particular for the effect of hydrostatic pressure on deformation and compressive strength. The mechanism evolved consists of two processes—one an elastic deformation which is a function of the strain or potential energy of the system. Failure occurs here by "brittle" rupture wherein the maximum extension or maximum internal tension is the criterion. The other is a deformation by means of a two-phase transfer mechanism and is a function of the thermodynamic potential relations of the system. This latter type is also a function of time and therefore a function of the rate of application of load. When both processes of this mechanism are operative failure occurs by shear; the criterion for this type of failure is given by a function of time, the strain or potential energy and the thermodynamic potential relations of the system. Expressions are derived for creep or plastic flow of polycrystalline substances from the thermodynamic potential relations which not only satisfy the well-known phenomena of creep in metals but also express recent empirical creep data of some substances immersed in liquids in which they are somewhat soluble. An expression is also derived for the "brittle" potential type of rupture under combined thrust and hydrostatic pressure.

THE thesis presented in this paper is that the phenomena of deformation, flow or creep, and rupture may be interpreted and correlated from a study of the internal energy stored up in the lattice as a result of deformation.

The energy of deformation may be subdivided into energy of work and energy of heat, that is, into an energy of position and an energy of motion. If this energy of deformation exceeds a certain critical limit, determined by the physical characteristics of the material and the amount of externally applied compensation, a release of the strain energy takes place in such a manner that the system does the least work. If the energy relations are such that release is effected through the potential component, i.e., work function, the system exhibits potential or brittle rupture and the system relieves itself of its strain energy by doing work in the direction of greatest extension which is the direction of least external constraint. If the stress and energy relations are such that release may be effected through the kinetic component, i.e., the work done on the substance is largely dissipated by heat transfer, the specimen deforms by means of a "two-phase" flow mechanism. This is the dominant effect in phenomena of creep and plastic deformation.

In general, deformation and failure are effected by a combination of these two mechanisms and observed as shear and as "gliding along shear planes."

Many of the ideas incorporated in this discussion have been tentatively put forth by other writers but the picture as a whole with its correlations and the theory of rupture presented appears to be new and is therefore presented with the hope that it will prove of interest. This subject needs stimulus for further work on deformation phenomena under hydrostatic confining pressure because it is believed by the writer, perhaps also by others, that further advances in our knowledge of crystal lattice forces will come from such studies.

EMPIRICAL HISTORY

Volume compressibility, like density or heat capacity, is insensitive to variations in structure. By that we mean the volume compressibility of a single crystal is the same as that of a polycrystalline aggregate of the same material. Shear strain, creep, and other related phenomena on the other hand, will vary with crystallographic

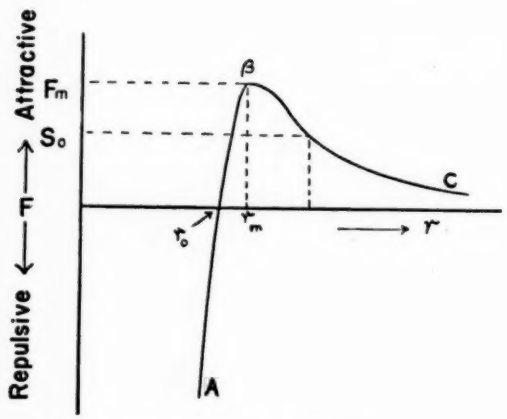

FIG. 1. Force *vs.* extension.

orientation, the geometry of grain boundaries, and other structural factors.

Under certain conditions the material may react like a "perfectly elastic body" whereas under other conditions it may react like a "viscous liquid." In general our material will be found to behave in some intermediate manner for which several words have been coined such as "elastico-viscous," "firmo-viscous," and even "elastic flow."

Some other phenomena which must also be correlated are: Strain hardening (work hardening) an effect for which yield stress increases with strain; and elastic afterworking. The stress is also found to vary with rate of deformation; for liquids the stress-flow rate slope is a constant related to the coefficient of viscosity. The type of deformation may also vary with the speed of loading and a "ductile" or "malleable" substance may, under certain conditions of rapid loading, behave as a "brittle" substance. Again "aging," which is presumably a slow transition toward a more stable state, is observed as a change of yield stress with time. A similar phenomenon may be observed in glass which although breaking readily along a fresh scratch does this with more difficulty after a lapse of time and eventually will no longer break cleanly along the scratch.

THE ENERGY FUNCTIONS

The current electrical theory of intercrystalline bonding forces is based essentially on an electrostatic model. The electrostatic potential φ at a distance r will include the sum of charge potentials proportional to r^{-1}, of dipole potentials proportional to r^{-2}, of quadrupoles proportional to r^{-3}, of octupoles proportional to r^{-4}, and so on. There are also additional terms arising from interactions, induction and dispersion effects. For example the character of the van der Waals forces has been correlated with polarization forces (always attractive) produced by quadrupoles on molecules which are regarded as deformable distributions of charge; the potential from this effect is proportional to r^{-8}. These forces have also been correlated with the polarization of one molecule by the time varying dipole moment of another; these interaction potentials have been computed as proportional to r^{-6}, with also terms of higher order as r^{-8} and r^{-10}.

From quantum-mechanical considerations the repulsive potential is given by the encroachment energy from overlapping wave functions of the atoms and expressible, to fairly high pressures, by an exponential[1] term. The Thomas-Fermi atom model has been suggested and applied[2] to calculations of densities at very high pressures, i.e., exceeding 10^6 bars (1 bar $=10^6$ dynes cm^{-1}).

The force field is given by the negative gradient of the electrostatic potential. Our present purpose will be satisfied by noting that we can write the attractive force F on a particular element in the form

$$F=\sum_i C_i r^{-i}-\sum_j C_j r^{-j}, \qquad (1)$$

where the C_i and C_j are, in general, complicated functions of space and direction. The derivative of F with respect to r/r_0 will denote the reciprocal of the linear compressibility, assuming linear symmetry. Volume cannot be arbitrarily substituted for r^3 because of asymmetry with respect to the space coordinates.

The coefficients C_i and C_j cannot, in general, be directly determined or computed; we may, however, expect to learn something of their respective importance from studies of deformation under high hydrostatic pressure. Initial compressibilities have been computed for some

[1] P. M. Morse, Phys. Rev. **34**, 57–64 (1929).
[2] J. C. Slater and H. M. Krutter, Phys. Rev. **47**, 559–568 (1935). H. Jensen, Zeits. f. Physik **111**, 373–385 (1938).

ionic cubic crystals.[3] Approximate correlations[4] of structure with certain physical properties such as viscosity have been obtained from an assumed two term expression. Although these simplified arbitrary expressions cannot be other than rough approximations they are able to extend the range of elastic theory[5] and also give us a very useful qualitative picture. Some explicit account may be taken of thermal energy pressure by adding a third term.[6] From such an assumed relation it is then possible to calculate the relative stability of certain types of lattices as functions of r.

Schematic plots of these two functions F[7] and ϕ are given in Figs. 1 and 2 for an arbitrarily assumed two-termed expression wherein $i=3$ and $j=9$. The horizontal scales are the same but the vertical scales differ.

The internal energy may be divided into two portions, a work function and a heat function, and expressed as

$$\epsilon=\psi+T\eta, \tag{2}$$

where ϵ denotes the internal energy, ψ the "maximum work" function, T the absolute temperature and η the entropy. Differentiation of this expression gives us

$$(\partial\epsilon/\partial r)_T=-\pi+T(\partial\pi/\partial T)_r, \tag{3}$$

where π is a compressional stress (a tensional stress will be expressed as a negative pressure). The integral

$$\int_\infty^r \pi dr=\psi(r)-\psi(\infty)=\phi(r) \tag{4}$$

is the portion used herein as the potential function, and $\epsilon=\psi=\phi$ for $T=0$.

The curve of Fig. 2 will also denote ψ as a function of r if the zero ordinate is replaced by the value $\psi(\infty)$ where $d\psi(\infty)/dT=-k$, k denoting Boltzmann's constant.

Similarly the integral of $Td\eta$ from $T=0$ to $T=T$ may be considered the thermal or kinetic function. A harmonic oscillator at temperature T has an *average* thermal energy of kT according to classical statistical mechanics. In summing up these energies for a system of oscillators, however, the mutual coupling terms are neglected. Some calculations made for metals using Debye functions wherein the Debye temperature depends on the elastic constants have indicated the usefulness of this method but further development is needed.

The mean internal energy curve will have a shape similar to the potential curve but with a minimum which lies at a higher level and is displaced in the direction of smaller r. Consequently the internal energy will at first decrease on application of pressure at constant temperature by loss of thermal energy exceeding that gained from the work function ψ. Although in a large system the fluctuations in energy of the oscillators tend to cancel out, across any surface a certain fraction of them will have larger energies than the mean and, under favorable circumstances, can migrate from their positions.

It might be anticipated that F_m, the maximum internal tension, of the $F-r$ plot should bear some relation to the cohesive tensile strength and r_m-r_0, where r_m is the separation distance for $F=F_m$ and r_0 the distance for $F=0$, to the maximum elastic strain. This must however be of the nature of an upper limit because of (a) localized high stress regions resulting from inequalities of load distribution and from distortions in the lattice structures caused by imperfections resulting from holes, fissures and inclusions of foreign elements, and (b) localized high energy levels resulting from thermal energy

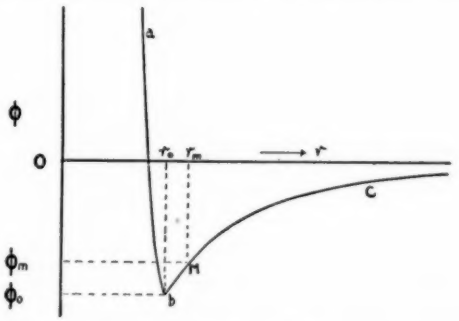

FIG. 2. "Strain energy function" *vs.* extension.

[3] M. Born and J. E. Mayer, Zeits. f. Physik **75**, 1–18 (1932). A. May, Phys. Rev. **52**, 339 (1937).

[4] References in R. H. Fowler, *Statistical Mechanics* (Cambridge University Press, 1936), Chapter 10.

[5] F. D. Murnaghan, Am. J. Math. **59**, 235–260 (1937), has used an arbitrary function similar in form to $Ar^{-2}-Br^{-4}$ for expressing pressure volume relations.

[6] J. Bardeen, J. Chem. Phys. **6**, 372–378 (1938).

[7] The term $-F$ will hereafter in this article be spoken of as internal pressure and F as internal tension. The terms pressure and tension without qualifying terms will refer to the external forces.

gradients and fluctuations. The calculated tensile strengths, F_m, are all much higher than the observed values which are indicated roughly by S_0 in the plot. In the following discussion F_m is used as the ideal elastic tensile strength and $r_m - r_0$ as the ideal maximum safe elastic extension. The actual values may be only about a tenth or less of these maxima.

It should be noted that these considerations are made for the case where the "two-phase" transfer mechanism does not operate. Care must therefore be exercised in drawing comparisons between theoretical and empirical results and this will be shown more clearly later.

Temperature

If the temperature of the system is increased, at constant pressure thermal energy is absorbed with increase in the internal pressure. The system expands doing work against the external surroundings until a new positional equilibrium is attained for the new F. In this way we obtain a family of curves for different T. Ignoring for the time being the change in slope of these curves and considering only the large scale differences, we note that the effective zero ordinate of the $F-r$ plot moves up and r_0 increases to some larger $(r_0)_T$. Similarly the mean minimum potential $(\phi_0)_T$ moves to a larger $(r_0)_T$ and higher up the right limb of the potential energy well which is therefore becoming shallower and shallower in the direction of increasing r. Eventually the right wall of this well would vanish and no further readjustments yield a stable configuration; the system actually breaks down long before this point is reached. If in this breakdown a reorganization in potential and kinetic functions of the components can take place for a new minimum $(\phi_0)_T$ the system melts, and if such a redistribution cannot be effected the system sublimes. The size and nature of the elemental units in this breakdown will depend on the variations in the interatomic bonds, the structure splitting up across bonds of least cohesive strength.

In this connection it might be of interest to note that if the thermal energy be assumed as proportional to v^{-1}, or to r^{-2}, the internal pressure contribution from this source will be proportional to r^{-3}. Under increasing hydrostatic pressure the other internal pressure terms of higher power, here assumed as r^{-9}, eventually dominate over the r^{-3} term and at an increasing rate. The thermal expansion should therefore decrease under hydrostatic pressure and approach zero at very high pressures. This conclusion, in conjunction with the third law, means that, for this model, the entropy must be zero at infinitely high pressure for all temperatures.[8] At moderate pressures the smaller powers of $1/r$ will play more effective roles and the initial rate of decrease of dilatation should, as for compressibility, be less for simple ionic lattices since here the attractive r^{-2} term is initially more effective than the r^{-3} term.

Hydrostatic Pressure

The same type of reasoning applies to systems under hydrostatic pressure at constant temperature but in this case the increase in potential is equal to the work done on the system. The system decreases in volume until an equilibrium between internal and external pressure has been achieved. The most stable pressure or phase configuration is the one best able to withstand the external pressure and therefore the one of higher density. A change of phase under pressure may take place either by reorganization of form (potential or work energy) or in part by change of form and in part by change of momenta (conversion to thermal energy). The pressure at which the latter type of phase change occurs will be a function of temperature; the former should be independent of temperature.

Silicate glasses should in general behave somewhat abnormally because these glasses are in a metastable energy state, i.e., the configuration stable for the high temperature kinetic and potential energy relationships has been frozen into the system. The internal forces should therefore be tensions but the configuration is presumably prevented from collapsing by the randomness of orientation inherited as a result of the previous thermal kinetic energy, that is to say, the glass is not only metastable from considerations of heterogeneous or phase equi-

[8] This was also suggested by G. N. Lewis, Zeits. f. physik. Chemie, Cohen Fest. Band **130**, 532–538 (1927), from other considerations.

librium but is also metastable from considerations of homogeneous equilibrium.

This is suggested as the reason why viscosity bears a relation to the previous thermal history and why anomalous heat capacity effects are observed in the annealing range.

Resistance to motion and reorientation is a function of viscosity so we should expect anomalous effects in highly viscous substances quenched from high temperatures. In fact we might expect a possible increase of compressibility with pressure since the system is in a state which is up on the right limb of the energy curve plotted in Fig. 2 and should be under internal tension.

Bridgman[9] observes anomalous effects in the compressibilities of quartz glass and of basalt glass but he suggests a different explanation for these behaviors. The results of Birch and Dow,[10] however, support the conclusion arrived at here because at higher temperatures, where rearrangements for a more stable configuration will take place more readily, they find the "abnormal" observed increase of compressibility with pressure becomes less pronounced and eventually disappears.

Unidirectional Pressure

If, instead of a hydrostatic pressure, a unidirectional pressure load π is applied to the system no external constraints will exist in the plane at right angles, resulting in an unbalanced energy distribution in the system. The spacing r along the line of thrust decreases by an amount $r-r_0$ and the strain energy increases, climbing up the left limb of the ϕ function plotted in Fig. 2.

It is possible to set up hypothetical unsymmetric arrangements of attractive and repulsive forces such that on contraction of the longitudinal elements the effect laterally is an increased net attraction with consequent contraction of these elements also. Such a condition yields a negative Poisson's ratio, σ, the ratio of lateral elastic extension to longitudinal elastic contraction under compression. A few examples of this phenomenon exist, but in general σ is positive and varies in magnitude between 0.25 and 0.50. As a rule then, the symmetry will be such that, as the longitudinal elements are contracted, the effective lateral r for Eq. (1) decreases and thus the system extends in the plane at right angles to the compression. The effective left limb of the strain energy curve ϕ of Fig. 2 moves to the right a distance $\sigma(r_\pi-r_0)$. When this extension reaches the value (r_m-r_0), the strain energy increasing to ϕ_m, the system becomes unstable and, on further extension, ruptures by moving into the region of no stress. This "brittle" potential rupture, observationally called breaking along tension cracks, will occur across surfaces that tend to parallel the axis of compressive thrust.

The ideal "potential" rupture condition, according to this presentation, is given by

$$r_\pi-r_0=(r_0-r_m)/\sigma \tag{5}$$

and the elastic or potential strength by

$$(F_\pi)=Ar_\pi^{-n}-Br_\pi^{-m}. \tag{6}$$

Thus the elastic strength in compression should be $1/\sigma$, or roughly three, times the elastic strength in tension. In general there is evidence of more or less "plasticity" in compressional and tensional test pieces of steel. Glass hard tool steel, in which a minimum of plasticity is observable, has a compressive strength of about 30 kilobars but even here there is some evidence of shear in the rupture. Direct comparisons for potential rupture cannot therefore be made but the tensile strength of this steel is not very different from the expected value. Such tests should be carried out at low temperatures.

In considering the effect of hydrostatic pressure alone we had only one region available to the system, i.e., the entire region was subjected to the hydrostatic pressure p. Here, however, there are two regions available to our system—one subjected to compressive stress π and one to zero compressive stress. The system therefore, if free of internal and external constraint, will move into and occupy the region of lower energy. If then, before the lateral strain energy can attain the value ϕ_m, the longitudinal energy has increased to a value such that its thermodynamic potential becomes equal to that of the liquid for

[9] P. W. Bridgman, Am. J. Sci. **237**, 7–18 (1939).
[10] F. Birch and R. B. Dow, Bull. Geol. Soc. Am. **47**, 1235–1256 (1936).

the region corresponding to zero compressive stress, i.e.,

$$\zeta(T,\pi,p)=\zeta'(T,p), \tag{7}$$

the prime referring to the liquid phase, then the solid would melt to the liquid phase at (T,p) provided the stressed region is permeable to, i.e., not be active on, the liquid.

The thermodynamic potential is defined by the expression

$$\zeta=\psi+\pi r \tag{8}$$

and $\partial\zeta/\partial\pi=r$.

A schematic plot of ζ as a function of r at the *stressed face* is given in Fig. 3. ζ will be observed to increase with increasing compression but to decrease with increasing tension until it reaches a minimum, ζ_0, at r_m. At the *free face* $(\zeta)_{FF}=(\psi_0)_{FF}$ and thus at this face ζ increases with ψ_0 for both tension and compression. It should perhaps be emphasized that in the direction at right angles to the stress ψ is always at its minimum value on the curve which however changes by virtue of the change in our expression for F.

The use of the terms "liquid" and "melting" may seem confusing and should perhaps be amplified. The process of the two-phase transfer type of mechanism suggested here involves the transition from an immobile solid phase to a mobile phase and thence back again to the solid. The mobile phase should more aptly be called the "fluid" phase and includes not only the condition ordinarily accepted as melting but also any other similar mechanism such as the one known as "migration of lattice points" and diffusion. To make this point somewhat clearer the creep relations will be derived later for a solid in contact with a liquid in which it is slightly soluble and, for this case, the fluid phase is the solution.

We have then two possible mechanisms to transport our system into the region of lower internal energy—one by snapping the cohesive bonds, determined by the strain energy potential; and the other by transition to, and flow of, a fluid phase, solid→fluid→solid; this is determined by the thermodynamic potential relations. The "fundamental strength" of our material is therefore not only a function of the strain energy potential but also of the thermodynamic potential.

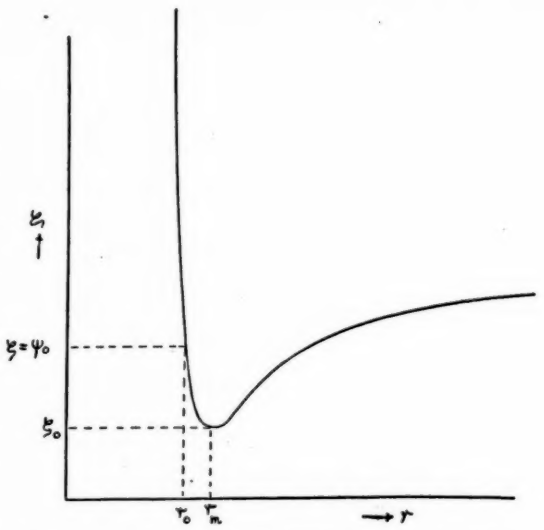

FIG. 3. Free energy for the stressed face *vs.* extension.

The internal energy of the system is merely a statistical mean of the lattice point energies and, on any surface, elements will be found with energy levels exceeding the mean value. The lattice structure is also more or less distorted because of impurities and other irregularities with resulting non-uniform stress distribution. Phase change is initiated at such regions of localized high energy values and results in still further localization of high stress areas. The process therefore tends to accelerate until the concentration of strain energy becomes too high to be borne by the remaining bonds and the specimen fails by shear, a combined "fluid" and "brittle" release.

An increase in compressive load thus acts similarly to an increase in temperature with respect to our "two-phase" mechanism. Phase change is initiated at, and proceeds from, loci of high energy levels at a finite rate, and not as an instantaneous disintegration of the lattice configuration. The time gradient of energy interchange set up by change in the external conditions is also an important factor. The transfer of thermal energy will lag behind that of strain energy. This is evident from explosive phenomena wherein the rotational and vibrational energies can be observed to lag behind the translational energy.

The fact that this phase-change type of deformation is a *function of time*, and the elastic type is not, has important consequences. Failure as a result of a rapidly applied large compressive load is by brittle fracture across surfaces parallel to or making small angles with the axis of load; as the rate of application is decreased failure will tend to occur as shear along surfaces which are at larger angles to the axis of load; if the application is slow enough and the thermodynamic potential relations are favorable the specimen will deform by "gliding along 45° planes," or by "flow."

If the load is not too great the shear may proceed in steps—"melting" at high energy points, shear of the remaining cohesive bonds, slipping, recementation by solidification, the cycle repeating itself as conditions again become favorable. The most favorable surface for this process is the 45°-plane along which the resultant shear stress is a maximum and equal to one-half the compressive load.

These statements need some qualification because the force and potential functions are not symmetric in space and therefore vary with orientation of the system. The curve of Fig. 1 is thus a function of a vector r and the lattice will therefore, if conditions are favorable, rupture or shear along surfaces across which the cohesive bond, F_m, is the least such as cleavage, parting, and twinning planes.

"Melting" can occur in specimens under tension, *viz.* along shear planes, but the phenomenon should not be so evident here because it will take place only at the free surfaces (see Eqs. (11b), (12b), (14b)).

Derivation of Expressions for "Creep" or "Plastic Flow"

The creep relations will be derived first for a solid under compressive load and immersed in a liquid in which it is somewhat soluble.

Assume an initially "ideal solid" in which the thermodynamic potential is the same for all the faces and equal to the potential of the solid in solution (solute), i.e., assume that the solid is in equilibrium with the saturated solution at temperature T and hydrostatic pressure p. If now the solid is loaded by a longitudinal compressive force π the thermodynamic potentials at the stressed and free faces of the solid and of the solute will no longer be equal and the system no longer in equilibrium so long as the stress exists.

In order to derive our thermodynamic equations the system is first divided into hypothetical isolated parts, namely the regions at the stressed surface, at the free face, and of the solution bulk. We also assume any coexistence of phases necessary for our derivations. The physical interpretation follows readily from this procedure and moreover we avoid any confusion that might be introduced from a compromise[11] between the thermodynamic and the physical picture.

The following formulae were derived by ordinary thermodynamic methods applied to stressed systems[12] and have been somewhat simplified for purposes of clarity.

We have

$$(\partial \ln a_2/\partial\pi)_{SF} = M/\rho RT \qquad (9a)$$

and

$$(\partial \ln a_2/\partial\pi)_{FF} = M\pi/\rho ERT, \qquad (9b)$$

where Eq. (9a) refers to the stressed face (subscript SF) and (9b) to the free face (subscript FF). a_2 denotes the activity of the solute, π the compressive stress, M the mole weight, ρ the density of the solid, R the gas constant ($R=83.156$ bar cm), and T the absolute temperature. E is Young's modulus of elasticity in compression, i.e., $E=dX/de$ where X is the stress (negative for pressure) and e the extension per unit length in the direction of the stress. For small stresses E may be approximated by a constant, generally of the order of 10^6 bars.

On integrating (11a) we have, at the stressed face,

$$\pi - \pi_0 = (\rho RT/M) \ln (a_2/a_{2_0}), \qquad (10a)$$

where ρ is the mean value for the integration limits.

---

[11] P. W. Bridgman, Phys. Rev. **7**, 215 (1916), derives an expression which may be correlated with (14a) and (14b). E. D. Williamson, Phys. Rev. **10**, 275 (1917). H. C. Boydell, Ec. Geol. **21**, 1 (1926). Boydell derives Poynting's expression which applies to a solid under hydrostatic pressure p_1 and liquid at p_2 where $p_1 > p_2$. Poynting's expression has the same form as (14a) of this paper.

[12] R. W. Goranson, *Thermodynamic Relations in Multicomponent Systems* (Carnegie Inst. Washington. Publ. No. 408, 1930). For usage of activity see R. W. Goranson, J. Chem. Phys. **5**, 107–112 (1937).

If the system is impervious to liquid and the load contact is a "perfect surface" then only the external free face can be in contact with the solution. Actually the system is, in general, never impervious to the liquid and perfect contact surfaces non-existent. Penetration occurs along crystal boundaries, across crystal cleavages and cracks. The stressed surfaces carry the load non-uniformly and contain high points of localized stress. As these high points are dissolved the stress distribution shifts to other high points and the process is repeated.

Thus at the stressed face solubility is increased by a compressive load and lowered by a tensile load. At the free face solubility is increased by either a compression or tension but by a much smaller factor. It should be noted however that the integral expression for (9b) is

$$\frac{\pi^2-\pi_0^2}{E}=\frac{\rho RT}{M}\ln\left(\frac{a_2}{a_{2_0}}\right), \tag{10b}$$

which may become large for large π. ρ and E are here mean values for the range of integration. This relation is the *plastic flow factor for tension.*

According to this interpretation it is found that, whereas under compressive load the solute concentration tends to increase at both stressed and free face, diffusion of solute away from these faces would leave the bulk of the solution supersaturated. Consequently deposition of solute should occur at unstressed places. If, however, the solution can supersaturate by an amount in excess of the relatively small increased solubility at the free faces, then crystallization will take place on these free surfaces which, under these conditions, act as nuclei for deposition. Our mechanism can thus be considered as a diffusion process along crystal grain boundaries wherein the solution acts as a transfer medium. This diffusion rate will approach a steady state when a dynamic equilibrium between rate of solution and rate of deposition has been established, and will be governed by the mobility of the solute in the solution, the path length, and the concentration head between the stressed and free faces.

If, by changing the load, we change only the concentration head of the *polycrystalline* substance then the change in the steady creep rate, $\dot{\epsilon}_s$, should be directly proportional to the change in activity, or

$$\frac{d\ln a_2}{d\pi}=B\frac{d\ln\dot{\epsilon}_s}{d\pi}, \tag{11}$$

where B is a constant. From (10a) and (11) we obtain

$$\pi-\pi_0=K\ln(\dot{\epsilon}_s/\dot{\epsilon}_0), \tag{12}$$

where K is a physical constant. This is the relation obtained empirically[13] for the steady creep rate of compressively loaded alabaster in contact with water.

As compressive load is increased the solubility at the stressed surface eventually becomes larger than the amount by which the solution can supersaturate. Under these conditions the solution will drop the excess solute in any available unstressed space. Consequently, the texture of the substance may thus become so loosened that it crumbles under the load.

The remainder of the discussion parallels that for plastic flow in polycrystalline metals. As before, we divide our system into hypothetical isolated portions and derive expressions for the stressed face and free face. We assume also the coexistence of two phases—the bound atoms of the solid and the free migrating atoms with energies exceeding those necessary to break the cohesive bonds of the crystal lattice. At the melting point this will be equivalent to the heat of melting.

The analogous relations to (9a) and (9b) connecting compressive stress π and "melting" temperature, T_m, in degrees absolute are readily derived as

$$\left(\frac{d\ln T_m}{d\pi}\right)_{SF}=-\frac{1}{\rho h} \tag{12a}$$

and

$$\left(\frac{d\ln T_m}{d\pi}\right)_{FF}=-\frac{\pi}{\rho E h}, \tag{12b}$$

where h is the heat of "melting" and the other quantities are as before.

The melting point at the stressed face is thus depressed for compression and raised for tension. This may be observed graphically from Fig. 3

[13] The experimental data were obtained by Griggs. To be offered for publication, with Goranson, in a future issue of the *Bulletin of the Geological Society of America.*

where the thermodynamic potential ζ is seen to increase with pressure and decrease with tension at the stressed face. The melting point at the free face is depressed for both compression and tension. Here $(\psi_0)_{FF}=(\zeta)_{FF}$ always increases. The ratio of lowering at the two faces is the same as that found for (9a) and (9b).

The number of atoms with Maxwellian energies in excess of that needed to break the lattice bonds, i.e., the number of free migrating atoms, increases with increase in temperature. At the melting point this fraction of the total number becomes unity. The factor

$$\theta=T/T_m, \tag{13}$$

where T denotes the constant experimental and T_m the melting temperature, has been used in correlating temperature *versus* creep data for different metals. The behavior of a low melting point metal is thus considered as equivalent in behavior to a high melting point metal at a correspondingly higher temperature to give the same θ, other factors remaining unchanged. The argument should be carried out in terms of energy but, as compensation is here effected through the h term this expression is a sufficiently satisfactory approximation.

On combining (12a) and (13) and integrating we have

$$\pi-\pi_0=\rho h \ln(\theta/\theta_0), \tag{14}$$

where ρ and h are here the mean values over the range of integration.

For a sufficiently large load, i.e., for relatively large creep rates, we may in the same manner as before write

$$\pi-\pi_0=K' \ln(\dot{\epsilon}_s/\dot{\epsilon}_0), \tag{15}$$

where K' is a physical constant and $\dot{\epsilon}_s$ the steady state or minimum creep rate. This is the expression that has been used for about thirty years to express the empirical relation between yield stress and minimum creep rate $\dot{\epsilon}_s$ in metal mosaics.

The expressions (12) and (15) were derived for relatively large creep rates and thus for compressive loads large enough to iron out the initial inequalities over a short period of time. Let us assume now that we are operating with either very small stresses or with a substance that does not "migrate" readily. For these conditions the number of migrating units will be relatively few and their paths much shorter. Thus, instead of being able to picture a statistical streaming action, we are slowed down to a hop-skip process and can no longer set up a steady mean flow. The crystallization process must be explicitly considered here and for these cases we have for mobility along the stressed surfaces.

$$K(\theta/\theta_0)=Ke^{(\pi-\pi_0)/\rho h} \tag{16a}$$

and for crystallization along the same surfaces

$$K(\theta_0/\theta)=Ke^{-(\pi-\pi_0)/\rho h}. \tag{16b}$$

The creep rate will be given by the difference between these two quantities or

$$(\dot{\epsilon}/\dot{\epsilon}_0)=K \sinh\frac{\pi-\pi_0}{\rho h}. \tag{17}$$

The same reasoning and therefore a similar sinh expression also replaces (12) for very small creep rates.

An expression of this type was obtained empirically[14] by combining analytically the empirical logarithmic relation for high creep rates (see Eq. (15)) with the linear relation between stress and creep rate observed for very low creep rates.

So far we have considered only the relation between steady creep rate and stress. When compressive load is first applied the irregularities in the structure of the polycrystalline material set up an initial localization of stress at the raised points and thus, for large enough loads, in an initially high creep rate. This rate gradually diminishes toward a steady state as the original inhomogeneities of texture become ironed out and the stress redistributes itself over larger and larger surface areas. The effective stress, for constant load, thus decreases with time. Finally the pore spaces in the texture become filled and the grains more or less reoriented into their most stable crystallographic configuration for an axial load distribution. If now a series of such creep-time tests is made for varying compressive loads on initially identical specimens this last state should be reached at

[14] For example see H. Mussmann, Ann. d. Physik **31**, 130 (1938).

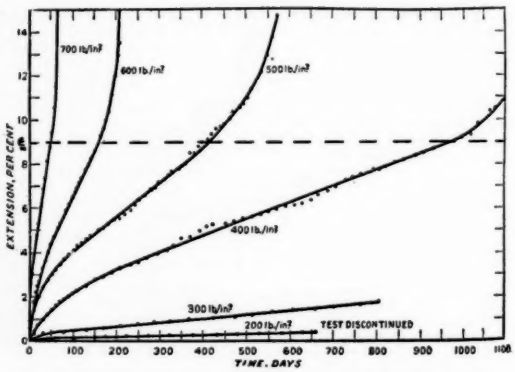

FIG. 4. Tensile creep tests on coarse-grained lead rods at room temperature. By suitable changes in coordinates this diagram can be made to express, to a fair approximation, the compressive creep tests of alabaster in water.

about the same longitudinal contraction ϵ_m provided none of the material has precipitated elsewhere. At this point the specimen has stabilized itself and from this point on should therefore behave more or less as a unit, i.e., approximate to the condition for a single crystal. Solution (or migration) then begins to work along crystallographic surfaces and will be most effective on surfaces across which the cohesive bonds are smallest, i.e., have the largest ζ, in the general 45° trend to the stress axis. If the load is large enough the specimen will then deform by a gliding action along 45° planes and the creep rate, measured by the rate of contraction, will appear to accelerate until the specimen "fails." This is graphically illustrated in Fig. 4.[15]

Plastic flow may also occur in single crystals but the effect in general is a gliding along cleavage, twinning, or parting planes from combined "melting" and snapping of bonds. Localized high stress regions may be set up in crystals, as was mentioned earlier, and thus an initially single crystal may, under a compressive load, finally become a mosaic of reoriented crystalline grains.

The energy at the external crystal faces cannot be denoted by the energy of the interior because of loss of symmetry at these external faces; the difference is known as surface tension. For ionic crystals this difference will be greatest along edges and at corners and least at the centers of faces; this is the reason for the initial skeleton growth of such crystals. With a high symmetry type of structure this difference might become greatest at re-entrants. For our system solution or melting will be most rapid at the stressed surfaces of highest ζ and growth by crystallization most rapid on the free faces of lowest ζ. These directions are, in general, indicated by the crystalline form and cleavage. For example, mica and related minerals will tend to grow with two crystal axes (cleavage planes) perpendicular to the axis of compressive load, asbestos and related minerals to elongate (one crystal axis) in the plane perpendicular to the stress. The best examples we have are the metamorphic rocks which have recrystallized according to this mechanism under high confining pressure (see below).

[15] Data taken from J. McKeown, J. Inst. Metals **60**, 207 (1937).

ELASTIC AFTERWORKING

There is a type of deformation which on loading is a contraction and on unloading a recovery by extension, according to the expression

$$\dot{\epsilon} = \epsilon_1 B/(t+\tau),$$

where $\dot{\epsilon}$ denotes the strain rate, ϵ_1 the purely elastic portion of the strain, B a constant, t the time and τ a time constant. This type of recovery, after unloading, is called "elastic afterworking" and has been observed in glass fibers, in steels, and in rocks.

This is the kind of deformation to be expected from materials which are relatively strong elastically. For these materials the strain is mainly an elastic one but, for a long continued application of a moderate load, a small amount of migration of lattice points will take place if the load is left on long enough. On release of load the material tends to recover elastically, i.e., instantaneously, but it cannot recover completely because under load lattice elements have migrated and then solidified in conformity with the equilibrium conditions existing while under load. These therefore formed bonds tying in this equilibrium state so that when load is released an opposing stress distribution is consequently initiated and the initial equilibrium conditions are attained only by a backward migration of these same elements in retracing their paths.

Work Hardening

The mechanism of work hardening should not require particular comment. There is a further consequence of this phenomenon: The reorientation and reorganization of a polycrystalline aggregate for greater elastic stability to a compressive load, for example, means that the material should then be weaker for a tensional load along the same axis. This is observable in push-pull load-extension diagrams of "overstrained" steels.

Effect of Hydrostatic Pressure on Strength

If hydrostatic pressure is applied to a crystal lattice, r decreases by an amount $r_0-r_p=\epsilon_p$ and if the electrostatic force field is symmetric in space the decrease will be uniform in all directions. If now an additional stress is applied by means of a superimposed unidirectional compressive load π then r along this axis will decrease to r_π by the additional amount $\epsilon_\pi=r_\pi-r_p$.

The lattice, assuming "normal" behavior, expands laterally doing work against the confining pressure until a new equilibrium is established between the repulsive, attractive, and external forces.

It might be anticipated that Poisson's ratio should bear a functional relation to r. The evidence from seismic data indicates, however, that within the earth σ remains approximately constant, at about 0.27, independent of pressure (depth).

The lateral extension will increase as the longitudinal compressive load is increased and thus r will gradually move back through r_0 to r_m at which point the specimen becomes unstable and ruptures. The load for this condition will represent the compressive strength of the specimen.

Rupture, here the "brittle" potential type of fracture, will occur then for the condition

$$\int_{F=-p}^{F=-\pi}\frac{dr}{dF}dF=\frac{\int_{F=0}^{F=-p}\frac{dr}{dF}dF-(r_m-r_0)}{\sigma},$$

where $[(\pi)_m-p]$ denotes the "elastic" compressive strength of the specimen under confining pressure p.

The slope of the $r-F$ curve,

$$\frac{dr}{dF}=\frac{r^{i+1}}{jC_j-iC_ir^{i-i}}$$

flattens rapidly as r decreases and approaches zero as a limit. This initial change in slope may be observed graphically in the curves of compressibility plotted as a function of pressure. Hence the smaller the r, and consequently the higher the hydrostatic confining pressure, the larger must be the unidirectional thrust for the same r_m-r_p but this distance, as a matter of fact, is itself also increasing by virtue of increasing p. The compressive strength of the specimen should therefore accelerate rapidly with increasing confining pressure and become infinitely strong elastically as the confining pressure continues to increase indefinitely. If, therefore, the compressive strength be plotted as ordinate and hydrostatic confining pressure as abscissa the curve should be found to rise gently at first and then to steepen rapidly, eventually becoming infinitely steep.

The above conclusions from this theory, depending entirely on seismic data, have been held in abeyance until they could be further confirmed. Recently confirmation has been obtained from the experimental work of Griggs.[16] Experimental work is also being conducted at the Geophysical Laboratory to verify the calculated strengths for steel. The initial pressure effect is complicated by the geometry of cracks but these cracks close up at a few thousand atmospheres pressure.

The curve of compressive strength *versus* hydrostatic confining pressure for substances which have polymorphic pressure modifications should exhibit discontinuities at such transformation points. In fact if such transformations took place rapidly while the substance was under unidirectional load the structure should break down. These points represent therefore loci of instability, so that the above conclusions would be applicable only to the homogeneous regions above and below such loci.

[16] D. T. Griggs, J. Geol. 44, 541–577 (1936). D. T. Griggs and J. F. Bell, Bull. Geol. Soc. Am. 49, 1723–46 (1938).

The energy levels rise very steeply and eventually for some value $\pi > p$ a state will be reached for which

$$\zeta(T, \pi, p) = \zeta'(T, p),$$

where these quantities are as before.

If this condition becomes fulfilled failure will then take place by plastic deformation or "plastic shear." In other words, a substance under axial compression will become not only stronger elastically but also more malleable with increasing hydrostatic confining pressure. This is shown very clearly from the experimental results of F. D. Adams and Coker.[17] Their results were not duplicated by Griggs but the reason for it should be fairly obvious. Adams and Coker's confining pressure was obtained by means of a pliable steel wall, Griggs' by means of a thin liquid. As soon as incipient melting takes place along, say, a shear plane the substance is relatively free to shear in Griggs' case because the only work involved is (*a*) that of breaking the remaining cohesive bonds across this plane and (*b*) that of exchanging regions with the pressure fluid, since the resistance to flow of the pressure fluid, for a finite rate, is a simple function of its viscosity. For Adams and Coker's case we have, in addition to (*a*), the work of pushing aside the supporting steel wall which is here the total lateral support. Release of strain energy can take place rapidly in the former case but only at a slow rate in the latter case.

Thus, although Griggs has expressed the belief that his results are more applicable to problems of geological deformation in depth and that rocks do not flow in the dry state, the conclusions arrived at herein do not support this contention as a general conclusion. These two apparently dissimilar experimental results are special cases of the same physical hypothesis described in this paper.

[17] F. D. Adams and E. G. Coker, *An Investigation into the Elastic Constants of Rocks* (Carnegie Inst. Washington, Publ. No. 46, 1906). F. D. Adams and J. A. Bancroft, J. Geol. 25, 597–658 (1917).

APRIL, 1940 JOURNAL OF CHEMICAL PHYSICS VOLUME 8

An Empirical Equation for Thermodynamic Properties of Light Hydrocarbons and Their Mixtures

I. Methane, Ethane, Propane and *n*-Butane

MANSON BENEDICT, GEORGE B. WEBB AND LOUIS C. RUBIN
Petroleum Research Laboratory, The M. W. Kellogg Company, Jersey City, New Jersey

(Received December 23, 1939)

An empirical equation is given for the isothermal variation with density of the work content of pure hydrocarbons in the gaseous or liquid state. From this fundamental equation are derived (a) an equation of state, (b) an equation for the fugacity, and (c) an equation for the isothermal variation of the enthalpy. These equations summarize P-V-T properties of the gaseous or liquid phase, critical properties, vapor pressures, and latent heats of evaporation. A procedure is suggested for determining numerical values of the parameters in the equation. Such values are given for methane, ethane, propane, and *n*-butane. A comparison is made between observed properties of these hydrocarbons and those predicted by the equations.

A. INTRODUCTION

RECENT experimental studies of pure light hydrocarbons by Sage and Lacey and co-workers and by Beattie and co-workers are useful in developing an equation to represent the thermodynamic properties of these substances. An equation for this purpose has several advantages: it permits interpolation of experimental data; it facilitates thermodynamic calculations involving integration and differentiation; it provides a concise summary of a large mass of data; and it provides a point of departure for the treatment of the thermodynamic properties of mixtures.

Concurrent with this advance in experimental

knowledge there has taken place development of statistico-mechanical methods for deducing the thermodynamic properties of fluids in bulk from the interaction energies of aggregates of the constituent molecules. A method for the rigorous treatment of this problem, as applied to gases, was first given by Ursell[1] and has recently been extended and clarified by Mayer and co-workers.[2] A less rigorous treatment, leading to a single equation describing the thermodynamic properties of both the liquid and gaseous phases, has been given by Lennard-Jones and co-workers.[3] These theoretical treatments are particularly valuable for suggesting the correct qualitative features of suitable equations. They do not lead to simple expressions in terms of familiar functions, and in the present state of our knowledge of molecular fields, they do not lead to correct numerical values for the properties of matter in bulk. It has, therefore, seemed worth while to attack the problem of representing the thermodynamic properties of hydrocarbons from a more empirical standpoint, and to use the theoretical results only to suggest the proper general characteristics of the formulation.

These theoretical analyses demonstrate that the phase integral summarizing all thermodynamic properties of a fluid may be expressed as the product of two factors, one arising from the internal degrees of freedom of each molecule and the other arising from the interaction energies between aggregates of two or more molecules. From the first factor may be derived equations for the specific heats, entropy, work content, and free energy of the fluid in the hypothetical ideal gas state. From the second factor may be derived equations for the difference between the thermodynamic properties of a real gas or liquid and the corresponding properties of the fluid in the hypothetical ideal gas state. The object of the present paper is to present an empirical equation for this second class of properties.

Definition of terms

Our equation expresses the isothermal variation with density of the work content A of a mole of gaseous or liquid hydrocarbons. The work content is also known as the Helmholtz free energy or the Gibbs ψ-function; it is related to the internal energy E, absolute temperature T, and entropy S by the equation

$$A=E-TS.$$

We are concerned with the residual work content $\tilde{A}$, here defined as the difference between the work content of a mole of hydrocarbons at molal density d and absolute temperature T and its work content in the hypothetical ideal gas state at the same density and temperature. The residual work content $\tilde{A}$ may be defined more rigorously by the equation:

$$\tilde{A}=A-RT\ln d-\lim_{d\to 0}(A-RT\ln d). \quad \text{(A1)}$$

The method of Ursell and Mayer may be used to prove that the limit occurring in Eq. (A1) exists and is finite.

An equation of the form (A1) is a fundamental equation in the sense that from it a number of thermodynamic properties of the fluid may be computed, no one of which alone would permit the computation of all the others. The thermodynamic properties of a fluid which may be computed from the fundamental equation of this paper include: (1) P-V-T properties of the gas or liquid phase. (2) Critical properties. (3) The effect of pressure on the enthalpy. (4) The effect of pressure on the free energy; i.e., the fugacity. (5) Vapor pressures. For instance, an equation of state in which the pressure P is expressed as a function of the density and temperature may be obtained by the relation:

$$P=RTd+d^2(\partial\tilde{A}/\partial d)_T. \quad \text{(A2)}$$

The fugacity f is given by:

$$RT\ln f=\tilde{A}+RT\ln dRT+P/d-RT, \quad \text{(A3)}$$

and the isothermal variation of the enthalpy H by:

$$H(T,d)-H(T,0)=-T^2\left(\frac{\partial\tilde{A}/T}{\partial T}\right)_d+P/d-RT. \quad \text{(A4)}$$

Conversely, the residual work content of the gas phase may be obtained by integration of an equation of state:

$$\tilde{A}=\int_0^d\frac{P-RTd}{d^2}\delta d. \quad \text{(A5)}$$

[1] Ursell, Proc. Camb. Phil. Soc. **23**, 685 (1927).

[2] Mayer, J. Chem. Phys. **5**, 67 (1937); Mayer and Ackermann, *Ibid.* **74**; Mayer and Harrison, *Ibid.* **6**, 87, 101 (1938).

[3] Lennard-Jones and Devonshire, Proc. Roy. Soc. London **A163**, 53 (1937).

Relationship to other equations of state

Of the many equations of state that have been proposed perhaps the best known are the van der Waals and the Beattie-Bridgeman equations. The van der Waals[4] equation,

$$P=\frac{RTd}{1-bd}-ad^2, \tag{A6}$$

has the advantage of simplicity, and for this reason is often used in discussing the thermodynamic relationships of the gaseous and liquid states and the critical region between them. By substituting the van der Waals equation of state (A6) in (A5), Eq. (A7) for the residual work content of the gas phase is obtained:

$$\tilde{A}=-RT\ln(1-bd)-ad. \tag{A7}$$

When derived in this way, Eq. (A7) applies rigorously only to the gas phase. In the van der Waals theory of the continuity of the liquid and gaseous states the assumption is made that this equation is valid for the liquid phase, as well. From this standpoint, Eq. (A7) is the fundamental equation of the van der Waals theory for both the gaseous and liquid phases. It may be used to calculate the equation of state and fugacity of either phase, and from them, the vapor pressure. Vapor pressures calculated in this way from the van der Waals equation are in only qualitative agreement with observed vapor pressures. This need not invalidate the significant assumption of the van der Waals theory, that a single fundamental equation can be found for both the liquid and gaseous phases, as the discrepancy may be due to the recognized failure of the van der Waals equation to correspond accurately to observed P-V-T data.

Among the many equations of state which have been proposed as improvements on the van der Waals equation, the Beattie-Bridgeman[5] equation,

$$\begin{aligned}P=&RTd+(B_0RT-A_0-Rc/T^2)d^2\\&+(-B_0bRT+A_0a-RB_0c/T^2)d^3\\&+RB_0bcd^4/T^2,\end{aligned} \tag{A8}$$

has, perhaps, most satisfactorily combined mathematical simplicity with accurate representation of P-V-T data over a wide temperature range. In its present form the Beattie-Bridgeman equation does not correspond accurately with the P-V-T properties of liquids or gases above their critical density, so that it cannot be used to calculate the residual work content above this density or the vapor pressure.

The present equation

The equation of state proposed in this article may be regarded as a modification of the Beattie-Bridgeman equation to enable it to represent more accurately the properties of fluids at high densities. The van der Waals assumption of the continuity of the liquid and gaseous states is retained, in that a common fundamental equation and a common equation of state are used for both gaseous and liquid phases. The fundamental equation proposed for expressing the dependence of the residual work content $\tilde{A}$ of a mole of gaseous or liquid hydrocarbon on the molal density d and absolute temperature T is:

$$\begin{aligned}\tilde{A}=&(B_0RT-A_0-C_0/T^2)d\\&+(bRT-a)d^2/2+a\alpha d^5/5\\&+\frac{cd^2}{T^2}\left[\frac{1-\exp(-\gamma d^2)}{\gamma d^2}-\frac{\exp(-\gamma d^2)}{2}\right].\end{aligned} \tag{A9}$$

The equation of state corresponding to (A9) is:

$$\begin{aligned}P=&RTd+(B_0RT-A_0-C_0/T^2)d^2\\&+(bRT-a)d^3+a\alpha d^6\\&+\frac{cd^3(1+\gamma d^2)\exp(-\gamma d^2)}{T^2}.\end{aligned} \tag{A10}$$

The isometrics of this equation of state have the same form as the isometrics of the Beattie-Bridgeman equation:

$$P=T\psi(d)-\phi(d)-\Gamma(d)/T^2. \tag{A11}$$

The parameters B_0, A_0, and C_0 of Eq. (A10) play the same role and have about the same numerical values as corresponding parameters in the Beattie-Bridgeman equation. The parameters b, a, c, γ, and α are not directly related to any occurring in the Beattie-Bridgeman equation.

[4] Van der Waals, *Die Continuität des Gasförmigen und Flüssigen Zustandes* (Barth, Leipzig, 1899).

[5] Beattie and Bridgeman, Proc. Am. Acad. Arts Sci. **63**, 229 (1928).

B. Considerations Influencing Adoption of Present Equation

The work of Ursell and Mayer may be used to prove that the residual work content $\tilde{A}$ of a gas can be expressed by the series

$$\tilde{A}=Q_1(T)d+Q_2(T)d^2+\cdots, \qquad \text{(B1)}$$

convergent in the region of stable existence of the gas phase. An equation for both the gaseous and liquid phases was sought which would reduce to (B1) at low densities, which would constitute a suitable compromise between simplicity of application and accurate correspondence with observed thermodynamic properties of gases and liquids, which would contain a minimum number of independent parameters to be fitted numerically, and which would summarize as well as possible the following classes of properties: (1) P-V-T properties of the gas phase. (2) Critical properties. (3) Vapor pressures. It is believed that emphasis on these properties results in the most generally satisfactory equations for pure light hydrocarbons on which to base the prediction of liquid-vapor equilibria of their mixtures. This is the ultimate object of the project described in part in this article.

The functional form of the equation finally adopted as most satisfactorily filling these three requirements was determined primarily from an examination of the P-V-T properties of the gas phase; then, for each hydrocarbon, the best numerical values of the parameters in the equation were estimated from a consideration of all three classes of properties.

Equation of state

In developing the equation of state, attention was first directed to the isometrics of $(P-Rtd)/d^2$ *versus* temperature; these are very nearly straight. For each hydrocarbon it was found that these isometrics could be represented by an equation of the form:

$$(P-RTd)/d^2=RTB(d)-A(d)-C(d)/T^2. \qquad \text{(B2)}$$

These isometrics are illustrated with the example of propane in Fig. 1. The plotted points are derived from the observed pressures of Beattie, Kay and Kaminsky;[6] the lines represent the equation of state for propane given in Section D.

Equations, consistent with expression (B1), were then sought to express the dependence of

[6] Beattie, Kay and Kaminsky, J. Am. Chem. Soc. **59**, 1589 (1937).

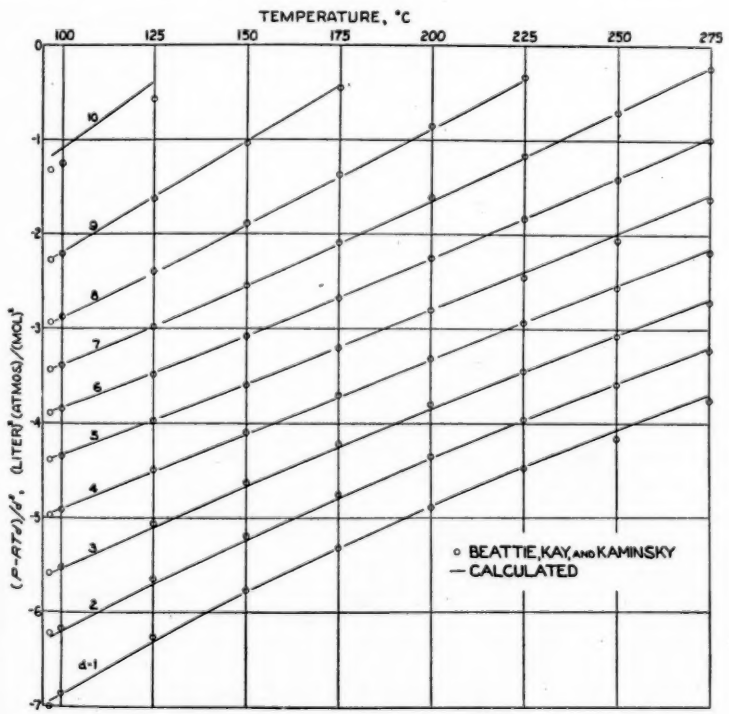

FIG. 1. Isometrics of gaseous propane.

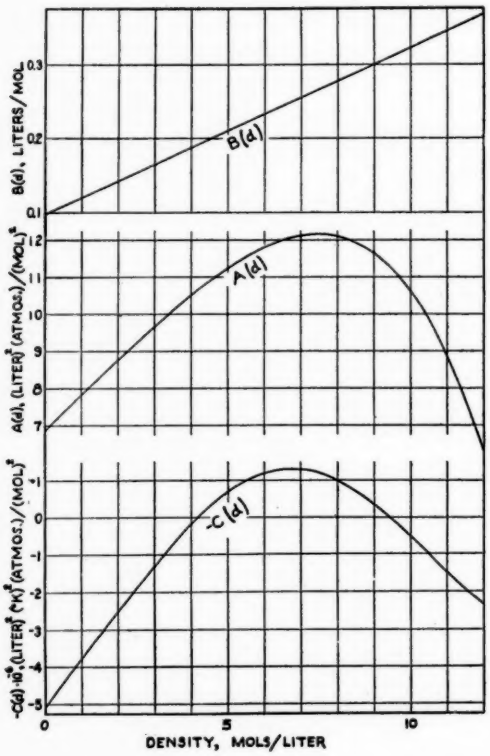

FIG. 2. Functions of density in equation of state.

$B(d)$, $A(d)$, and $C(d)$ on density. It was found that $B(d)$ could be represented by the simple linear equation

$$B(d)=B_0+bd, \qquad \text{(B3)}$$

but that plots of $A(d)$ and $C(d)$ against density showed marked curvature. $A(d)$ was finally represented by an equation of the form:

$$A(d)=A_0+ad(1-\alpha d^3), \qquad \text{(B4)}$$

and $C(d)$ by an equation of the form:

$$C(d)=C_0-cd(1+\gamma d^2)\exp(-\gamma d^2). \qquad \text{(B5)}$$

A simple polynomial would have sufficed to express $C(d)$ for the gas phase, but in order to represent the fugacities of the liquid phase at high densities and low temperatures, the more complicated expression (B5) was required.

The functions $B(d)$, $A(d)$, and $C(d)$ for propane are illustrated in Fig. 2. The same qualitative features of these functions were found for each hydrocarbon studied. The properties of $C(d)$ are of especial interest. Since

$$(\partial^2 P/\partial T^2)_d=-6d^2C(d)/T^4, \qquad \text{(B6)}$$

$-C(d)$ has the sign of the curvature of the isometrics. It appears to be a general rule that the isometrics of the gas phase at densities less than the critical have negative curvature.[5] Near the critical density the curvature of the isometrics becomes positive, as first noted by Sydney Young.[7] The isometrics of the compressed liquid phase at still higher density have negative curvature, as shown by Bridgman.[8] These properties of the isometrics of real gases and liquids are paralleled by Eq. (B5) for $C(d)$. As shown in Fig. 2, $-C(d)$ is negative up to approximately the critical density. Between this density and about twice the critical density, it is positive. Above twice the critical density, in the region corresponding to the compressed liquid, $C(d)$ is again negative.

When expressions (B2), (B3), (B4), and (B5)

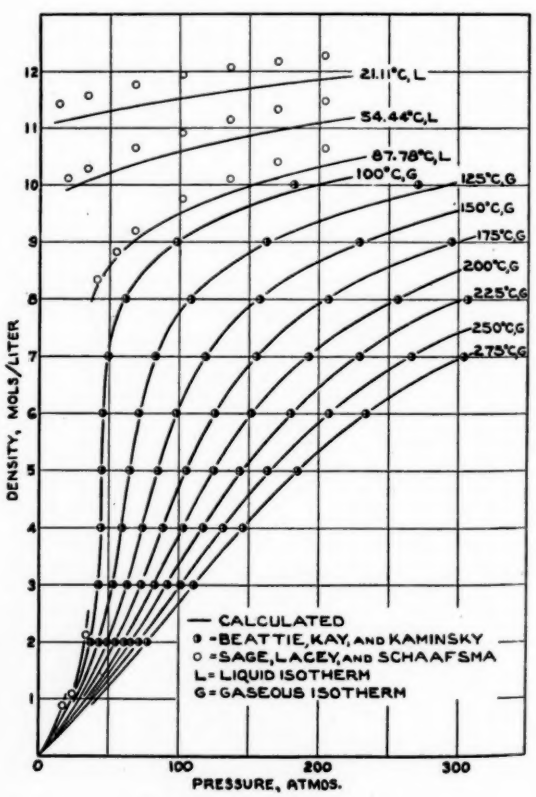

FIG. 3. Isotherms of propane.

[7] Young, Proc. Phys. Soc. London **13**, 602 (1895).
[8] Bridgman, Proc. Am. Acad. Arts Sci. **66**, 185 (1931).

are combined, the equation of state (B7) is obtained. This is the isometric form of

$$P=RTd+d^2\left\{RT[B_0+bd]-[A_0+ad-a\alpha d^4]\right.$$
$$\left.-\frac{1}{T^2}[C_0-cd(1+\gamma d^2)\exp(-\gamma d^2)]\right\}, \quad \text{(B7)}$$

Eq. (A10), useful in computing pressures at constant density. This equation is integrable and differentiable with respect to density, volume, and temperature. Its eight parameters is the smallest number with which the P-V-T properties of the gas phase could be represented up to about twice the critical density. In Section E it is shown that the average error in calculated pressures up to this density is only 0.34 percent. Owing primarily to limitations in Eq. (B4) for $A(d)$, the error at higher densities becomes much larger; better agreement at higher densities could not have been obtained without the use of several more parameters.

To illustrate in terms of familiar properties the agreement of equation of state (B7) with observed data, isotherms of density versus pressure for propane are plotted in Fig. 3. This figure is typical of all hydrocarbons studied. The complex dependence of density on pressure, especially near the critical temperature, 96.8°C, is clearly shown. Up to 9 moles per liter, about twice the critical density, the equation of state accurately reproduces this dependence. Above this density, the equation predicts densities too low by from 2 to 3 percent, because of the limitations of the equation noted in the preceding paragraph.

Critical properties

Since the equation of state (B7) reproduces observed P-V-T properties of the gas phase in the critical region, it necessarily satisfies our second requirement, that it summarize observed critical properties. Except for methane, calculated and observed critical temperatures and pressures agree within 0.25°C and 0.4 atmos., respectively. However, it should be noted that our equation describes what may be termed the "classical" picture of the critical region between liquid and vapor; at each temperature below the critical point it leads to only one pair of phases of different densities which can be in equilibrium. This picture differs from the recent observations of Maass[9] and the predictions of the theory of Mayer,[2] which indicate that for several degrees below the critical temperature it is possible for an infinite number of phases of different density to coexist.

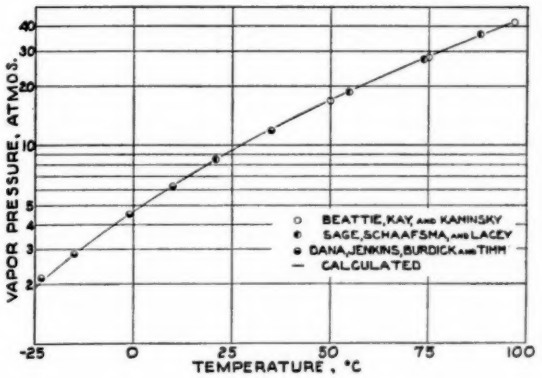

FIG. 4. Vapor pressure of propane.

Vapor pressures

The fundamental equation (A9), summarizing P-V-T properties of both phases, critical properties, and vapor pressures, was developed from the equation of state as follows.

(1) An equation for the residual work content of the gas phase was obtained by substitution of equation of state (B7) in the thermodynamic relation (A5).

(2) It was then assumed that the resulting Eq. (A9) was valid for the liquid phase also, as in the van der Waals treatment of the continuity between the gaseous and liquid states.

This assumption may be tested by seeing how well vapor pressures computed from an equation of the form (A9) agree with observed data. Detailed comparison between observed and calculated vapor pressures is deferred to Section E. Here it may be stated that the average error in calculated vapor pressures above one atmosphere is only 1.1 percent. This justifies the use of Eq. (A9) as a fundamental equation for both the gaseous and liquid phases.

Figure 4 illustrates vapor pressures of propane predicted by the equation and those observed by various authorities. Approximately the same

[9] Maass, Chem. Rev. **23**, 17 (1938).

agreement is found for vapor pressures of methane, ethane, and *n*-butane.

To calculate vapor pressures from the fundamental equation (A9), Eq. (B8) for the fugacity f is first obtained from it by the thermodynamic relation (A3).

$$RT \ln f = RT \ln dRT + 2d(B_0RT - A_0 - C_0/T^2) + 3d^2(bRT - a)/2 + 6a\alpha d^5/5 + \frac{cd^2}{T^2}\left[\frac{1-\exp(-\gamma d^2)}{\gamma d^2} + \frac{\exp(-\gamma d^2)}{2} + \gamma d^2 \exp(-\gamma d^2)\right]. \quad \text{(B8)}$$

A gaseous density d^G and a liquid density d^L are found by trial such that

$$P(d^G, T) = P(d^L, T) \quad \text{(B9)}$$

and

$$RT \ln f(d^G, T) = RT \ln f(d^L, T). \quad \text{(B10)}$$

P is the calculated vapor pressure at absolute temperature T.

Isothermal variation of enthalpy

From fundamental equation (A9) and thermodynamic relation (A4) it is possible to derive an equation for the change in enthalpy H with density at constant temperature. We obtain:

$$H(T,d) - H(T,0) = (B_0RT - 2A_0 - 4C_0/T^2)d + (2bRT - 3a)d^2/2 + 6a\alpha d^5/5 + \frac{cd^2}{T^2}\left[3\frac{1-\exp(-\gamma d^2)}{\gamma d^2} - \frac{\exp(-\gamma d^2)}{2} + \gamma d^2 \exp(-\gamma d^2)\right]. \quad \text{(B11)}$$

Eq. (B11) may be used to compute the change in enthalpy of the gas upon isothermal expansion or to compute the latent heat of evaporation of the liquid. In the latter application, the densities of the saturated liquid and vapor which satisfy Eqs. (B9) and (B10) above should be used, rather than the observed saturation densities.

Simplified equations for the gas phase

It is an advantage of the present formulation that simpler equations can be used when the density does not exceed one-half the critical density. When fundamental equation (A9) is expanded in ascending powers of the density, we obtain:

$$\tilde{A} = (B_0RT - A_0 - C_0/T^2)d + (bRT - a + c/T^2)d^2/2 + a\alpha d^5/5 - c\gamma^2 d^6/12T^2 + \cdots. \quad \text{(B12)}$$

At low densities the terms in the fifth and higher powers of d may be neglected in comparison with the others. We then have for the fundamental equation:

$$\tilde{A} = Q_1 d + Q_2 d^2,$$

where

$$Q_1 = B_0RT - A_0 - C_0/T^2, \quad Q_2 = (bRT - a + c/T^2)/2; \quad \text{(B13)}$$

for the equation of state:

$$P = RTd + Q_1 d^2 + 2Q_2 d^3; \quad \text{B(14)}$$

for the fugacity:

$$RT \ln f = RT \ln dRT + 2Q_1 d + 3Q_2 d^2; \quad \text{(B15)}$$

and for the isothermal variation of the enthalpy:

$$H(T,d) - H(T,0) = (B_0RT - 2A_0 - 4C_0/T^2)d + (2bRT - 3a + 5c/T^2)d^2/2. \quad \text{(B16)}$$

The fundamental equation (B13) for the gas phase at low densities is in the form (B1) required by general statistico-mechanical considerations, except that a definite temperature dependence is here proposed for the coefficients Q_1 and Q_2. It may be noted that Q_1 and Q_2 are related to the coefficients in the "virial" equation of state,

$$P/RTd = 1 + \beta_1 d + \beta_2 d^2 + \cdots, \quad \text{(B17)}$$

as follows:

$$\beta_1 = Q_1/RT \quad \text{(B18)}$$

and

$$\beta_2 = 2Q_2/RT. \quad \text{(B19)}$$

Table I indicates the order of magnitude of the errors made by using the simplified equations.

TABLE I. *Comparison of simplified and complete equations for propane. Density = 2.565 moles/l. Temp. = 96.81°C.*

EQUATION	SIMPLIFIED	COMPLETE
Pressure, atmos.	39.108	39.121
Fugacity, atmos.	26.737	26.743
Enthalpy, *l*-atmos./mole	−55.134	−55.147

Here, the pressure, fugacity, and isothermal change in enthalpy of propane at its critical temperature and one-half its critical density have been calculated with the simplied Eqs. (B14), (B15) and (B16) and with the complete Eqs. (B7), (B8) and (B11). At lower densities the errors resulting from using the simplified equations are still smaller, so that for most purposes it is permissible to use them when the density is less than one-half the critical. On the other hand, the simplified equations may not be used for the gas phase at higher density or for the liquid phase, since the errors rapidly become larger as the density increases.

C. Determination of the Numerical Values of the Parameters from Experimental Data

The foregoing general remarks on the considerations which led to the form of the present equation may be made more concrete by an outline of the procedure followed in determining from experimental data the most suitable numerical values of the parameters for a particular hydrocarbon. This procedure will be found convenient in fitting the present equation to substances other than those treated in this article.

(1) Interpolate experimental P-V-T data for the gas phase to even temperatures and densities. Pressures at these even temperatures and densities will be referred to as the observed pressures, P_{obs}.

(2) At each density fit an equation of the form:

$$P=RTd+d^2[RTB(d)-A(d)-C(d)/T^2] \quad (C1)$$

to the observed pressures by the method of least squares; give equal weight to each pressure.

(3) Plot $B(d)$, determined in step (2), against density. Pass a straight line through the points; give greater weight to the points at the higher densities. The equation of this line is:

$$B=B_0+bd. \quad (C2)$$

(4) Let the "cohesive pressure," π_{obs}, be defined by the equation:

$$\pi_{obs}=RT(d+B_0d^2+bd^3)-P_{obs}. \quad (C3)$$

At each density fit an equation of the form:

$$\pi=d^2[A'(d)+C'(d)/T^2] \quad (C4)$$

to the cohesive pressures by the method of least squares; give equal weight to each pressure.

(5) Find by trial a value of γ such that when $C'(d)$ is plotted against $d(1+\gamma d^2)\exp(-\gamma d^2)$ the points fall on an approximately straight line. Pass a straight line through these points; give greater weight to the points at the higher densities. The equation of this line is:

$$C'(d)=C_0-cd(1+\gamma d^2)\exp(-\gamma d^2). \quad (C5)$$

(6) Let A_{obs} be defined by the equation:

$$d^2A_{obs}=\pi_{obs} -\frac{d^2}{T^2}[C_0-cd(1+\gamma d^2)\exp(-\gamma d^2)]. \quad (C6)$$

If $B(d)$ and $C'(d)$ have been properly determined, A_{obs} will be practically independent of temperature. "Best" values of $A(d)$, denoted by $A''(d)$, are selected as follows: At densities near the critical take the value of A_{obs} at the critical temperature; in this way the equation being fitted will be more nearly consistent with observed critical properties. At other densities use an average value of A_{obs}.

(7) Find by trial a value of α such that when $A''(d)$ is plotted against $d(1-\alpha d^3)$ the points fall on an approximately straight line. Pass a straight line through these points; give greatest weight to the points in the neighborhood of the critical density. The equation of this line is:

$$A''(d)=A_0+ad(1-\alpha d^3). \quad (C7)$$

(8) The values of A_0, a and α, given in Eq. (C7); C_0, c and γ, given in Eq. (C5); and B_0 and b, given in Eq. (C2) constitute provisional values of these eight parameters. If these provisional values give a satisfactory representation of the observed pressures and critical properties, the values of b, a, c, γ, and α may be accepted as final.

(9) There remains the adjustment of B_0, A_0, and C_0, to give the best representation of observed vapor pressures. At each temperature, with provisional values of B_0, A_0, and C_0 and final values of the other parameters, compute $RT\ln f$ at the observed vapor pressure for the gaseous and

TABLE II. *Numerical values of parameters. Units: atmospheres, liters, g-mole, °K. Atomic weights: C=12.000, H=1.0078. Universal gas constant: R=0.08207. T (°K)=t (°C)+273.13.*

	METHANE	ETHANE	PROPANE	*n*-BUTANE
B_0	0.0426000	0.0627724	0.0973130	0.124361
A_0	1.85500	4.15556	6.87225	10.0847
$C_0 \cdot 10^{-6}$	0.0225700	0.179592	0.508256	0.992830
b	0.00338004	0.0111220	0.0225000	0.0399983
a	0.0494000	0.345160	0.947700	1.88231
$c \cdot 10^{-6}$	0.00254500	0.0327670	0.129000	0.316400
γ	0.0060000	0.0118000	0.0220000	0.0340000
α	0.000124359	0.000243389	0.000607175	0.00110132

liquid phases, as follows: Find by trial a liquid density d^L and a vapor density d^G such that when these densities are substituted in equation of state (B7), the computed pressures equal the observed vapor pressure. Compute the vapor fugacity f^G and the liquid fugacity f^L at d^G and d^L, respectively, by means of Eq. (B8).

B_0, A_0, and C_0 have now to be adjusted so that f^G and f^L at the observed vapor pressure are made as nearly equal as possible. The effect on the calculated fugacities of adjusting B_0, A_0, and C_0 may be estimated through its effect on Q_1, defined as:

$$Q_1 = B_0RT - A_0 - C_0/T^2. \tag{C8}$$

It may be proved that

$$RT(\partial \ln f/\partial Q_1)_P = d, \tag{C9}$$

so that the effect on f of changing B_0, A_0, and C_0 by ΔB_0, ΔA_0, and ΔC_0 is given to the first order by:

$$RT\Delta \ln f = d\Delta Q_1 = d(RT\Delta B_0 - \Delta A_0 - \Delta C_0/T^2). \tag{C10}$$

To make f^G and f^L equal at the observed vapor pressure, Q_1 must therefore be changed by an amount ΔQ_1, given by:

$$\Delta Q_1 = \frac{RT \ln f^G/f^L}{d^L - d^G}. \tag{C11}$$

TABLE III. *Summarized comparison of observed properties of light hydrocarbons with those predicted by present equation.*

	METHANE	ETHANE	PROPANE	*n*-BUTANE	AVE. FOR 4 HYDROCARBONS
1. *Pressures of Gaseous Phase*					
Source of Data	[10,11,13]	[13,14,15]	[6,21]	[22,24]	
Range of Density, moles/liter	2 to 18	0.5 to 10	1 to 9	0.5 to 7	
Range of Temperature, °C	−70 to 200	25 to 275	96.81 to 275	150 to 300	
Ave. % Dev. of Pressures	0.34	0.31	0.40	0.31	0.34
Observed Normal Density, g/l.	0.7168	1.3566	1.8325 (25°C)	2.70324	
% Deviation	−0.01	+0.15	−0.005	−0.10	0.07
2. *Critical Properties*					
Source of Data	[12]	[15,16]	[18]	[22]	
Deviation of Pressure, atmos.	−1.5	−0.17	−0.42	−0.05	−0.54
Deviation of Temperature, °C	−0.3	−0.25	−0.16	−0.06	−0.19
Deviation of Density, moles/liter	+0.06	+0.06	0.00	+0.13	+0.06
3. *Properties of Saturated Liquid*					
Source of Data	[12]	[14,17]	[18,19,20]	[20,22,23]	
Range of Temperature, °C	−139.50 to −85.13	−50 to 25	−25 to 75	4.44 to 121.11	
Range of Vapor Pressure, atmos.	4.51 to 41.81	5.45 to 41.37	2.01 to 28.0	1.20 to 22.48	
Ave. % Dev. of Densities	2.7	2.7	2.3	1.2	2.2
Ave. % Dev. of Vapor Pressures	2.4	0.4	1.0	0.7	1.1

[10] Kvalnes and Gaddy, J. Am. Chem. Soc. **53**, 394 (1931).
[11] Michels and Nederbragt, Physica **3**, 569 (1936).
[12] Keyes, Taylor and Smith, J. Math. Phys. (M.I.T.) **1**, 211 (1922).
[13] Int. Crit. Tab., Vol. 3, p. 3.
[14] Beattie, Hadlock and Poffenberger, J. Chem. Phys. **3**, 93 (1935).
[15] Beattie, Su and Simard, J. Am. Chem. Soc. **61**, 924, 926 (1939).
[16] Sage, Webster and Lacey, Ind. Eng. Chem. **29**, 685 (1937).
[17] Int. Crit. Tab., Vol. 3, p. 230.
[18] Beattie, Poffenberger and Hadlock, J. Chem. Phys. **3**, 96 (1935).
[19] Sage, Schaafsma and Lacey, Ind. Eng. Chem. **26**, 1218 (1934).
[20] Dana, Jenkins, Burdick and Timm, Refrig. Eng. **12**, 387 (1926).
[21] Kemp and Egan, J. Am. Chem. Soc. **60**, 1521 (1938).
[22] Beattie, Simard and Su, J. Am. Chem. Soc. **61**, 24, 26 (1939).
[23] Sage, Webster and Lacey, Ind. Eng. Chem. **29**, 1188 (1937).
[24] Breckers, Bull. Soc. Chim. Belg. **39**, 470 (1930).

TABLE IV. *Deviations of pressures calculated by equation of state from observed pressures for gaseous n-butane.*[22]

DENSITY, MOLES/LITER		0.5	1	2	3	4	5	6	7	8	
TEMP. °C		PRESSURE, NORMAL ATMOSPHERES									AVERAGE % DEV.
150	Obs.	14.68	24.68	34.39							
	% Dev.	−0.07	−0.04	−0.06							0.06
152.01	Obs.					37.46	37.76	43.40	73.27	168.11	
	% Dev.					−0.11	−0.82	−0.51	+0.33	(−5.39)	0.44
175	Obs.	15.91	27.50	41.31	47.89	52.20	58.30	74.32	120.59	239.49	
	% Dev.	−0.06	+0.04	+0.56	+0.69	−0.33	−1.60	−0.57	+0.24	(−3.87)	0.51
200	Obs.	17.11	30.24	47.88	58.99	68.61	81.96	109.23	172.87	315.71	
	% Dev.	−0.12	+0.07	+0.56	+0.66	−0.20	−1.05	−0.13	+0.38	(−3.31)	0.40
225	Obs.	18.30	32.92	54.29	69.93	85.20	106.23	145.02	225.65		
	% Dev.	−0.11	+0.03	+0.48	+0.50	−0.13	−0.63	+0.23	+0.47		0.32
250	Obs.	19.48	35.55	60.62	80.74	101.84	130.80	181.11	278.51		
	% Dev.	−0.10	0.00	+0.43	+0.27	−0.16	−0.44	+0.31	+0.42		0.27
275	Obs.	20.65	38.18	66.82	91.58	118.57	155.59	217.50	331.20		
	% Dev.	−0.10	+0.05	+0.31	+0.17	−0.19	−0.37	+0.30	+0.25		0.22
300	Obs.	21.81	40.76	72.97	102.28	135.27	180.56	253.96			
	% Dev.	−0.05	+0.05	+0.22	−0.01	−0.32	−0.36	+0.17			0.17
Average % Deviation		0.09	0.04	0.37	0.38	0.21	0.75	0.32	0.35	(4.19)	
Over-all Ave. % Dev.											0.31

These values of ΔQ_1 are to be fitted by an equation of the form:

$$\Delta Q_1 = RT\Delta B_0 - \Delta A_0 - \Delta C_0/T^2. \qquad \text{(C12)}$$

Find by trial values of ΔB_0, ΔA_0, and ΔC_0 such that ΔQ_1 computed by (C11) is represented as well as possible, subject to the restrictions: (a) ΔQ_1 vanishes at the critical temperature. (b) ΔQ_1 is made as small as possible between the critical temperature and the highest temperature at which gaseous pressures are to be computed. Requirement (a) ensures that the calculated critical properties will not be affected by adjusting B_0, A_0, and C_0: requirement (b) ensures that gaseous pressures will be changed as little as possible while fitting the vapor pressure data.

To obtain the final value of B_0, A_0 or C_0, add ΔB_0, ΔA_0 or ΔC_0 to the provisional value of the corresponding parameter.

(10) As a check on the process described in the preceding paragraphs, observed vapor pressures and observed P-V-T properties of the gas phase should be compared with those computed with final values of the eight parameters.

D. NUMERICAL VALUES OF THE PARAMETERS

In Table II are listed numerical values of the eight parameters B_0, A_0, C_0, b, a, c, γ, and α for the hydrocarbons methane, ethane, propane, and *n*-butane. These values were determined by the procedure outlined in Section C from the data listed in Table III of Section E, following. These data comprise: (1) P-V-T properties of the gas and liquid phases up to 1.8 times the critical density. (2) Critical properties. (3) Vapor pressures above one atmos.

Atomic weights, the value of the universal gas constant R and the centigrade temperature of the ice point listed in Table II should be used in conjunction with the parameters given there, because they were employed in fitting the equation to the experimental data.

It is, of course, impossible to assign unique values accurate to six significant figures to each of these parameters. Nevertheless the full six figures given in Table II should be used in calculating the properties of liquids, and four or five should be used for gases. A change of one in the sixth place of one constant by itself will alter the calculated pressure of a liquid by about 0.01

TABLE V. *Miscellaneous properties of n-butane.*

1. *Properties of Gas at Low Pressure*

	Obs.[24]	% Dev.
Normal density, g/liter	2.70324	−0.10

2. *Critical Properties*

	Obs.[22]	Obs.-Calc.
Pressure, atmos.	37.48	−0.05
Temperature, °K	425.14	−0.06
Density, moles/liter	3.88	+0.13

3. *Properties of Saturated Liquid*

	Density, moles/l.		Vapor Press., atmos.	
Temp., °C.	Obs.	% Dev.	Obs.	% Dev.
4.44	10.26[20]	+0.6	1.20[20]	+1.2
37.78	9.66[23]	+2.2	3.51[23]	−1.0
71.11	8.93[23]	+1.8	8.23[23]	−0.4
100.00	8.07[23]	+0.6	15.19[23]	−0.5
			15.09[22]	−1.1
121.11	7.26[23]	−0.8	22.48[23]	+0.1

atmos. However, it is possible to change all the constants simultaneously by about 5 percent without seriously prejudicing the calculated results. This point should be borne in mind in any attempted correlation of the constants with other properties of the hydrocarbons.

E. Comparison of Observed and Calculated Properties of Light Hydrocarbons

There is not space here for a detailed comparison of observed properties of methane, ethane, propane, and *n*-butane with those predicted by the present equation. Table III summarizes the results of such a comparison and indicates the source of the data used. Since the predictions of the equation correspond about equally well with experimental data for each hydrocarbon, the detailed comparison for *n*-butane, given in Tables IV and V, may be considered as typical of the results for methane, ethane, and propane as well. In these tables, "% Dev." is defined by

$$100\,\frac{\text{Obs. Property} - \text{Calc. Property}}{\text{Obs. Property}},$$

and "Ave. % Dev." is the average of the absolute values of the individual deviations.

Tables IV and V illustrate the agreement between observed data for *n*-butane and values calculated by the equation of state. Similar tables for methane, ethane, and propane give about as good agreement between observed and calculated properties as here illustrated for *n*-butane. A comparison between the columns in Table III helps to show this point.

It was impossible to fit the points for *n*-butane (Table IV) at 8 moles/liter, about twice the critical density, and these were not used in determining the parameters. Excluding these three points, the average deviation of the calculated pressures is 0.31 percent. Up to 4 moles/liter the average deviation is only 0.22 percent, whereas over approximately the same density range the average deviation from the Beattie-Bridgeman equation[22] is 0.36 percent. It may be said that the equation fits the data well for all four hydrocarbons up to about 1.8 times the critical density, but above this density calculated pressures are high.

In Part 2 calculated critical properties are shown to be in good agreement with those observed by Beattie, Simard and Su.[22] Table III, Part 2, shows fair agreement for the other three hydrocarbons. Calculated critical pressures are somewhat high, though with the exception of methane the deviations are less than 0.5 atmos.

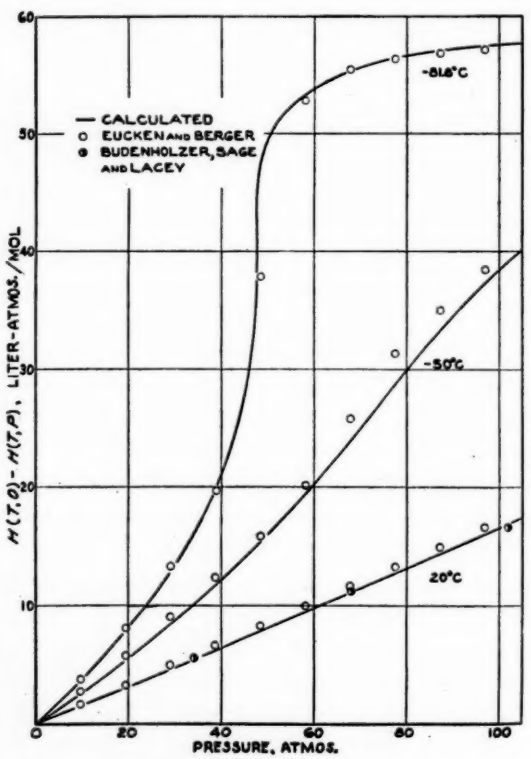

FIG. 5. Effect of pressure on enthalpy of methane.

Calculated critical temperatures are from 0.06 to 0.3°C high.

In Part 3 of Table V calculated vapor pressures of *n*-butane are shown to agree with observed vapor pressures practically within experimental error. Calculated liquid densities differ from observed liquid densities with an average deviation of 1.2 percent. For the other hydrocarbons as well as for *n*-butane calculated liquid densities are from 0 to 3 percent low. Vapor pressures agree well down to pressures of the order of 2 atmos.; at lower pressures calculated vapor pressures are low.

The average deviations summarized in Table III indicate the error resulting when the present equations are used to compute thermodynamic properties of these hydrocarbons within the regions of density, pressure, and temperature in which the equations have been fitted. Caution should be exercised in using the present equations at higher densities or lower temperatures. Extrapolation to higher temperatures or lower densities is less hazardous.

The use of the equation for calculating thermodynamic properties other than those considered in evaluating the parameters is illustrated by the following examples: (1) the effect of pressure on the enthalpy of methane, and (2) the latent heat of evaporation of *n*-butane.

Eucken and Berger[25] have determined the effect of pressure on the enthalpy of methane calorimetrically below 20°C, and Budenholzer, Sage and Lacey[26] have computed it from Joule-Thomson coefficients measured above 21.11°C. In Fig. 5 experimental values of $H(0, T) - H(P, T)$ at −81.8, −50, and 20°C are compared with those calculated by Eqs. (B7) and (B11). The agreement at −81.8°C, the computed critical temperature, and at 20°C, is probably within the error of the measurements. At −50°C the agreement is less satisfactory.

The calculated latent heat of evaporation of *n*-butane at 37.78°C is compared below with that measured calorimetrically by Sage, Webster and Lacey:[23]

Calculated	202.6	liter-atmos./mole
Observed	201.1	liter-atmos./mole

The calculated latent heat is the difference in enthalpy between the liquid and vapor, each evaluated by Eq. (B11) at the calculated saturation density.

The minor discrepancies between observed properties of pure hydrocarbons and those calculated by the present equation, although real, do not seriously impair the value of the present equation. It provides in a single expression a concise and reasonably accurate summary of several classes of thermodynamic data pertaining to hydrocarbons and covers a wider range of data than any equation proposed up to the present time. It may be applied both to the gas phase and to the saturated liquid. Perhaps the greatest value of the equation is that it provides a point of departure for the prediction of thermodynamic properties of mixtures.

The next paper of this series will show how the present equation may be generalized to describe the thermodynamic properties of mixtures. Work is also planned on extending the equation to substances other than those treated in this first paper.

ACKNOWLEDGMENT

Thanks are due Professor James A. Beattie, of the Massachusetts Institute of Technology, for valuable suggestions in the development of this equation. The financial assistance of the Polymerization Process Corporation is gratefully acknowledged.

[25] Eucken and Berger, Zeits. f. ges. Kälte-ind. **41**, 145 (1934).
[26] Budenholzer, Sage and Lacey, Ind. Eng. Chem. **31**, 369 (1939).

Consistent Notation for Point Positions in Space Groups

L. W. McKeehan
Sloane Physics Laboratory, Yale University, New Haven, Connecticut
(Received February 14, 1940)

ANYONE who has had much to do with special and general point positions in space groups of high symmetry has been delayed by the rather awkward notation in available tables, the best of which are the "International tables for the determination of crystal structures."[1] The coordinates of the different points of a single set, when written on the typewriter, take from 3 characters as a minimum to 11 as a maximum; e.g., xyz; $\frac{1}{4}-x$, $\frac{1}{4}-y$, $\frac{1}{4}-z$. In addition it may be remarked that mistakes in copying fractions, printed or typed, are especially easy and that the derivation of point coordinates by application of symmetry operations is hindered by an unsymmetrical notation. This is written to point out that a consistent notation with exactly 6 characters per point is easy to devise and remember. It is suggested that future tabulations take advantage of this simplification. This suggestion was, in fact, made some years ago,[2] but has not hitherto been published.

The only fractions which appear with arbitrary parameters added to or subtracted from them are $\frac{1}{6}$, $\frac{1}{4}$, $\frac{1}{3}$, $\frac{1}{2}$, $\frac{2}{3}$, $\frac{3}{4}$, $\frac{5}{6}$. Besides these there appear without additions the fractions $\frac{1}{8}$, $\frac{3}{8}$, $\frac{5}{8}$, $\frac{7}{8}$, and without fractional parts the multiplier 2 affecting an arbitrary parameter. The problem is to express all these in exactly two typed characters so that six consecutive characters will always be necessary and sufficient.

Adopting a duodecimal basis and suppressing the denominator (10 on this basis, 12 on a decimal basis) the fractions to which parameters are added or subtracted become 2, 3, 4, 6, 8, 9, t (using t for "ten"). The fractions that appear alone are similarly 16, 46, 76, $t6$. (Denominator 100 suppressed.) The addition of two fractions can now be represented merely by writing them together, $3u$ for $3+u$, and as is customary in some degree already, a negative quantity can be shown by overlining, $3\bar{u}$ for $3-u$. The multiplier 2 is consistently suppressed, the symbol for the parameter being written twice, $\bar{u}\bar{u}$ for $2\bar{u}$. Wherever a space would otherwise appear a zero is inserted. This completes the system of notation. It may be remarked that the letters chosen for representing parameters should be those which are not made unsightly or ambiguous by overlining or underlining (the latter will be preferred by typists). The only conventional set of three consecutive letters which meets this criterion is the set u, v, w. If it is desired to use different letters for one, two, and three parameter sets the best choices are m; r, s; u, v, w. Another way of designating parameters without occupying more space than is available is to use superscript letters (or numbers 1, 2, 3) for added fractions, subscript letters (or numbers) for subtracted fractions. This is easier in typing but has the disadvantage of using a small type size in printing.

As examples two point position sets are copied below in the present standard notation and translated into the suggested consistent notation.

Space Group $D_{3d}{}^4-H\bar{3}1c$ Point position $18(f)$

old $(000;\ \frac{1}{3}\ \frac{2}{3}\ 0;\ \frac{2}{3}\ \frac{1}{3}\ 0)+$
$x\ \bar{x}\ \frac{1}{4};\ x,\ 2x,\ \frac{1}{4};\ 2\bar{x},\ \bar{x},\ \frac{1}{4};$
$\bar{x}\ x\ \frac{3}{4};\ \bar{x},\ 2\bar{x},\ \frac{3}{4};\ 2x,\ x,\ \frac{3}{4}.$

new $(000000;\ 408000;\ 804000)+$
$0u0\bar{u}30;\ 0uuu30;\ \bar{u}\bar{u}0\bar{u}30;$
$0\bar{u}0u90;\ 0\bar{u}\bar{u}\bar{u}90;\ uu0u90.$

Space Group O^4-F4_13 Point position $48(f)$

old $(000;\ 0\ \frac{1}{2}\ \frac{1}{2};\ \frac{1}{2}\ 0\ \frac{1}{2};\ \frac{1}{2}\ \frac{1}{2}\ 0)+$
$\frac{1}{8},x,\frac{1}{4}-x;\ \frac{1}{4}-x,\frac{1}{8},x;\ x,\frac{1}{4}-x,\frac{1}{8};\ \frac{1}{8},\bar{x},\frac{3}{4}+x;$
$\frac{3}{4}+x,\frac{1}{8},\bar{x};\ \bar{x},\frac{3}{4}+x,\frac{1}{8};\ \frac{3}{8},x,\frac{1}{4}+x;\ \frac{1}{4}+x,\frac{3}{8},x;$
$x,\frac{1}{4}+x,\frac{3}{8};\ \frac{3}{8},\bar{x},\frac{3}{4}-x;\ \frac{3}{4}-x,\frac{3}{8},\bar{x};\ \bar{x},\frac{3}{4}-x,\frac{3}{8}.$

new $(000000;\ 006060;\ 600060;\ 606000)+$
$160u3\bar{u};\ 3\bar{u}160u;\ 0u3\bar{u}16;\ 160\bar{u}9u;$
$9u160\bar{u};\ 0\bar{u}9u16;\ 460u3u;\ 3u460u;$
$0u3u46;\ 460\bar{u}9\bar{u};\ 9\bar{u}460\bar{u};\ 0\bar{u}9\bar{u}46.$

[1] Leading title: *Internationale Tabellen zur Bestimmung von Kristallstrukturen* (Gebrüder Borntraeger, Berlin, 1935).

[2] At a meeting of the American Academy of Arts and Sciences, October 8, 1935.

LETTERS TO THE EDITOR

This section will accept reports of new work, provided these are terse and contain few figures, and especially few halftone cuts. The Editorial Board will not hold itself responsible for opinions expressed by the correspondents. Contributions to this section should not exceed 600 words in length and must reach the office of the Managing Editor not later than the 15th of the month preceding that of the issue in which the letter is to appear. No proof will be sent to the authors. The usual publication charge ($3.00 per page) will not be made and no reprints will be furnished free.

Transformations in Monolayers

It appears from the letter to the Editor by Harkins and Boyd[1] that many parts of my article[2] have been overlooked.

Points of transformation.—The thermodynamical definitions given on p. 932 are valid however indefinite the limits of the surface phase may be.

Mesomorphous phase.—This is analogous to a liquid crystal, not because it lies between the solid and liquid states, but for reasons and experimental evidence which have been given in a special paragraph, p. 945.

Liquid phase.—In other temperature ranges, the condensation from the gaseous to the solid or mesomorphous phases is also a first-order transformation. This is not peculiar only to the liquid. As for the compressibility, there can be no comparison with the three-dimensional liquid, since in the film all the molecules are oriented with reference to the same plane and the compressibility is measured only in that plane. The heat expansion of three-dimensional paraffin crystals is incomparably smaller in the direction of the chains than in the two other directions of the unit cell.[3]

Isotropic film.—We are enabled to estimate the degree of anisotropy of liquid films by comparing the measured areas at different points of the isotherms to the area $A = V^{2/3}$. Actually it happens that, *when* $T \geq T_{cc}$, the areas at the point M are close to the calculated values. This is an experimental fact, an explanation of which I have tried to give, p. 941.

State of a film.—This is defined when three of the four variables A, π, T, pH, are fixed. Part of the misunderstanding of Harkins and Boyd comes from the fact that they compare molecular areas without defining the temperature and the pressure. Thus they compare to the numbers of column 4 of my Table I, which are relative to molecular areas of the liquid film *under its vapor pressure and at temperatures* $T \geq T_{cc}$, values found for $T < T_{cc}$ (column 2, Table II of H. and B.) and even areas at the point 0 (transition to the crystal). The value of 57A² for myristic acid is in agreement with Adam and Jessop's classical isotherms ($T = 34°$), while the smaller area of 45A² may be found at 17° (see Fig. 17).

General diagram.—My diagram has been incompletely and wrongly reproduced by Harkins and Boyd. Especially the isotherm relative to $T > T_{cc}$ is missing, while all the discussion on the isotropy at the point M concerns precisely that case.

Areas in the solid and mesomorphous states.—The state of the solidified film between 19.5 and 18.5A² is metastable. This can be easily detected by registration of the isotherm (see Figs. 7 and 14 and read legend); when using the ordinary method, there is no wonder if the film seems to collapse at 19.5A².

The areas of 18.5, 19.5, 20.5, 23.5A² per chain are average values. With the actual technique it is impossible to estimate the molecular area with a precision greater than ±1 percent (errors on the area, volume of the solvent deposited, weighing of the substance). With the exception of a few studies on single crystals, x-ray analysis gives data with the same indetermination. So that even the values given by H. and B. in columns 3 and 4 agree in majority with the x-ray data. Besides, it should be kept in mind that palmitic acid at 20° is already in the expanded mesomorphous form ($T_m = 18°$) and that the area of 23.5 for stearic acid is found at room temperature on substrates between distilled water and HCl $N/500$, while it rises to 24.5 when reaching $N/100$. The important point is that, even when the area at the sublimation point is larger than 24A², the value of 23.5 unquestionably appears at higher pressures as a second-order point (p. 946).

Concerning alcohols, although their characteristic areas seem to agree with those for acids (see H. and B.'s own values), it would be more reasonable to compare them with those found by x-ray analysis of the same alcohols.

Van der Waals forces do act by raising the melting and critical temperatures. But it seems doubtful whether, *in the same state*, the packing of the molecules increases with the chain length. This is a matter of discussion based on such feeble evidence as variations of less than 0.5 percent in the measured areas. For the moment, we are able to say that, within the precision of both methods, there is correspondence between the x-ray and monolayer measurements.

D. G. DERVICHIAN

Laboratoire de Chimie Physique,
Faculté des Sciences,
Paris, France,
March 13, 1940.

[1] Harkins and Boyd, J. Chem. Phys. **8**, 129 (1940).
[2] Dervichian, J. Chem. Phys. **7**, 931–48 (1939).
[3] Müller, Proc. Roy. Soc. **A127**, 417 (1930).

Mechanism of the Exchange Reaction Between Gaseous Bromine and Hydrogen Bromide

Liberatore and Wiig[1] have presented conclusive evidence for a rapid homogeneous interchange reaction between Br_2 and HBr in the gaseous state at room temperatures. Their data show the reaction to be nearly but not quite at equilibrium in two minutes and to be homogeneous and nonphotochemical. As a mechanism, the authors suggest a chain involving the production of Br atoms by the ionization processes associated with the radioactive bromine radiation, the Br atoms reacting according to

$$Br + HBr^* = HBr + Br^* \quad (1)$$

or

$$Br + BrBr^* = BrBr + Br^* \quad (2)$$

to establish uniform distribution of the radioactive isotopes.

In this connection it may be of interest to consider experiments performed under conditions nearly identical with those of Liberatore and Wiig with the principal difference that the intensity of the radioactive radiations was nearly 20,000-fold smaller. The actual number of radioactive atoms present during a typical experiment was 1.5×10^5 while Liberatore and Wiig give 3.5×10^9 as the value for their experiments. At these lower activities the reaction was within ten percent of completion in two minutes and was not appreciably affected either by painting the reaction vessel black or coating the inner surface with paraffin. For these reasons it seems certain that the suggested mechanism is not the principal one involved in the reaction. The alternative mechanism mentioned by the authors, a direct reaction between Br_2 and HBr through a HBr_3 complex, appears to be the correct one.

The data require that this reaction have an activation energy less than 11 kilocalories. Such a value does not appear to be entirely unreasonable.

Additional experiments have shown that I_2 and HI undergo a similarly fast reaction both in the gaseous state and when dissolved in dry pentane.

W. F. Libby

Department of Chemistry,
University of California,
Berkeley, California,
February 16, 1940.

[1] L. C. Liberatore and E. O. Wiig, J. Chem. Phys. **8**, 165 (1940).

Thermal Diffusion Separation of Different Gases of the Same Molecular Weight

Most of the work done by means of the recently developed thermal diffusion method[1-3] has been directed toward the separation of isotopes and isotopic compounds. In order to find experimentally some of the factors other than mass which influence separations, we have applied the thermal diffusion method to the separation of different gases of the same molecular weight (to the nearest whole mass unit). In such cases any separation which might occur would be due to the difference in structure of the molecules and to their different forces of attraction and repulsion.

The apparatus used was a brass column nine feet long with an outer jacket cooled by tap water at 20°C and an inner tube heated by means of No. 22 Chromel wire to about 225°C. Mixtures of gases were placed into an intermediate chamber which was 0.7 cm thick and had an inner radius of 1.0 cm. The combinations of gases used were carbon dioxide and propane, nitrogen and ethylene, etc., the runs being made for various concentrations.

Table I.

Combination	Composition in Mole Percent			
	Before Diffusion	After Diffusion		Difference ±0.4
		Top	Bottom	
1. CO_2 and C_3H_8	34.4% CO_2	36.5	33.6	2.9
	53.6	55.9	52.9	3.0
	69.1	70.2	67.9	2.3
2. CO_2 and N_2O	36.1% CO_2	37.1	35.2	1.9
	42.5	43.3	41.4	1.9
	54.5	55.0	53.4	1.6
	70.1	70.4	69.0	1.4
3. CO and N_2	26.8% CO	26.7	26.8	−0.1
	38.0	37.6	37.9	−0.3
4. CO and C_2H_4	33.8% CO	35.5	29.7	5.8
	46.7	48.8	41.4	7.4
	58.8	61.2	55.1	6.1
	73.4	77.2	72.8	4.4
5. N_2 and C_2H_4	34.8% N_2	38.2	31.6	6.6
	48.3	53.0	45.1	7.9
	69.3	72.8	66.1	6.7

The results of the work are summarized in Table I. The percentage compositions after thermal diffusion are the averages of at least four measurements. For each of the combinations listed except CO and N_2, the separations were quite substantial. In the case of CO and N_2, the molecules are so similar that no separation was found, the observed deviations being within the experimental error. The probable error in each case was about ±0.4 percent.

Remarkably enough, carbon dioxide could be partially separated from nitrous oxide, the carbon dioxide tending to go to the top. No explanation for this is apparent, at least not when compared to the results for CO and N_2. In the other cases the larger of two molecules of the same molecular weight was found to go to the bottom. This result is probably to be related to the fact that the bulkier molecules have lower inverse power repulsive forces than do the compact molecules.

The slight mass differences between carbon dioxide and propane or between ethylene and carbon monoxide or nitrogen are not sufficient to account for the observed separations. Even if the masses differed by a whole atomic unit, the separations on that account would not be as large as observed for a column only nine feet long. Accordingly, the separation must be attributed to differences in structure.

Experimental studies of other combinations are under way. Full details of the work will be published shortly.

F. T. Wall
C. E. Holley, Jr.

Noyes Chemical Laboratory,
University of Illinois,
Urbana, Illinois,
February 29, 1940.

[1] K. Clusius and G. Dichel, Naturwiss. **26**, 546 (1938); **27**, 148, 487 (1939).
[2] A. Bramley and A. K. Brewer, J. Chem. Phys. **7**, 553, 972 (1939); Science **90**, 165 (1939).
[3] W. H. Furry, R. C. Jones and L. Onsager, Phys. Rev. **55**, 1083 (1939). (Theoretical paper.)

Windows for Studying the Optical Properties of Hydrogen Fluoride Gas

Following the remarks of Freed, McMurry, and Rosenbaum[1] on the use of artificial corundum in optics, we should emphasize that the preliminary researches, interrupted in August by the present events, have led us to certain conclusions relative to the materials which could constitute windows resisting the action of HF. These researches have as their aim, extension of our results regarding liquefied HCl to hydrogen fluoride.[2]

In dilute solution, certain organic glasses, in particular Duroïd, are inattackable by HF; those which are colorless may serve in the visible spectrum; they are deprived of double refraction and can be used in polarimetry, as Mlle F. Perrier has demonstrated. Duroïd is yellow colored, but does not show in infra-red (under about 4 mm) important bands up to 1.2μ; *it allowed us to discover a wide and weak band about 0.93μ, distinct from that of the gas, in the aqueous solution of hydrogen fluoride (about 40 percent in weight).*

In contact with a concentrated solution of HF, gas or pure liquid, all organic substances which we have tried, have been attacked (probably by dehydration); the fluorite itself tarnishes more or less quickly, especially at a high temperature (perhaps by the formation of CaF_2, HF). We have taken instead artificial white corundum (white sapphire), of which we have been able to obtain, in France, some plates of 22 mm diameter, parallel to the axis. We have verified that this substance does not show bands of absorption between 1850A and 2.5μ, and that it is not attacked by the gas HF, even at high temperatures (our experiments were made during an hour at 300°C).

B. Vodar
R. Freymann
Yeou Ta

Laboratoires de Physique de la Sorbonne,
Paris, France,
January 20, 1940.

[1] Freed, McMurry and Rosenbaum, J. Chem. Phys. **7**, 853 (1940).
[2] J. de phys. et rad. **9**, 282 (1939).

Exchange Reactions Between Gaseous Alkyl Bromides, Bromine and Hydrogen Bromide

An investigation, with the aid of radioactive bromine, of the exchange reactions of ethyl bromide with bromine and with hydrogen bromide confirms our recent conclusion[1] that the exchange reaction between bromine and hydrogen bromide proceeds by an atom chain. That this last exchange is a bimolecular reaction[2] going through a HBr_3 complex and requiring an energy of activation less than 11 kcal. appears to be highly improbable.

Gaseous Br_2 containing radioactive bromine when mixed with ethyl bromide for various periods of time up to two hours shows no exchange at all. Similar results have been obtained with HBr and C_2H_5Br. The mixture of Br_2 and C_2H_5Br was also exposed to the full light of a 500-watt tungsten lamp for 9 hours without any detectable exchange at room temperatures. When heated, exchange sets in. These results are all in agreement with an atom mechanism. Rapid exchange takes place when HBr and C_2H_5Br are heated to 200–300°, but this probably occurs through the equilibrium $C_2H_5Br \rightleftarrows C_2H_4+HBr$.

If the exchange reaction between HBr and Br_2, which is very rapid at room temperatures, proceeds through a bimolecular reaction as Libby[2] suggests, then exchange should also occur between C_2H_5Br and Br_2, since the strength of the C−Br bond (*ca.* 65 kcal.) is less than that of the H−Br bond (*ca.* 86 kcal.). Calculations by a semi-empirical method developed by Hirschfelder[3] of the energies of activation for these two reactions yield values of 37 and 31 kcal., respectively. Similar calculations for the Br atom exchange reactions with C_2H_5Br and with HBr yield values of about 25 and less than 5 kcal., respectively. Thus, of these four reactions only the HBr+Br atom exchange would be expected to occur at room temperatures, in agreement with our experiments.

The atom chain reaction appears to be the only possible mechanism, though the Br atom concentrations in Libby's experiments might seem to be too small. In our $HBr+Br_2$ experiments the Br atom concentration resulting from radioactive processes was larger (30 : 1) than that due to thermal dissociation of bromine. The latter is much larger than the former in Libby's experiments, however. The Br atom concentration at room temperatures may be estimated by extrapolation of the data of Perman and Atkinson[4] at 650–1050° or of Bodenstein and Cramer[5] at 800–1200°.

Calculations indicate that to account for Libby's results under our experimental conditions in two minutes about 225 collisions per cc of HBr with Br atoms would be required, whereas from the data of Perman and Atkinson the thermal Br atom concentration is sufficient to yield only 10 collisions. Bodenstein and Cramer's data give even fewer collisions. However, such an extrapolation might easily be too low by a factor of 100 or more. Thus Libby's results may also be accounted for by an atom chain reaction initiated by bromine atoms produced thermally.

More complete details of these investigations of the exchange reactions of Br_2 and HBr with C_2H_5Br and other alkyl bromides will appear shortly.

L. C. Liberatore
E. O. Wiig

University of Rochester,
Rochester, New York,
March 14, 1940.

[1] Liberatore and Wiig, J. Chem. Phys. **8**, 165 (1940).
[2] Libby, J. Chem. Phys. **8**, 348 (1940).
[3] University of Wisconsin Symposium on the Kinetics of Homogeneous Gas Reactions, June, 1939.
[4] Lewis and Randall, *Thermodynamics* (McGraw-Hill Book Co., New York, 1923), p. 514.
[5] Bodenstein and Cramer, Zeits. f. Elektrochem. **22**, 327 (1916).

The Absorption Spectra of Liquid HF and of its Aqueous Solution in the Region λλ8000–11,000

The absorption spectra of liquid HF and of HF in aqueous solution have been photographed in the region λλ8000–11,000 with a dispersion of about 60A per mm. In the case of the anhydrous HF a copper cell was used, with windows of MgO (artificial crystal) clamped directly onto the ends of the tube. The MgO is not attacked by anhydrous HF and appears to have greater mechanical strength than glass.

The absorption band of anhydrous HF in the liquid state is very similar to the band of liquid water at λ9722 as reported by Badger and Bauer,[1] though it is somewhat broader. The position of the band maximum determined at several temperatures is given in the following table. The large probable error indicated arises from the difficulty in estimating the maximum of a broad band in this region where the trend in plate sensitivity is large.

TABLE I. *The maximum of the band of liquid* HF *as a function of temperature.*

t(°C)	λ_{max}(A)
19	9940±75
0	9990
−30	10140
−60	10300
−75	10380

Salant and Kirkpatrick[2] have found that the third harmonic band of unassociated HF gas is located at λ8790. From the data just given it is evident that the frequency decrease in going from the gas to the liquid is very large even at the boiling point, namely about 1320 cm^{-1}. This shift in the HF frequency, which must be due mainly to the formation of hydrogen bonds of the type F−H···F, is large in comparison with the shift in OH frequency on the formation of the O−H···O linkage. The third harmonic OH band of methyl alcohol, for example, is found at λ9490 in the vapor[3] and at λ10,070 in the liquid,[1] so that the frequency shift is about 600 cm^{-1}.

The large difference in the magnitudes of the frequency shifts just mentioned is very interesting in view of the fact that the energies of the hydrogen bonds in associated HF and CH_3OH are so nearly the same, being 6.7 and 6.2 kcal. per mole,[4] respectively.

The absorption spectrum of HF in aqueous solution has also been examined at HF concentrations of 25 and 50 percent and at 0° and at 25°C. In no case does a cursory examination reveal any significant difference between the solution band and the λ9722 band of water in either position or shape.

AUSTIN L. WAHRHAFTIG

Gates and Crellin Laboratories of Chemistry,
California Institute of Technology,
Pasadena, California,
March 11, 1940.

[1] Badger and Bauer, J. Chem. Phys. **5**, 840 (1937).
[2] Salant and Kirkpatrick, Phys. Rev. **48**, 945 (1935).
[3] Badger and Bauer, J. Chem. Phys. **4**, 469 (1936).
[4] L. Pauling, *The Nature of the Chemical Bond* (Cornell University Press, 1939), p. 313.